PFC/RR85-10

DOE/ET-15013-151

STRUCTURAL BEHAVIOR OF INTERNALLY COOLED CABLED SUPERCONDUCTORS UNDER TRANSVERSE LOAD

PART I - EXPLORATORY TESTS

PART II - THEORY AND COMPARISON WITH EXPLORATORY TEST DATA

H. Becker[1], E.S. Bobrov[1], C. Chen[1], P.G. Marston[1], D.B. Montgomery[1], P. Neshe[2], D. Tognarelli[2]

(1 - MIT, 2 - Manlabs)

June 1985

Plasma Fusion Center

Massachusetts Institute of Technology

Cambridge, MA, USA

SUMMARY

Investigations were conducted into the transverse structural stiffness and static strength of internally cooled cabled superconductors (ICCS) in order to determine their effective stiffness and ultimate load-carrying capacity. Experiments were performed at room temperature (about 293 K) and in liquid nitrogen (about 80 K) to determine the effect of corner restraints from epoxy cement, the influence of the conductor cable on the effective stiffness of the conduit, and the relation of material strength to the structural character of the conduit. Theoretical calculations have been made in an attempt to help understand the structural response.

On the basis of the theoretical and experimental evaluations, it appears that the presence of corner fill is a major factor for ICCS transverse strength and stiffness.

SYMBOLS

A	Area, in^2
B	Magnetic field intensity, tesla
D	Diameter of tube, in
E	Young's modulus, psi
E_f	E of foundation, psi
E_i	E of insulator, psi
E_s	E of steel, psi
E_t	Tangent modulus, $(d\sigma/d\epsilon)$
h	Height of stack, in
I	Cirrent, amp
K_{IC}	Plane strain fracture toughness, ksi-$in^{\frac{1}{2}}$
L	Length of strip or column, in
N	Internal loading in conduit wall, lb/in
P	Force applied to stack, lb
p	Pressure, psi
q	General loading, lb/in or psi
R	Radius in conduit corner, in
S-N	Fatigue curve
W	Width of conduit, in
y	Coordinate, in
$\frac{da}{dN}$	Crack growth per cycle, (in)
Δ	Compressive deflection of conduit, in
ϵ	Strain
ν	Poisson's ration
σ	Stress, psi
σ_{cr}	Critical (or buckling) stress, psi
σ_{pl}	Proportional limit stress, psi
σ_u	Ultimate strength, psi
σ_n	Yield strength, psi

TABLE OF CONTENTS

TABLE OF CONTENTS, cont.

LIST OF FIGURES

LIST OF TABLES

PART I

GENERAL INTRODUCTION AND EXPLORATORY TESTS ON TRANSVERSELY LOADED ICCS

GENERAL INTRODUCTION

Statement of Problem

Interest in the use of ICCS has accelerated in recent years because of both the potentially greater cryogenic stability and the potential savings from magnet compactness when ICCS-wound magnets are compared with magnets wound of superconductors in a helium pool.

Research by investigators outside MIT has led to the belief that at certain fields and current densities the conduits of a full ICCS winding cannot withstand the integrated inplane Lorentz loading. That view is contrary to experimental data obtained during exploratory tests by MIT[1,2]. The more recent study[2] indicates that an ALCATOR DCT type ICCS can survive the TF coil static transverse design pressure of 7250 psi with a safety factor of 3[3]. It remains to develop a scientific basis for describing the behavior of an ICCS under both static and cyclic transverse loads, under axial loads, under internal pressure, and under the combination of all those loads. That requires a combination of theoretical analysis and well-designed experiments.

Structural Environment

If a coil winding is fashioned from an internally cooled cabled superconductor (ICCS), then the conductor conduit walls may be required to resist the transverse loading integrated through the coil thickness. The resultant wall stresses could be high enough to impair the structural integrity of the coil.

The transverse Lorentz loading also may induce longitudinal hoop tension in the conductor. In addition, the conduit must react the helium pressure from coolant flow and possibly a large internal overpressure caused by a quench. There also may be transient and static thermal stresses within the coil. Stresses from these effects must be combined with those from the transverse loading to yield values for comparison with allowables so that coil factors of safety may be determined.

There is little problem predicting response of an ICCS to longitudinal (axial) loading. It may be necessary to account for the axial load-carrying capacity of the cable. However, that presents little difficulty. Consequently, there is no need, at present, to investigate axial response. Therefore, the investigation of conduit behavior has been confined to transverse loading.

Past Activities

SIN (Suisse Institut Nucleaire) conducted ICCS design studies in connection with engineering of the Swiss Large Coil Task (LCT)[3]. The effort was based on experience gained from their OMEGA coils at CERN. They performed theoretical analyses and tests on several unpotted conduit configurations (Figure 1) without lateral restraint[4,5]. They studied the influence of various corner radii and distribution of the 316L structural material from which the conduit was to have been made. Moderate strength and stiffness appeared to be achievable using a small outside corner radius so that the corner thickness was greater than the wall thickness. SIN/BBC (Brown, Boverie et Cie) also conducted cost analyses which led them to conclude that a conduit ICCS would be too expensive to produce and it was abandoned in favor of a copper-solder-superconductor monolith with a central helium channel.

Westinghouse evaluated stiffness and strength of unpotted formed-sheet conduits of 304 steel (Figure 2) through analyses and experiments conducted as part of their LCT engineering[6]. They also measured the transverse stiffness of the cable at several void fractions. It was concluded that the conduits in a fully wound coil would not be able to support the design normal pressure. As a result, they wound the coil turns into grooves in machined aluminum alloy plates, with a maximum of four turns to a groove at the low field region.

Scoping studies to determine transverse loading effects on aluminum alloy ICCS conduits[1] were conducted at MIT. It was one aspect of ICCS technology development for MHD and fusion magnets. Some tests were conducted on potted arrays (Figure 3). They indicated that reasonably good strength was achievable in a fully wound coil. Tests were also run on unpotted, single conductors. They confirmed the Westinghouse data.

MIT Current Program

During the past year, design studies on ALCATOR DCT have considered a fully wound ICCS for toroidal and poloidal field coils. Those studies simulated the test program and related analytic studies to be described in this report. The goal has been to determine whether a fully wound ICCS coil can survive structurally in a fusion magnet with appropriate safety factors on static, cyclic, and transient dynamic loads. (That problem is separate from the electrical survivability of the cable superconductor). The program has been designed to elicit the details of the conductor structural

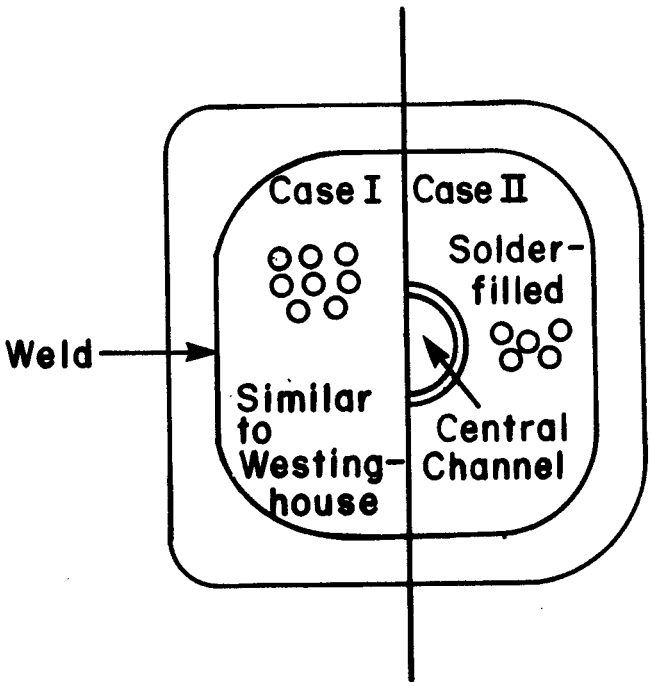

Fig. 1 SIN ICCS Shapes

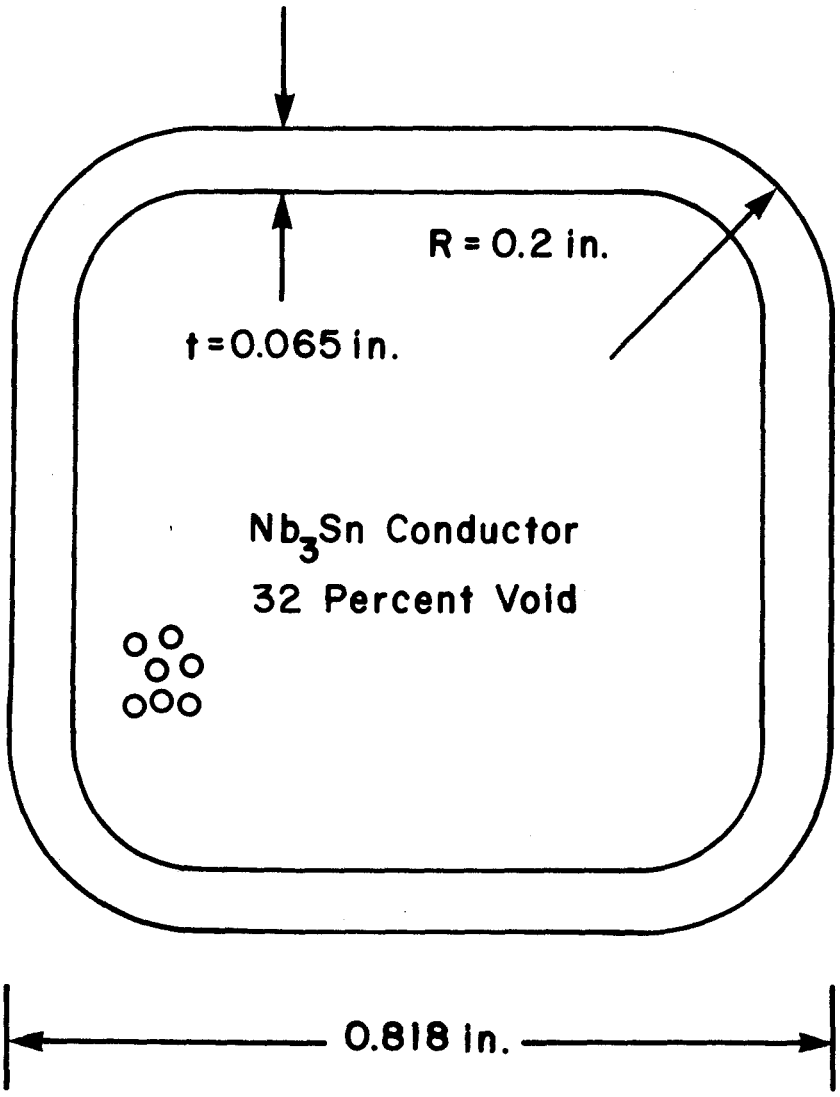

Fig. 2 Westinghouse ICCS Shapes

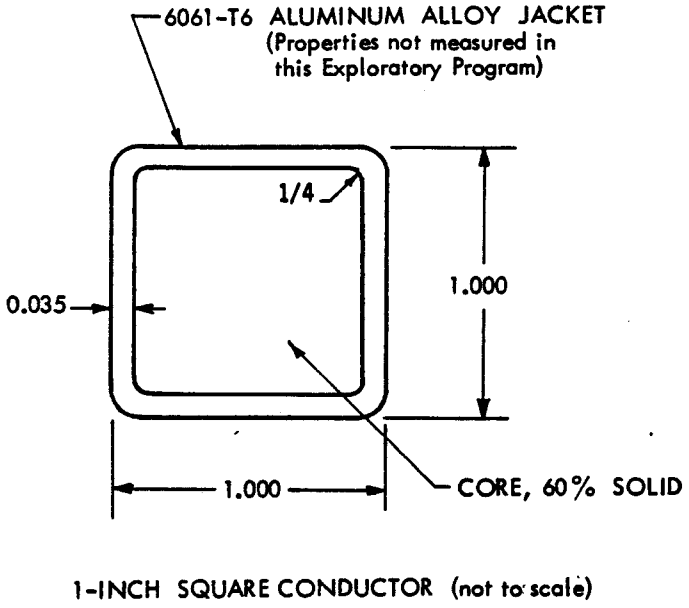

1-INCH SQUARE CONDUCTOR (not to scale)

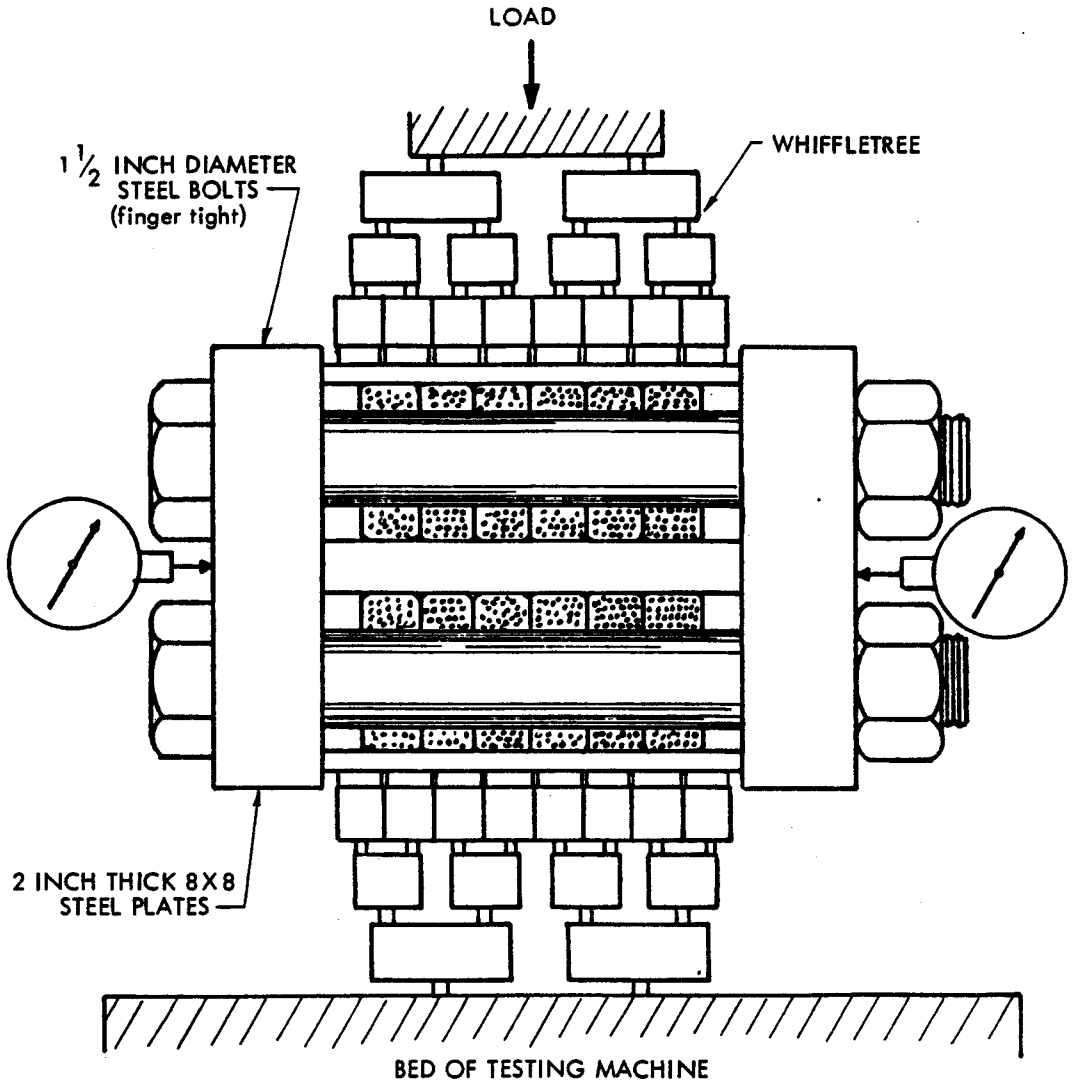

Fig. 3 MIT Potted Array of Aluminum Conduit ICCS

performance through experiments and calculations in order to generate a rational procedure for structural design and analysis of a real coil. Potted arrays were tested under conditions as close as possible to real magnet structural behavior.

At the time of this writing that process is not yet complete. However, it is felt that sufficient progress has been made to indicate that a fully wound coil is feasible for static loading.

Some Aspects of Compression Behavior

When a structure is loaded in compression, there is an adjustment of the loading device to the surface of the structure during the period of low load application. This usually is a nonlinear process with the nonlinearity dependent on the smoothness of each contact surface and on the general character of the structure to be loaded.

In the case of a compression stress-strain curve for a single bar of material, the initial nonlinear range usually is small compared with the more-or-less linear range before plasticity begins (Figure 4). If short blocks were to be built up into a stack the same height as the bar, there would be nonlinear behavior at each interface and the nonlinear region of the stress-strain curve could be large, as shown in Figure 4. In addition, there may be almost no linear range before inelasticity begins. That behavior has been observed during experiments to determine the compressive stiffness of superconducting cable stacks such as employed in high energy physics magnets[7].

If relatively soft sheets were to be placed between hard blocks, the initial nonlinear range could be larger than for a stack of blocks alone. If a stack were to consist of box-like elements, such as ICCS conduits, the nonlinear structural behavior would be amplified further because of the complex load paths between layers, particularly if there were no filler material between the box mating corners and if the corners were to be rounded as in an ICCS (Figure 5).

Conductors might be wrapped with fiberglass cloth wound into pancakes and then impregnated. (Prepreg cloth could also be used as insulation.) Under those conditions, the structural behavior would depend upon the load paths across the wrapping which would probably have lower stiffness and greater initial nonlinearity than if adjacent conductors were separated by thin laminated sheets that were cured before introduction into the winding.

The magnitudes of those motions were learned during the step-by-step exploratory test program. It was unrealistic to attempt to design an *ab initio* test program. Furthermore, learning

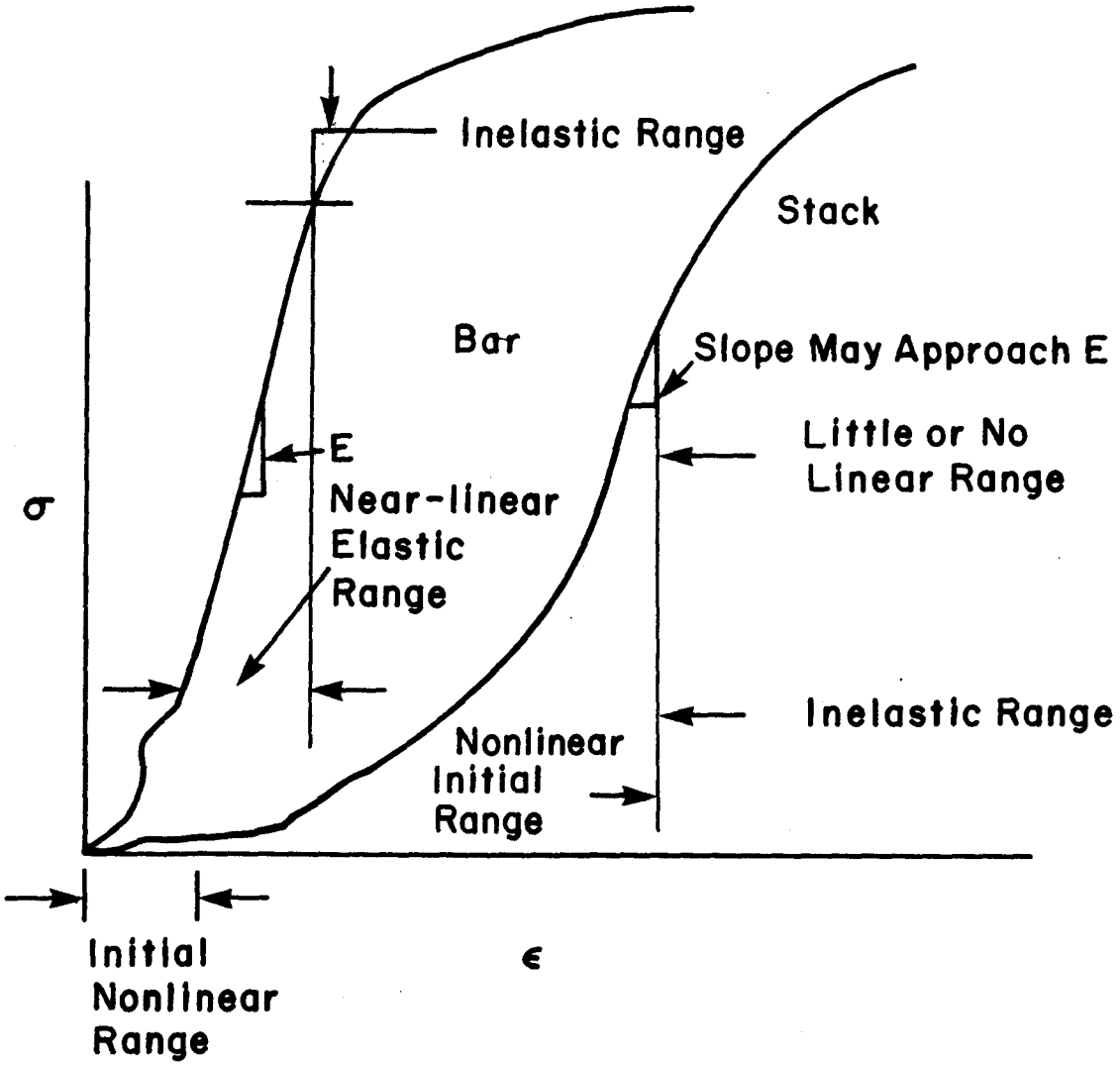

Fig. 4 Schematic Stress-Strain Curves, Bar vs. Stack

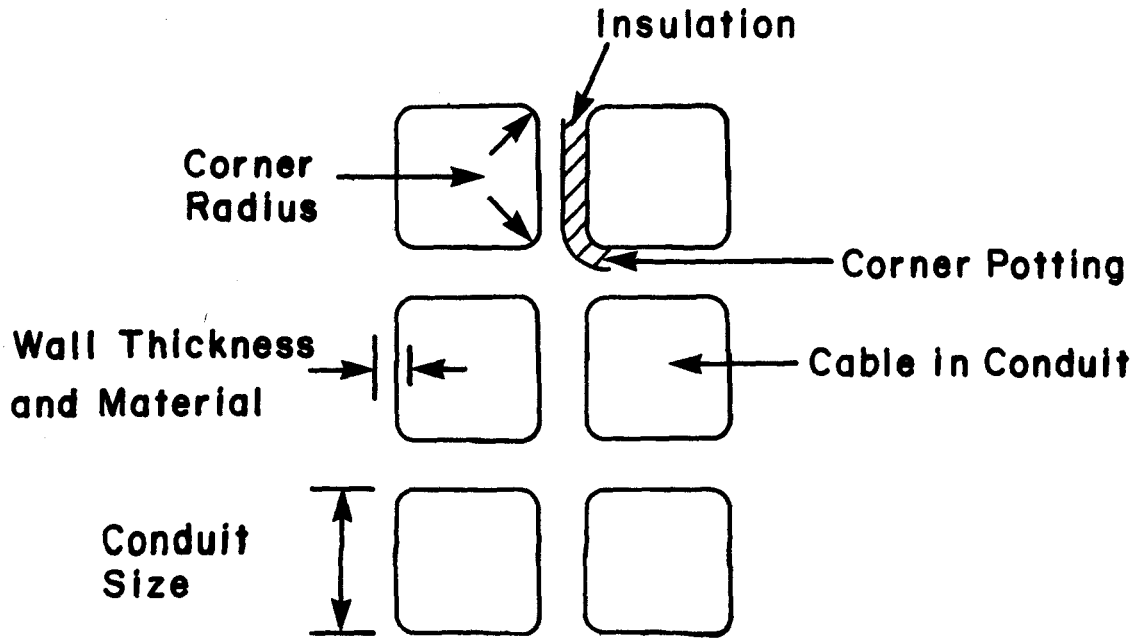

Fig. 5 Array Schematic Showing Factors That Can Affect Stack Transverse Stiffness and Strength

the phenomenology of stack behavior was an iterative process involving a few test runs, followed by some elementary analysis. It is only after having reached the present level of understanding that it appears feasible to design the systematic test program contemplated for the follow-on effort.

Materials

The structural performance of an ICCS depends upon the materials from which the components are fabricated. Candidate conduit materials and relevant structural properties are summarized in Table 1. In the current program only the static properties were important. Subsequent studies will include fatigue. Eventually, the effects of irradiation will have to be measured, as has been done on organic composite insulators[6].

No stress-strain curves were measured for any of the conduit materials in this exploratory program. The filled conduits contained Oxford Superconducting Technologies superconducting cable with the following characteristics:

Nb_3Sn wires 0.7 mm in diameter with Cu/sc = 1.8/1.

Wire triplets were twisted with 1 inch pitch.

3 triplets were twisted with 1.5 inch pitch.

3 of those were twisted with 3 inch pitch.

3 of those were twisted into a subcable with 6 inch pitch.

6 subcables were twisted with a 12 inch pitch to form a 486 wire cable.

The cable was wrapped with 0.001 inch thick stainless steel foil.

The wrapped cable was enclosed in a tube formed from JBK-75 steel strip 0.064 inch thick and 3.07 inches wide.

The combination was processed to final shape with a void fraction of 32 percent.

The conductor then normally would be reacted. However, the present tests were performed on unreacted conductors.

As a result of the forming and turks-heading operations, the JBK-75 iron superalloy conduit was highly cold worked. An attempt was made to determine the corner yield strength at room temperature for which a value of the order of 200,000 psi was found. The 77 K value was not measured. In future, measurements will be made on reacted conduit material.

Table 1. **Material Structural Properties Relevant to Conduit Survivability**

Component	Product Form	Candidate Material	Fabrication Process	Relevant Structural Property							
				E	ν	σ_{tu}	σ_{ty}	σ_{cy}	S-N	K_{IC}	$\frac{da}{dN}$
Cable	Wire	Cu:NbTi	N/A	x		x	x				
		$Cu:Nb_3Sn$	N/A								
Conduit	Sheet	JBK-75, One of Several Incoloys	Potting, Welding, Compressing Turks-heading, Bending, Heat-treating	x	x	x^2	x	x	x^2	x^2	x^2
Insulation	Laminate	Fiberglass with epoxy or polyimide	Pressure Molded	x^3			x^3	x^3			
	Cloth	Glass	Wrap around conductor and pot								
Potting Compound	Monomer plus curing agent (unfilled, filled)	epoxy, polyimide	Impregnation	x	x		x	x			

1 Both longitudinal and transverse, where applicable to conduit behavior

2 Base metal and weld

3 Perpendicular to layer

The epoxy filler was a common two-part resin for which the Young's modulus at 300 K is typically 0.3 msi and is of the order of 0.6 msi at 77 K.

The insulator was strips of G-10CR for which the reported transverse stiffness is in the 1 to 2 msi range.

The conduits exhibited numerous variations in cross section shape (Figure 6). In preparing some of the specimens for the empty conduit stack tests, it was necessary to remove the cable. This was accomplished by driving it out with an arbor press. The cable came out with little effort.

Exploratory Test Program

The exploratory test program has been designed to enlarge upon the aluminum conduit element and stack tests of reference 1 by using the steel conduit and winding configuration planned for the ALCATOR DCT TF and PF coils. The early tests in the current program were performed at 300 K on single stacks three conduit widths high[2]. As data were acquired, further tests were conducted in parallel with elementary calculations to help understand the significance of lateral restraint, corner potting. influence of the cable, and effect of test temperature. The culmination of that effort was a set of tests on parallel stacks of unpotted and potted conduits and circular tubes.

The exploratory test program included transverse strength and stiffness studies of conduits and circular tubes. The types of tests are summarized in Table 2.

The 1×3 unsupported conduit stack tests provided the insight needed to design the 2×3 supported stack tests, which were intended to simulate coil structural behavior. The tube tests helped reveal the need for corner filling to achieve high strength.

The structural features of major concern are strength and stiffness. In order to facilitate acquisition of those properties, the test data are presented as pressure-strain curves. The pressure is $p = P/A$ where P is the machine load (pounds) and A is the planform area of a stack (in^2). Strain, ϵ, is Δ/h where Δ is the compression deflection of a stack as a function of load and h is the initial stack height. That procedure veils details of stress and strain distributions within a stack. However, it provides data for practical coil design. Pressure-strain curves are presented in the report. The raw data (loads and deflections) are on file in the Plasma Fusion Center.

Throughout the conduct of this exploratory program, simplified strength-of-materials estimates

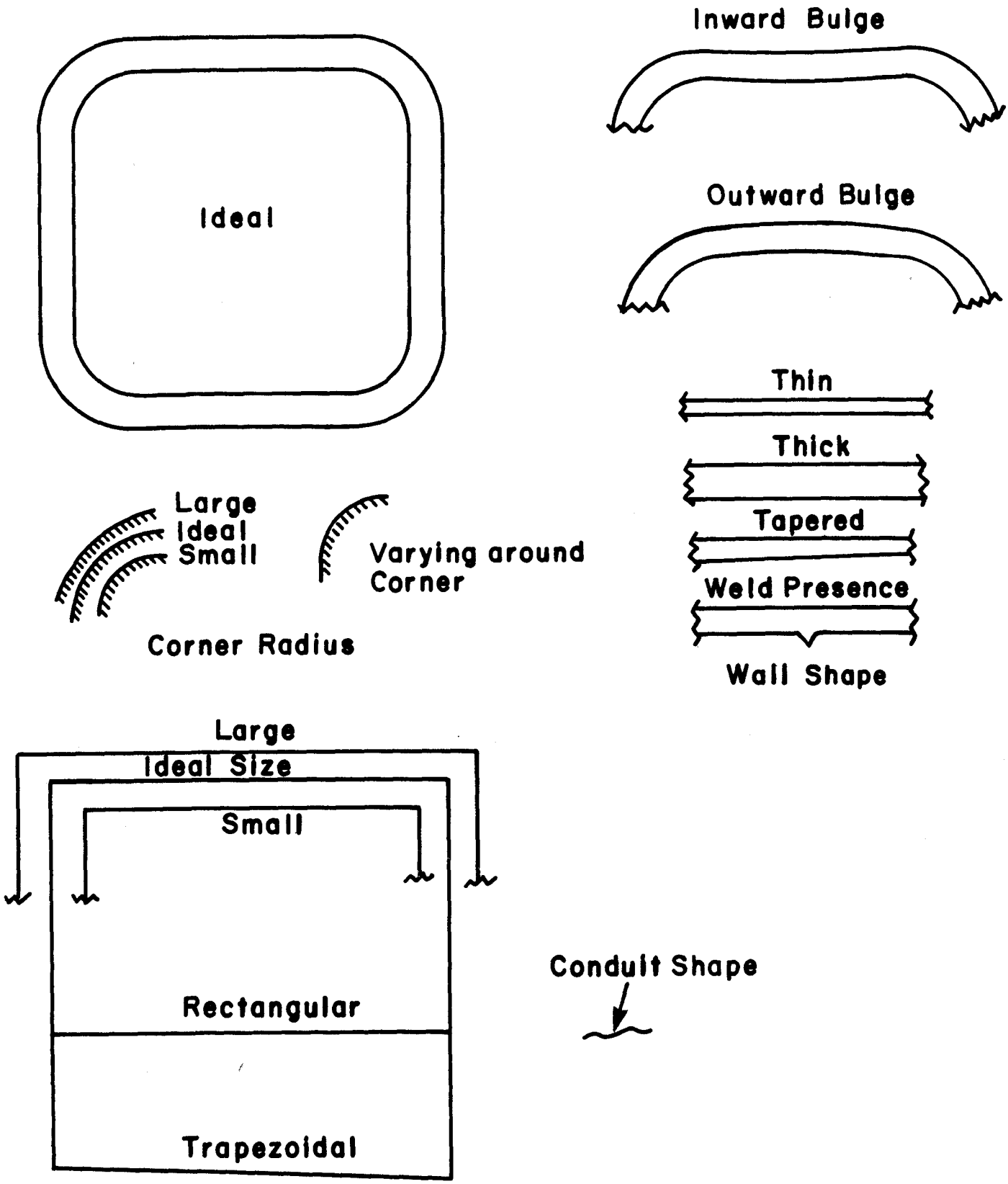

Fig. 6 Deviations in Conduit Shape From Ideal

Table 2. **Summary of Transverse Load Exploratory Tests**

Test Type, Material	Stack No.	Temp (K)		Stack Condition		Filling		Notes
		293	77	L[1]	P[1]	E[2]	F[2]	
Cable in Conduit	1	x		NA	NA	NA	NA	
Unsupported ICCS	2	x		x		x		
One Column	3	x		x		x		
Three High (1×3),	4	x			x	x		
JBK-75	5	x			x	x		
Laterally			x		x		x	Three
Supported	6	x			x		x	runs one
ICCS			x		x		x	stack
Two Columns	7		x		x		x	100 cycles
Three High								at 8 ksi max
(2×3),	8		x	x			x	
JBK-75	9		x		x	x		
	10		x	x		x		
Laterally	11		x		x	x		0.875 in.
Supported	12		x	x		x		diameter
Circular	13		x		x	x		0.41 in.
Tubes, 304 SS	14		x	x		x		diameter

1. L = Loose, P = Potted

2. E = Empty, F = Filled

were made to help assess the probable reliability of the data. In addition, cross-checks were applied (such as a comparison of 1×3 conduit results with 2×3 results). In a few cases, tests were rerun. These procedures also led to the decision to use teflon spray on all supported stack tests, after the first 2×3 conduit run, in an attempt to minimize friction effects that appeared to be present during that run. Comparisons also were made with the SIN data on empty, loose single conduits.

Form of Report

The report is presented in four Parts. Part I contains the experimental results of the transverse load exploratory program and qualitative discussions of conduit behavior under transverse load, including internal pressure response.

Part II covers the theory for ICCS structural response to transverse loads and compares theoretical predictions with experimental results of Part I. Plane strain finite element analyses were performed on transversely loaded empty single conduits, both loose and potted, to help understand the general structural behavior and to reveal the sensitivity to variations in lateral restraint. The variations could arise from deviations in potting and insulation material stiffnesses and thicknesses. An analysis was also performed on a single free conduit under internal pressure. Strength of materials calculations were performed to determine strengths of the conduit arrays, strengths and stiffnesses of the tube arrays, and the contact pressure on the insulation.

Part III will present additional test data from a supplementary test program now underway, which includes effects of axial loading and internal pressure. Part IV will contain the theory for superconductors under combined load, an analysis of the structural nature of a wound coil in a case, and a procedure for design of a structurally reliable coil/case system.

CABLE TRANSVERSE RIGIDITY

Introduction

An ICCS carries current through a magnetic field that probably can be assumed approximately constant across the cable. That induces a nearly linear variation of transverse pressure. Mechanical tests cannot simulate that behavior easily. In fact, when force was applied to one side of a cable the pressure did not appear constant across the cable, as will be shown. Photographs and mechanical data indicate a more complex response, due to the ICCS fabrication details.

A strip of all-copper simulated superconductor cable was loaded transversely at room temperature to determine the behavior in the conduit. Load-deflection data were obtained and photographs of the cable ends were taken to provide the desired information. The measurements were similar to those made by Westinghouse[6].

Test Arrangement

Each end of the specimen assembly was polished metallurgically. That was accomplished by filling the interior of the test specimen with hot wax before polishing. Afterward, the wax was melted out and the cable was cleaned. The polished faces revealed the cable wires which could be photographed easily during the test (Figure 7).

After polishing, one wall was removed from the ICCS conduit and the modified conductor was held in a steel machinist's vise which provided stiff support to the three remaining walls of the conduit (Figure 8).

The steel ram shown in Figure 8 was fabricated with a contour on one edge that matched the shape of the inner surface of the conduit. It was placed upon the exposed face of the cable with 0.005 inches clearance on the vertical sides so that it could slide between the insides of the conduit vertical walls when driven down by the force of the 60,000 pound Baldwin hydraulic universal testing machine in which the cable stiffness test was performed.

A pair of dial gauges, reading to 0.001 inch, straddled the conduit. They measured the vertical motion of the machine crosshead with respect to the base. (The machine rigidity for that arrangement was found to be several orders of magnitude greater than the cable).

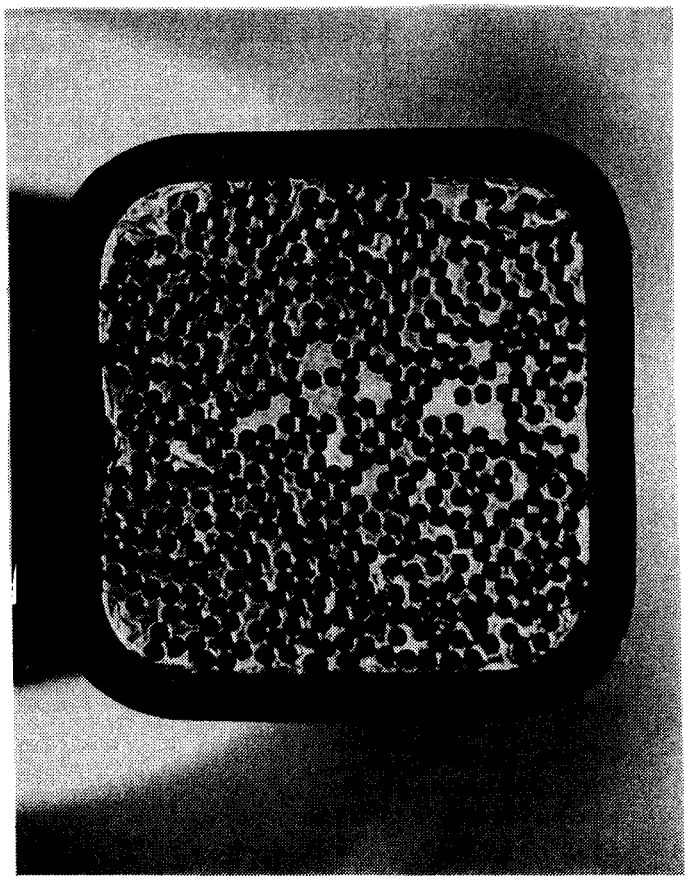

Fig. 7 Photograph Showing Ends of Cable

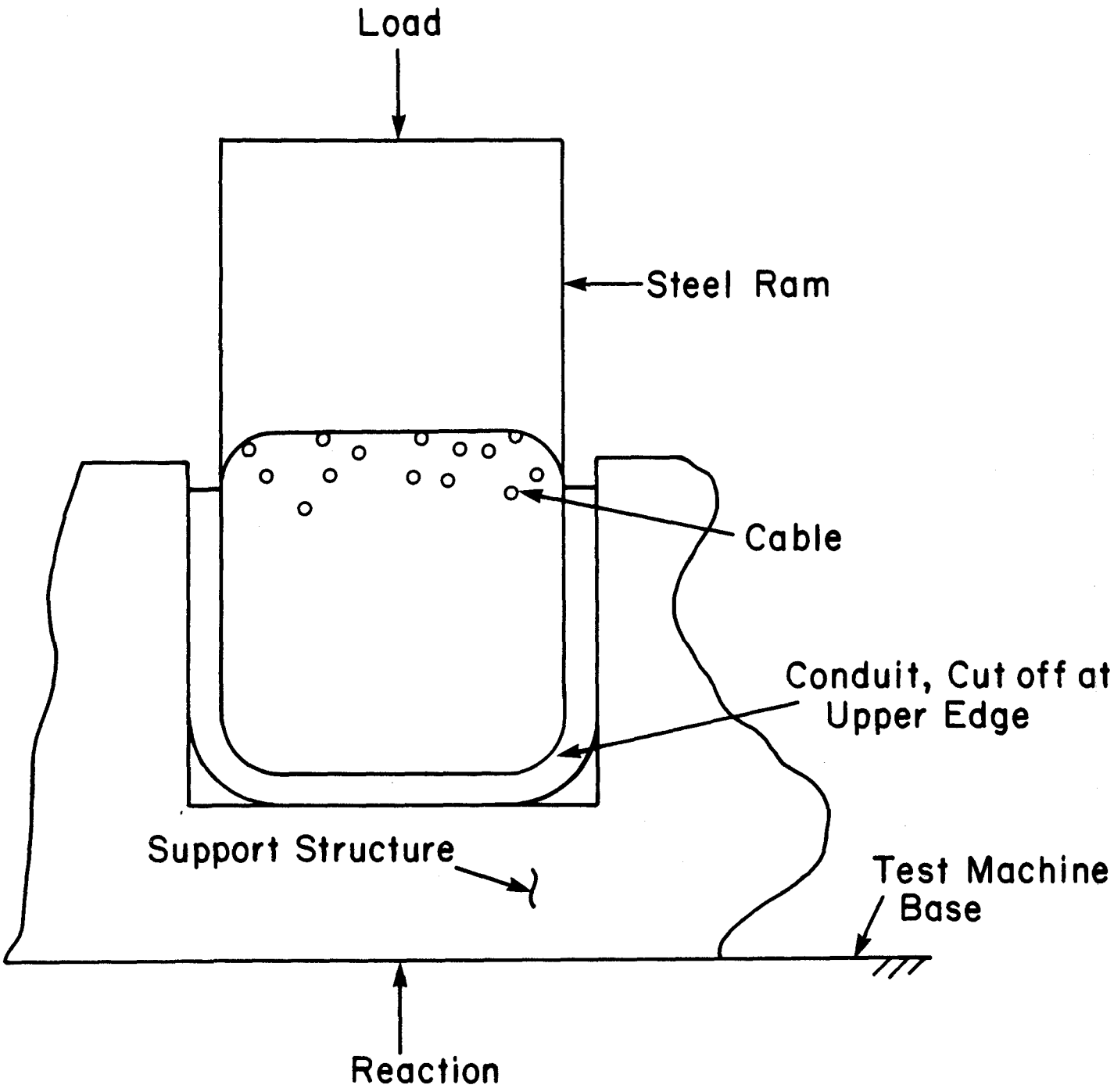

Fig. 8 Cable-in-Conduit Test Arrangement

Test Procedure

Load was applied at arbitrary values determined by observing the specimen distortion at one load level before proceeding to the next. The load was held constant at each level while a photograph was taken of the cable end. The duration of that action was of the order of half a minute. The dial gauges were read and the data were recorded while the photographs were being taken. In this preliminary exploratory test, no intermediate readings of permanent deformation were made. Only the final value was measured.

Data

The pressure-strain plot appears on Figure 9. The data points lie within a moderate scatter band the estimated average of which is reasonably linear. A study of the photographs indicated a behavior pattern which, when used to reassess the load-deflection behavior, indicated the possibility of stick-slip action. It is emphasized by the dotted arcs shown in the figure.

The effective stiffness was determined by drawing straight lines through the highest and lowest points on Figure 9 and then selecting the arithmetic mean between those extremes. As can be seen, the effective Young's modulus, $\Delta\sigma/\Delta\epsilon$, was found to be 0.097 msi.

Discussion of Behavior

The load-deflection plot is only a crude indicator that stick-slip action occurred during the test. The photographs of the cable end provide more direct verification. One method of observing the effect would be through the use of a flicker comparator of photograph pairs taken at different loads. Without a comparator, stereoscopy may be used. It provides an illusion of an axial three-dimensional depth effect that indicates vertical shifting of the wire ends.

Figure 10 contains several stereoscopic pairs. The column on the left repeats the near-zero load photograph while that on the right displays pictures taken at increasingly higher loads. If the left eye focuses on the left photograph of any pair while the right eye reads the right photograph, the depth illusion becomes apparent.

The illusion of depth has no significance. The only value is in enabling the viewer to observe that deformation occurs by random movement of irregular, randomly located zones with an increase in zone number and size with load. The behavior pattern can be likened to load-induced grain distortion and movement in a metal. The stick-slip action arises when each new zone is formed or

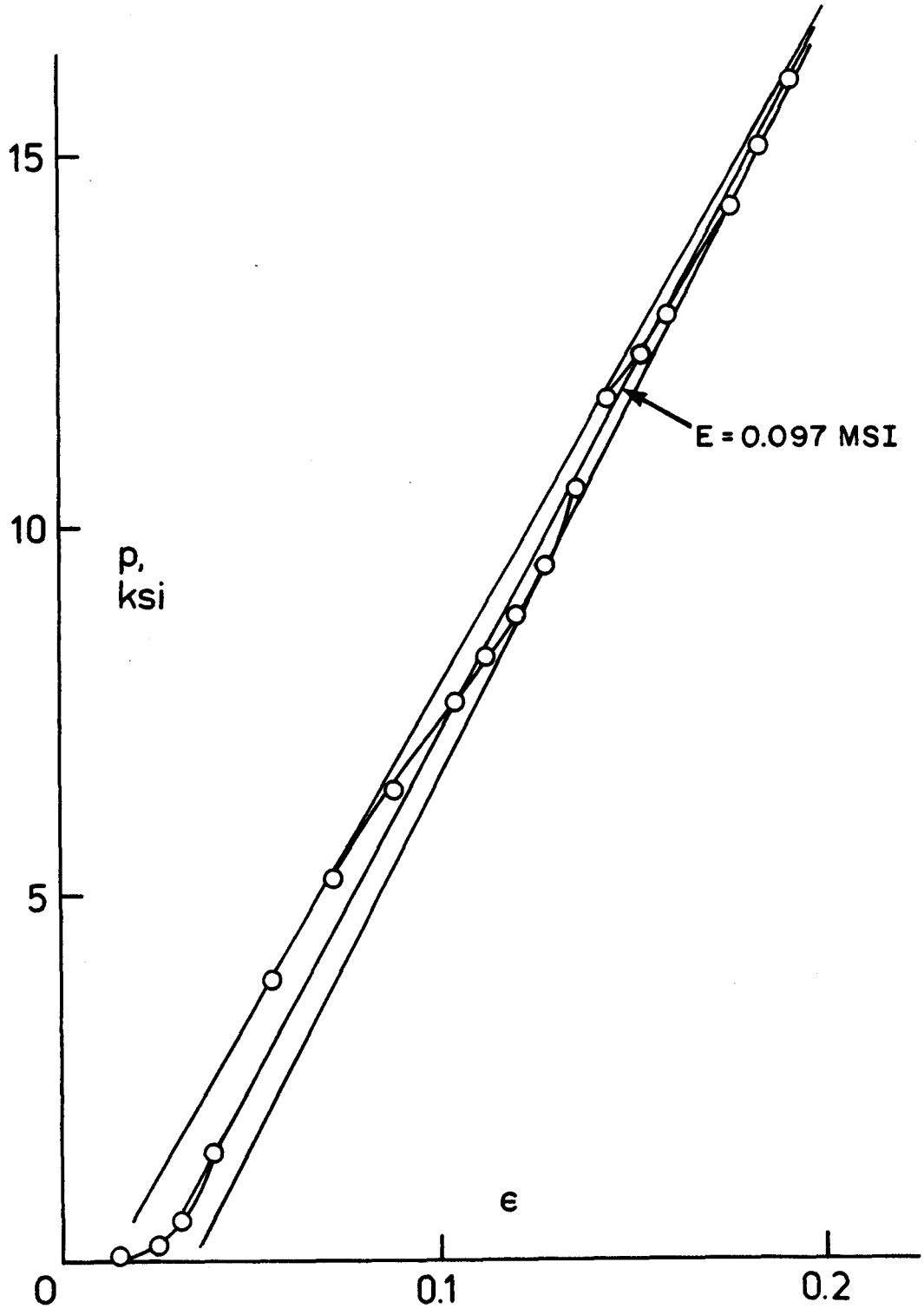

Fig. 9 Cable Transverse Stiffness as Derived From Pressure-Strain Curve

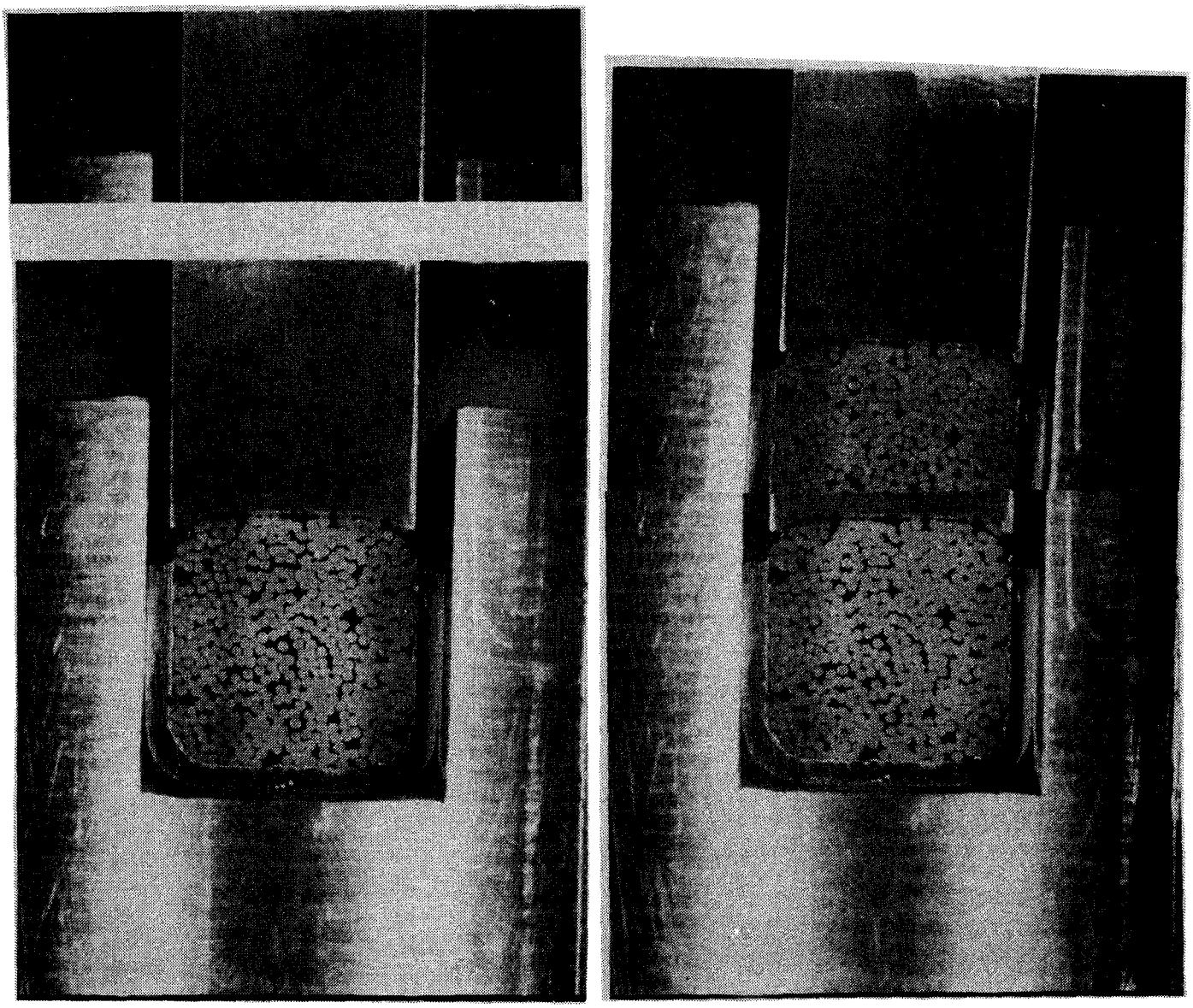

No Load 0 mils 685 lbs. 20 mils

Fig. 10 Stereo Pairs Depicting Wire Movements Within a Compressed Cable

when it suddenly changes shape.

There also could be friction between the conduit wall and the cable stainless steel.

These results cause difficulty in determining how the cable load is distributed to the conduit walls. Furthermore, it is probable that different degrees of compaction will lead to different types of behavior and equivalent transverse stiffnesses.

1×3 CONDUIT STACK TESTS

Introduction

Four room temperature tests were performed on single conduit width, three-high stacks of empty conduits (Table 2, stacks 2 - 5) to learn magnitudes of loads leading to conduit failure and deflections to be expected.

Information was obtained on the character of the deflection data as a function of dial gauge location. The effect of potting was explored. An examination was made of the relation of the MIT data to Westinghouse and SIN results. In Part II, the experimental stress-strain curves are compared with theoretical predictions.

The results from the 1×3 stack experiments were used to design the 2 ×3 stack test program and tube stack experiments.

Results

The pressure-strain data appear on Figure 11 for the four room temperature tests on unsupported single stacks. The curves from the loose-specimen tests are seen to be nearly identical at a stiffness of 0.26 msi and an apparent strength approaching 5,000 psi. The strength is comparable to the value measured by BBC[5]. However, the MIT test shows greater conduit stiffness. The stiffness and strength determined by MIT are comparable to values obtained by Westinghouse[6] (and by PPPL in their in-house studies).

Vertical deflection data for stack 4 were obtained from dial gauges contacting the inner surfaces of the conduit. However, there was a problem with positioning the gauge contacts. It was decided to obtain deflection data from measurements of crosshead motions in future tests.

The strengths and stiffnesses of the potted arrays are seen to be greater than those of the loose arrays. It would appear that failure would occur on the potted arrays at pressures considerably greater than 5,000 psi although they were not restrained laterally.

The equivalent lateral strains in the near-linear range of the fifth array were of the order of half the vertical strains in the loose arrays but approximately double the strains of array 4. This apparent inconsistency was another reason for questioning the data taken on array 3 with interior dial gauges. It was decided to disregard the array 3 data and to design the 2×3 tests on the basis of the results from arrays 2, 4, and 5.

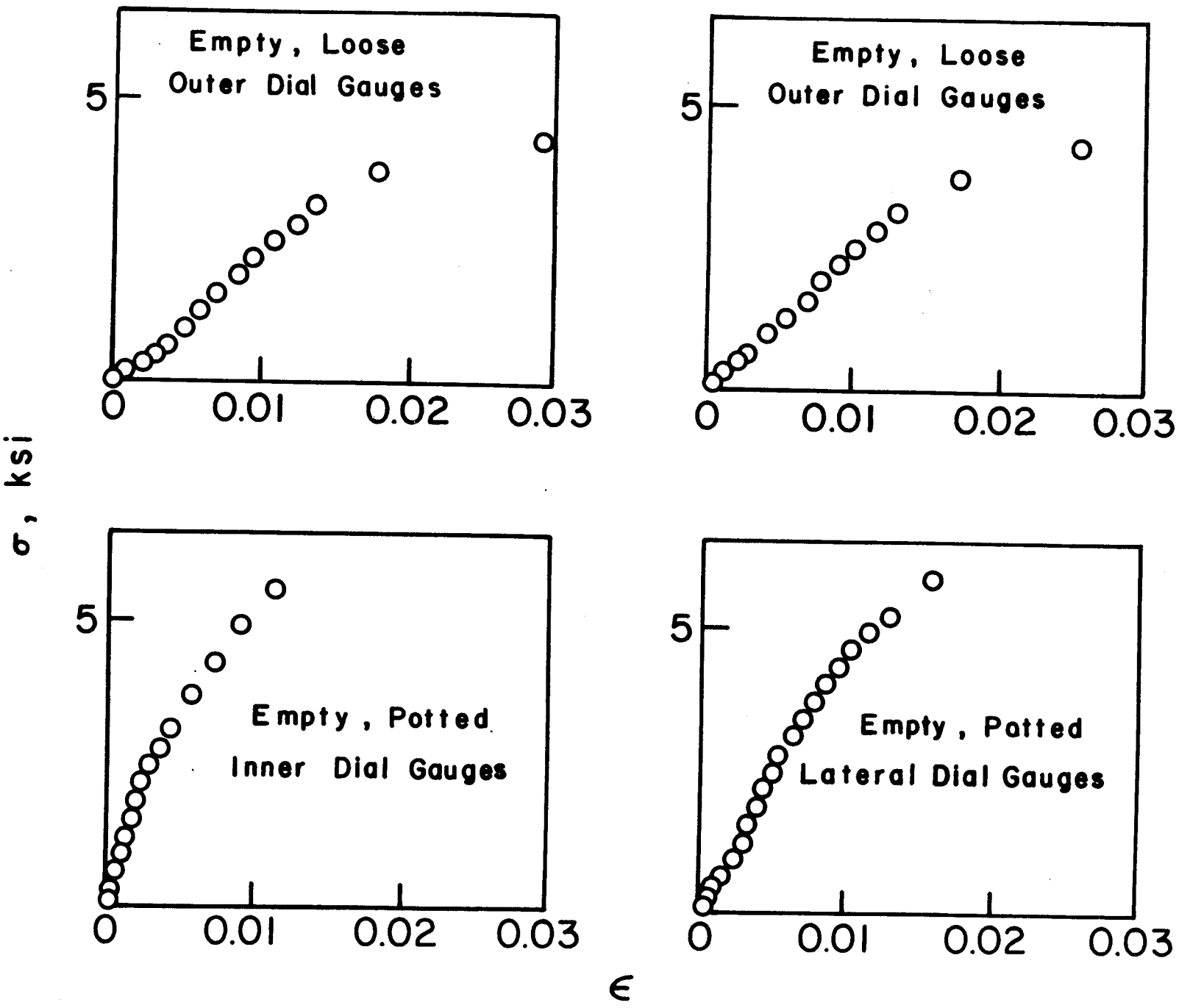

Fig. 11 Pressure-Strain Curves for 1×3 Stacks

2×3 CONDUIT STACK TESTS

Introduction

The 2×3 stack tests represented an initial attempt to assess the structural integrity of the ALCATOR DCT TF coil winding under Lorentz loading, which would induce a peak operation pressure of 7250 psi. The pack stiffnesses and strengths were measured both to learn the nature of the structural behavior and to compare the experimental data with theory.

An actual coil winding will include insulation and potting. The conduits will contain cabled conductor. Lateral restraint will be provided by the toroidal continuity of the wedged coils in the magnet throat region, where the peak pressure occurs. Two test specimens (Table 2, stacks 6 and 7) simulated that combination of conditions. The other three specimens were fabricated to help pinpoint the influences of the cable and potting.

Most test loadings were run to levels high enough to approach failure (but not to reach it) thereby enabling estimates of safety factors based on ultimate compression strength.

Test Arrangements

The configurations of the 2×3 conduit stack test specimens are shown in Figure 12. The specimen dimensions appear in Table 3. The test types and conditions are listed in Table 3. They are also identified on the pertinent pressure-strain graphs below.

Table 3

2×3 Conduit Stack Test Specimens

Loaded Areas and Heights

Stack	Area (in^2)	Height (in)
6, CFP	6.80	3.00
7. CFP	6.85	3.00
8, CFL	6.69	3.00
9, CEP	6.36	2.96
10, CEL	6.70	3.03

The 2×3 tests were performed in liquid nitrogen inside a styrofoam box fabricated to contain the specimens, the lateral restraint frame, and the bottom reaction anvil (Figure 12). Figure 13 shows a cemented array in place within the box before and after positioning of the lateral restraint

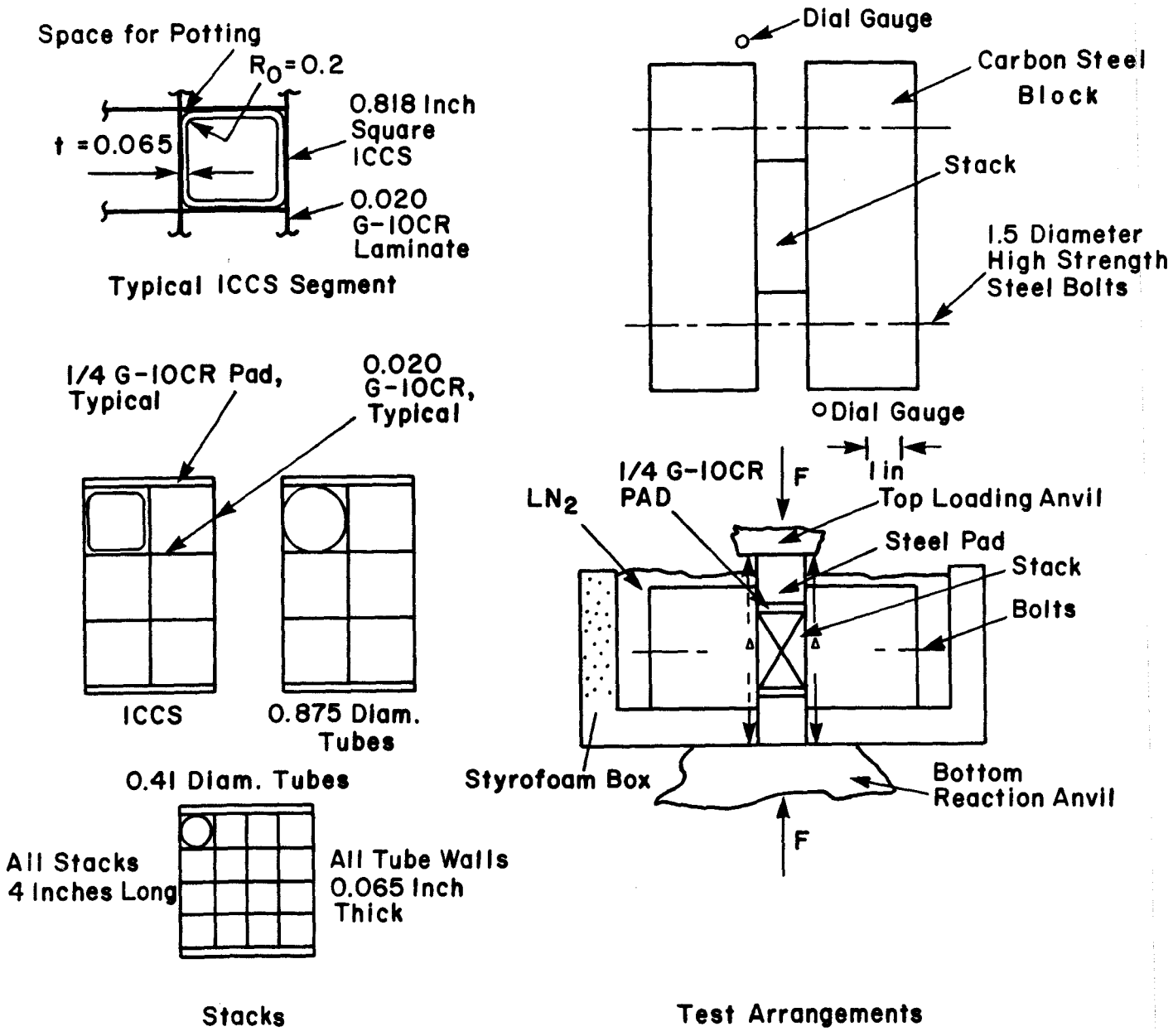

Fig. 12 Multiple Array Stacks and Test Arrangements

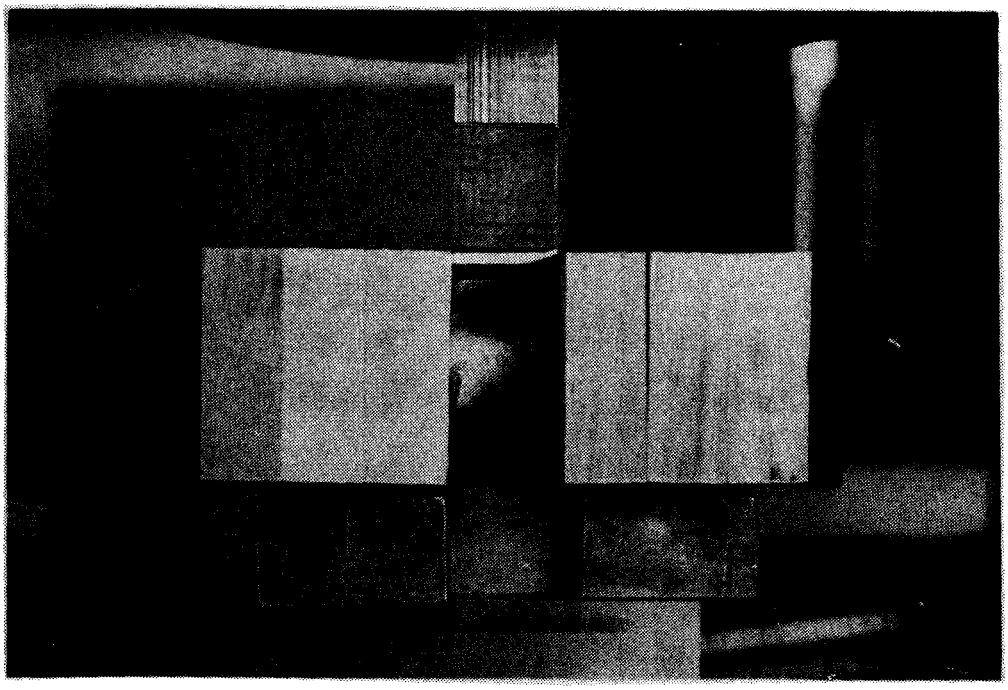

Fig. 13 Typical 2×3 Stack Test Being Assembled In LN_2 Box

frame.

The cemented stacks were prepared and cured before insertion into the restraint frame. The loose stacks had to be assembled in the box inside the restraint frame, which required development of assembly procedures to ensure alignment.

On examination of the data from the first run on stack 6, it was apparent that the stack compression was resisted by friction from the restraint frame. Subsequently, all exposed surfaces of the test stacks, and also of the loading plates and restraint frame, were sprayed with teflon to minimize friction. This was also done on all interior and exterior horizontal and vertical strips of G-10CR insulation in the loose stacks.

The styrofoam box with the steel reaction plate was placed on the lower platen of the press. The specimen and restraint frame were positioned in the box and the bolts were pulled up "finger tight." The diagonally opposite dial gauges (direct reading to 0.001 inch) were installed to indicate motion between the lower face of the machine rim and the top of the platen (Figure 12).

Loading was accomplished in the 300,000 pound hydraulic press at Manlabs. A calibration of the force gauge on the press revealed an error of less than one percent. The gauge is marked in 2,000 pound increments. It was read at 1,000 or 2,000 pound increments to within 200 pounds. That deviation corresponds to approximately 30 psi pressure on the specimen.

Test Procedure

The cavity of the styrofoam box was filled with liquid nitrogen (at ambient atmospheric pressure) to a level several inches above the top of the specimen. The loading began when the fluid stopped bubbling. Addition of fluid was not required more than once during a run. It was done without interrupting the loading process. The liquid nitrogen level was maintained a minimum of an inch above the top of the test specimen.

Loading was applied in the increments mentioned above, the magnitudes of which were selected after examination of the load-deflection data obtained during the early stages of a run. After application of a load increment, the load was held constant while the dial gauges were read and the data were recorded. That involved about one-half minute and application of the load increment required approximately another 15 seconds.

In addition to the stack tests, a calibration test was performed on the machine load path

stiffness using a solid block of 304 steel in place of a stack. No side restraints were used because of the large rigidity of the block compared to typical stack stiffnesses.

Data Reduction

The machine calibration curve deflection was subtracted from the specimen deflection at each load level. Loads were converted to stresses, $\sigma = P/A$, using the specimen projected area (Table 3). Deflections were converted to strains, $\epsilon = \Delta/h$, using the specimen height.

Results

The apparently large stiffness observed during the first CFP runs (Figure 14), was thought to be due in part to friction between the stack sides and the restraint frame faces. Consequently, the restraint frame faces were teflon-sprayed to minimize that effect, as was mentioned previously.

The stiffness was seen to be high during the second run as well. When the arrangement was disassembled, there was some evidence of specimen scratching. This indicated hangup which might have been due in part to assembly error and in part to insufficient teflon coating. These difficulties were apparently removed by teflon-coating the stack faces as well as the restraint frame, and by taking extreme care in aligning the stack within the frame. Subsequent test results on all stacks yielded stiffness data more in line with scoping calculations.

The third run on stack 6 yielded results that seemed more in line with order of magnitude calculations. They included the initial nonlinearity, attainment of a peak tangent modulus of 0.49 msi at a pressure of 12,000 psi (indicating initiation of inelasticity), and gradually increasing inelastic behavior at higher pressures. The test was stopped arbitrarily at 22,200 psi. At that pressure level there still appeared to be additional load-carrying capacity in the CFP stack, which was intended to simulate the prototype ALCATOR DCT coil.

In theory, the cable would have been loaded to 7100 psi at the 0.074 strain level, corresponding to the peak pressure of 22,200 psi. If the cable load (pw = 7000×0.69) is subtracted from the load on a conduit in the stack (pw = 22,200×0.82) the net load on the conduit wall would have been 13,400 lb/in. That translates into a stress, $\sigma = 13{,}400/(2\times0.065) = 103{,}000$ psi which is below the reported yield strength of JBK-75 at 77 K (nominally 130,000 psi). It also indicates that the cable could have been reacting one-fifth of the applied load.

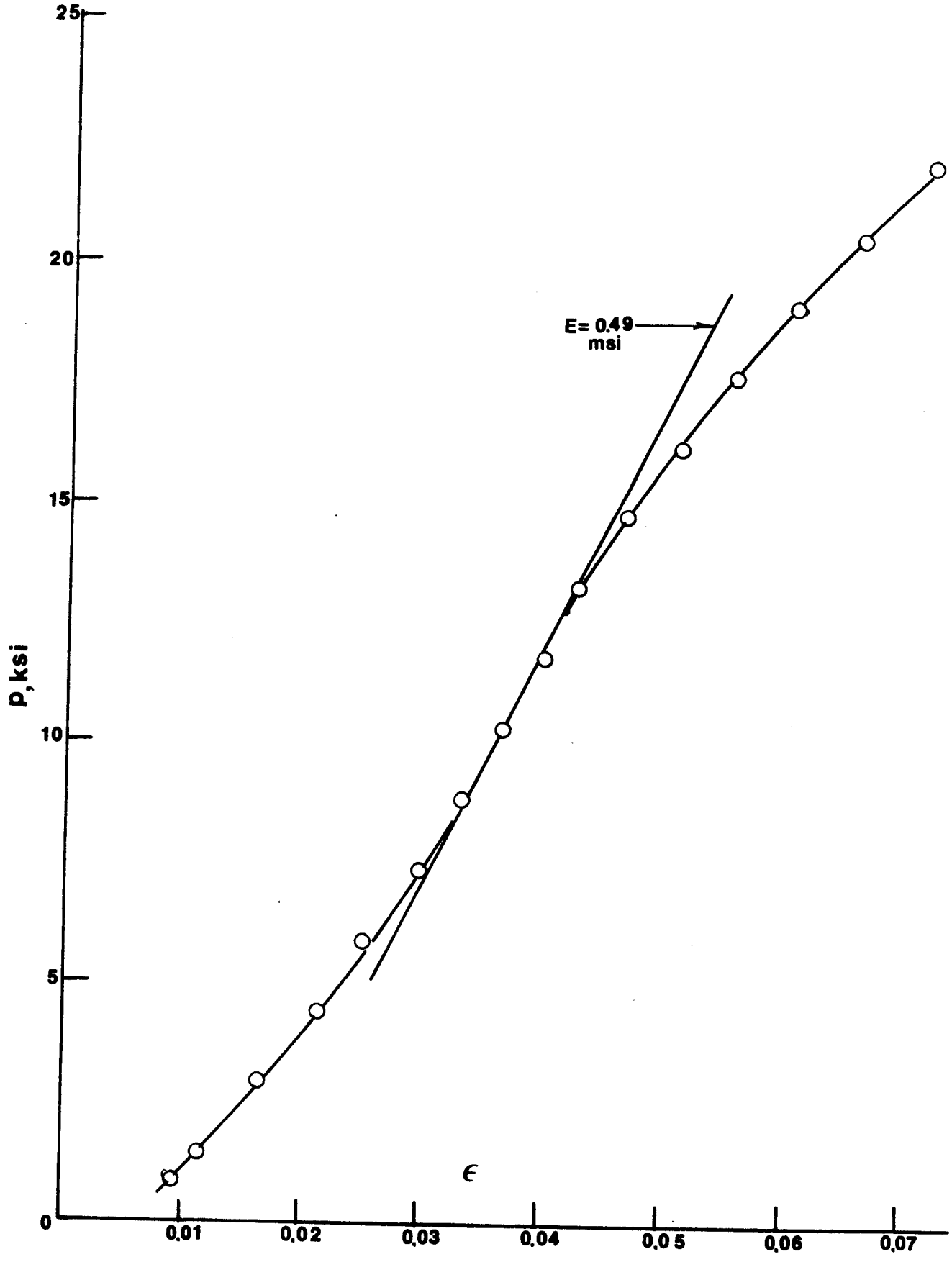

Fig. 14 Pressure-Strain Data from CFP Stacks

Loud noises were heard throughout the runs, such as snapping and cracking that might be associated with fracturing of cement bonds and cracking of insulation. When the third run was completed, the six conduit lengths were seen to be loose in the stack and the insulation was cracked at numerous locations. Almost all insulator strips were cracked along the lines at the conduit corner tangents (Figure 15). That effect presumably was caused by the high contact pressures along those lines, as discussed in Part II.

A comparison of the stack tests with the SIN single conduit tests is shown in Figure 16. The stiffness is seen to be one-fifth that of the thickened-corner SIN conduit, but much greater than for either of the two rounded-corner SIN conduits.

Stack 7 (CFP) was loaded 100 times from zero to a maximum pressure of 8000 psi. Some cement cracks were observed afterward. The cumulative permanent compression strain was 0.004, indicating the possibility of creep since the pressure presumably was below the level at which plastic straining might have been expected if the curve of Figure 14 is used for comparison. The loading was conducted manually. Since the total test time was of the order of two hours, it appears that creep is an effect to be considered in designing a fully wound coil and, consequently, accurate creep data are required.

The CFL (stack 8) behavior mimicked that of the CFP stack up to approximately 12,000 psi, with the CFP displaying slightly greater stiffness (Figure 17). Above that pressure the disparity between the two increased. At approximately 20,000 psi the CFL stack stiffness appeared to increase. Disassembly revealed scratches in the teflon coating indicating hangup between the stack and support frame. Consequently, the stiffness of the CFL stack actually may have been less than observed. A new specimen and a retest would be required to resolve that issue. However, it was decided not to proceed with it during this exploratory program.

After the CFL run, small cracks were observed in the welds of the restraint-frame plates (which had been fabricated from welded sets of one-inch-thick plates since the desired three inch thick stock had not been readily available when the frames were fabricated). Four-inch-square bar stock was located and machined to 3.575-inch-square cross section restraint plates, which were stiffer than the original plates.

Two runs were conducted on the CEP stack (number 9) using the new plates (Figure 18).

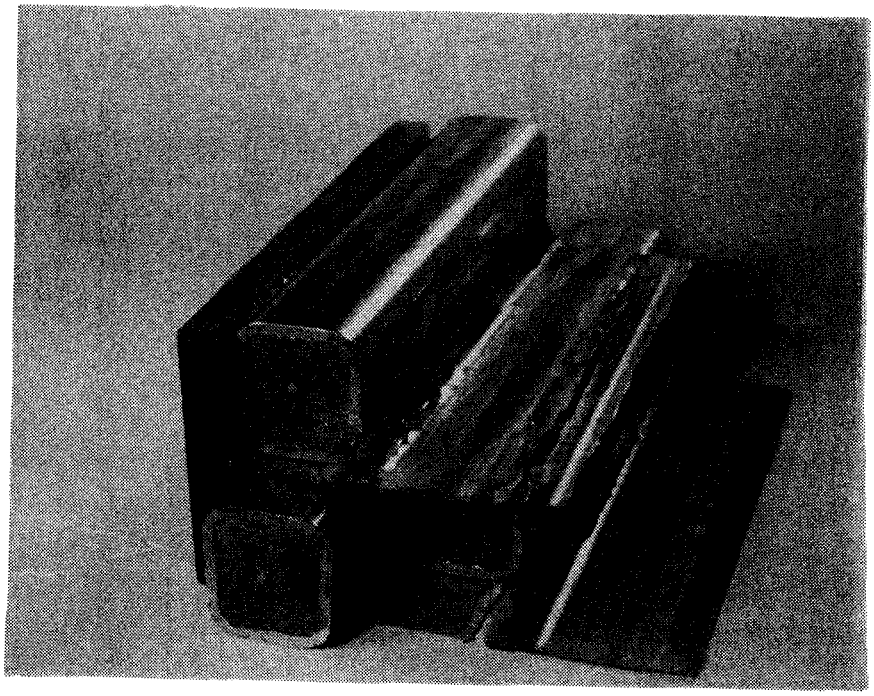

Fig. 15 Corner Cracks in Insulation of Stack 6

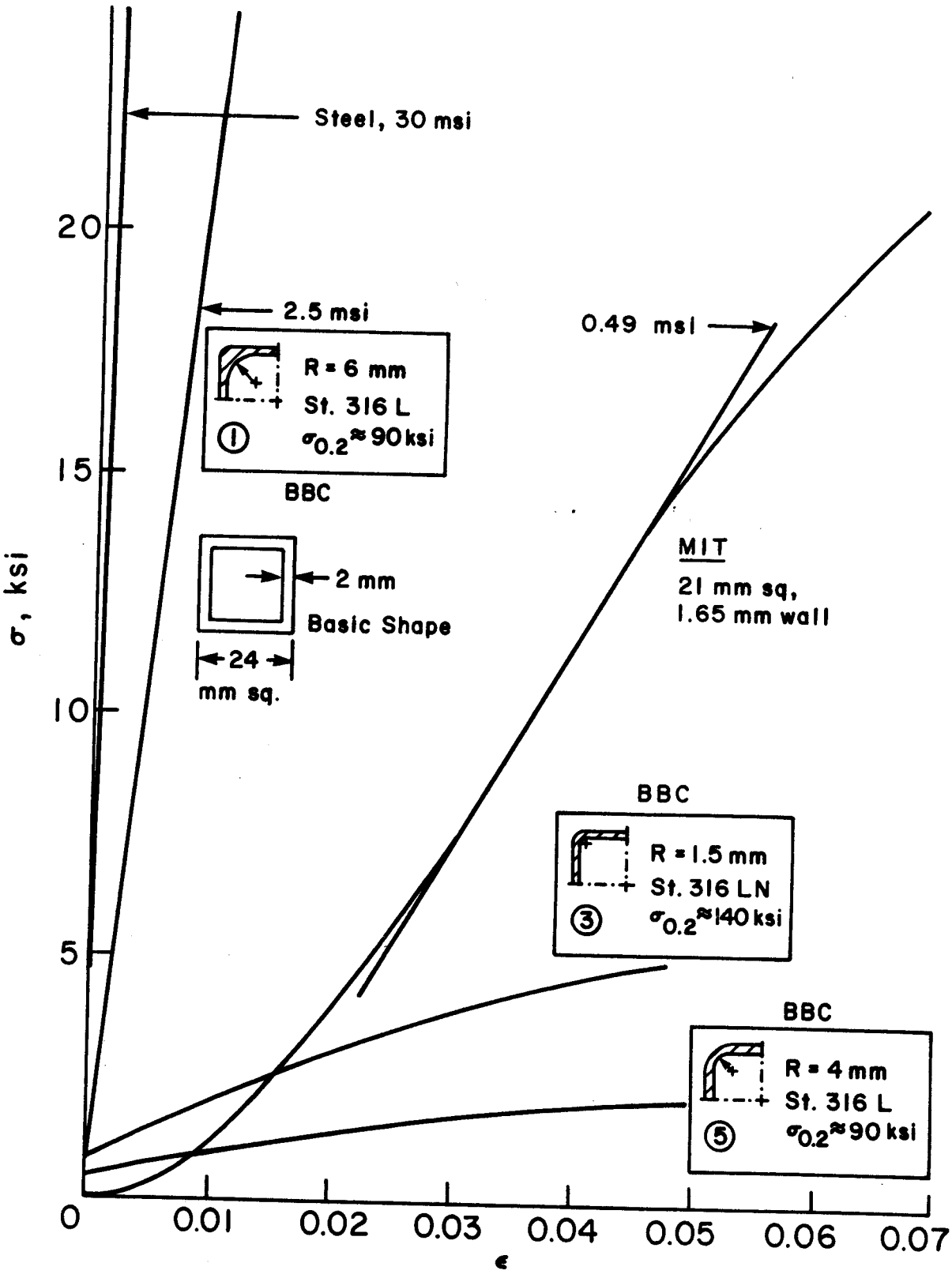

Fig. 16 Comparison of CFP Stack Behavior with SIN Behavior

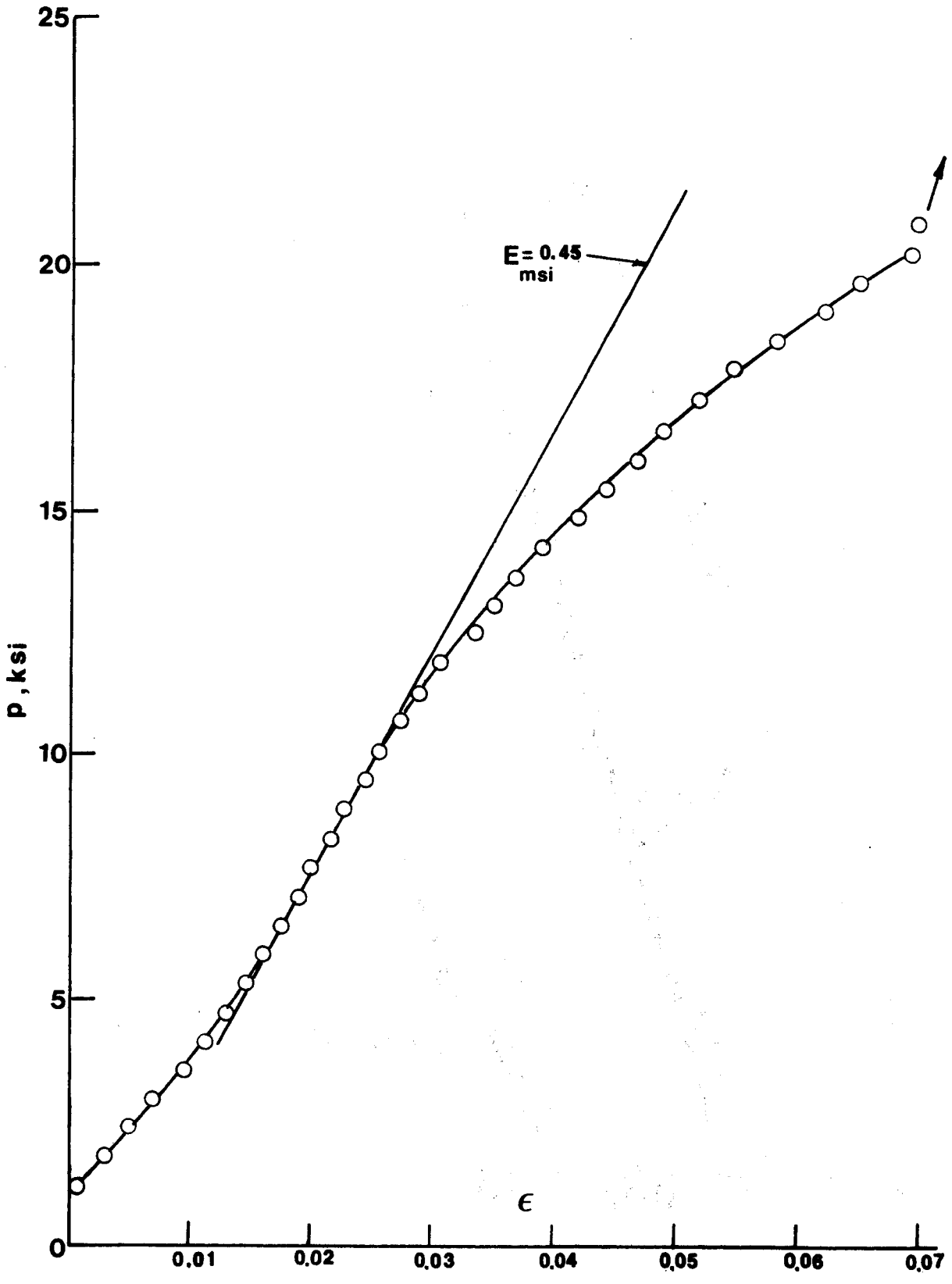

Fig. 17 Pressure-Strain Data from CFL Stack

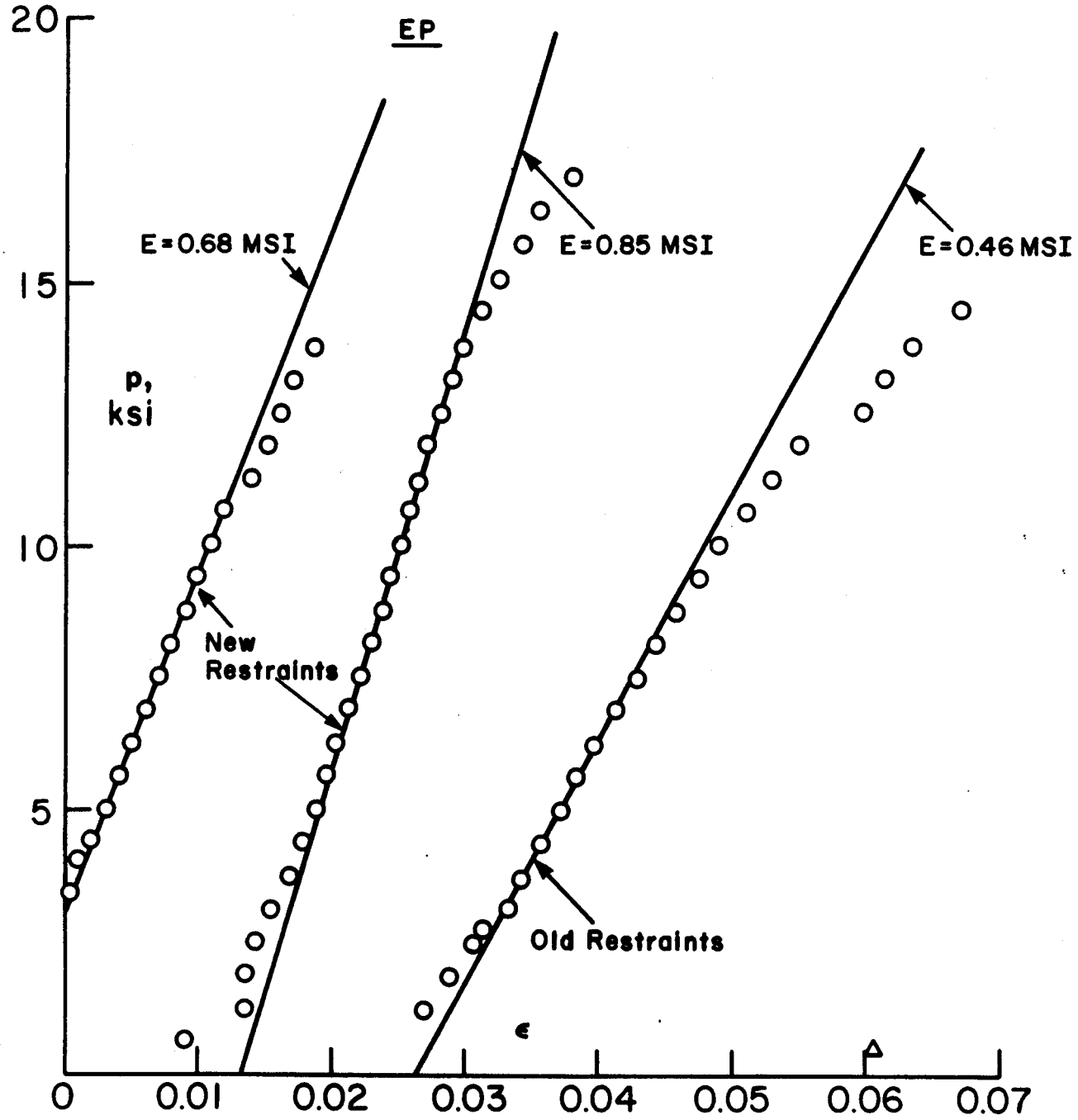

Fig. 18 Pressure-Strain Data from CEP Stack

They yielded stiffnesses of 0.69 msi and 0.85 msi which were greater than observed previously. It was decided to return to the original frame structure, which was used in the remaining tests since the welds were not broken. The next run on CEP indicated a stiffness of 0.46 msi which is comparable with previous data. Also, the onset of inelastic behavior began at approximately 7500 psi pressure compared with a value of 10,000 psi when the stack had been supported by the stiffer plates. That result indicated the potential gain in coil stiffness if the lateral restraint were to be infinitely large, which it would be in a wedged-coil magnet since the interfaces between adjacent coils would not move laterally.

It also indicated the need to know reliably the stiffness of the support frame and to be able to control it to a selected value for each test.

The CEL test (stack 10, Figure 19) yielded a peak tangent modulus of 0.29 msi and inelasticity onset at 5000 psi pressure, which demonstrated that it was the weakest and least rigid of all the conduit stack specimens. At the maximum strain level of 0.046 the cable might have been under 4500 psi pressure, which implies that it could have been supporting 30 percent of the applied load.

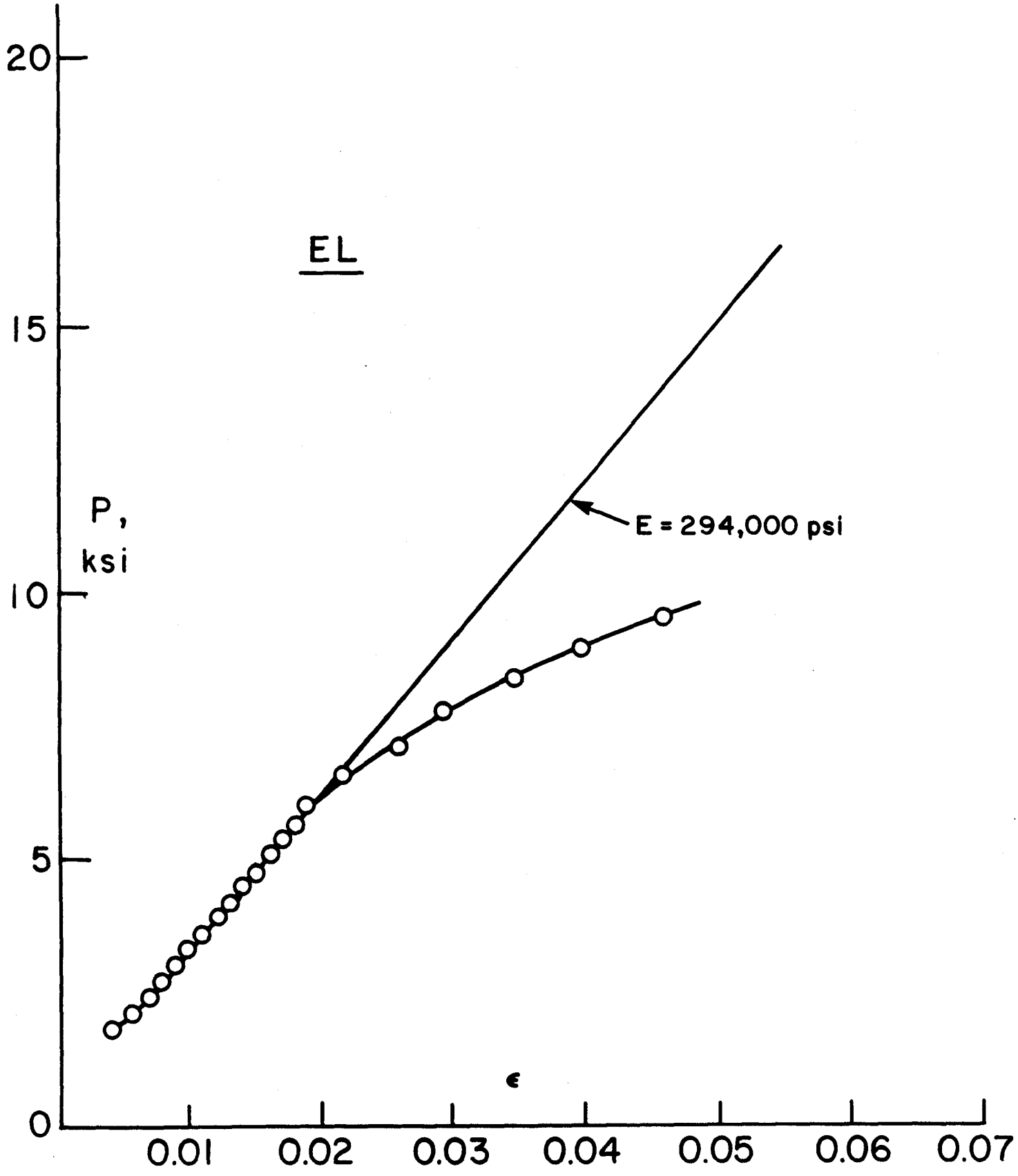

Fig. 19 Pressure-Strain Data from CEL Stack

TUBE STACK TESTS

Introduction

The four tube stack tests (Table 2, runs 11 - 14) were performed primarily to accentuate the importance of potting to stiffness and strength of the conduit corners. The two tests on unpotted tube arrays also permit a comparison with strength of materials analyses of linear elastic stiffness and the initiation of inelasticity (Part II).

Test Arrangements

The tube tests were performed on four inch lengths of 304 steel tubes. All wall thicknesses were 0.065 inch. The outer diameters were 0.875 inch (to approximate the conduit size) and 0.410 inch (to help understand the conduit corner behavior). The potted arrays were cemented into units before placement in the test arrangement. All exterior surfaces were teflon-sprayed.

The loose tubes and insulator strips were assembled into stacks between the inner teflon-coated faces of the support frame whereas the potted arrays only had to be positioned in the frame. Figure 12 depicts the general arrangements for the two types of stacks. The numbers of rows and columns for the 0.410 tubes were chosen to provide stacks with cross-sectional dimensions approaching those of the 2×3 conduit arrays and the 0.875 tube arrays in order to avoid extensive reworking of the restraint frame and the G-10 loading pads.

The same loading and deflection-reading procedures were used as for the 2×3 stack tests.

Results

The stiffness of the 0.875 potted array (0.53 msi, Figure 20a) was approximately three times the stiffness of the loose array (0.19 msi, Figure 20b). The strength ratio apparently was greater than three. The onset of plasticity in the potted array (0.825 EP) appeared to occur at more than 7500 psi, which was an order of magnitude greater than the run 1 value of the unpotted array. The maximum potted 0.875 tube stiffness of 0.53 msi agrees reasonably well with the potted conduit value of 0.46 msi. The plasticity at 17,500 psi indicated the strength of the tube configuration was lower than that of the filled and potted conduit, but was comparable with the value for the empty, potted conduit.

The two 0.875 EL curves (Figure 20b) indicate considerable cold work during run 1. The initial slope of the second run was used to determine the nominal elastic stiffness (0.19 msi). Most of the

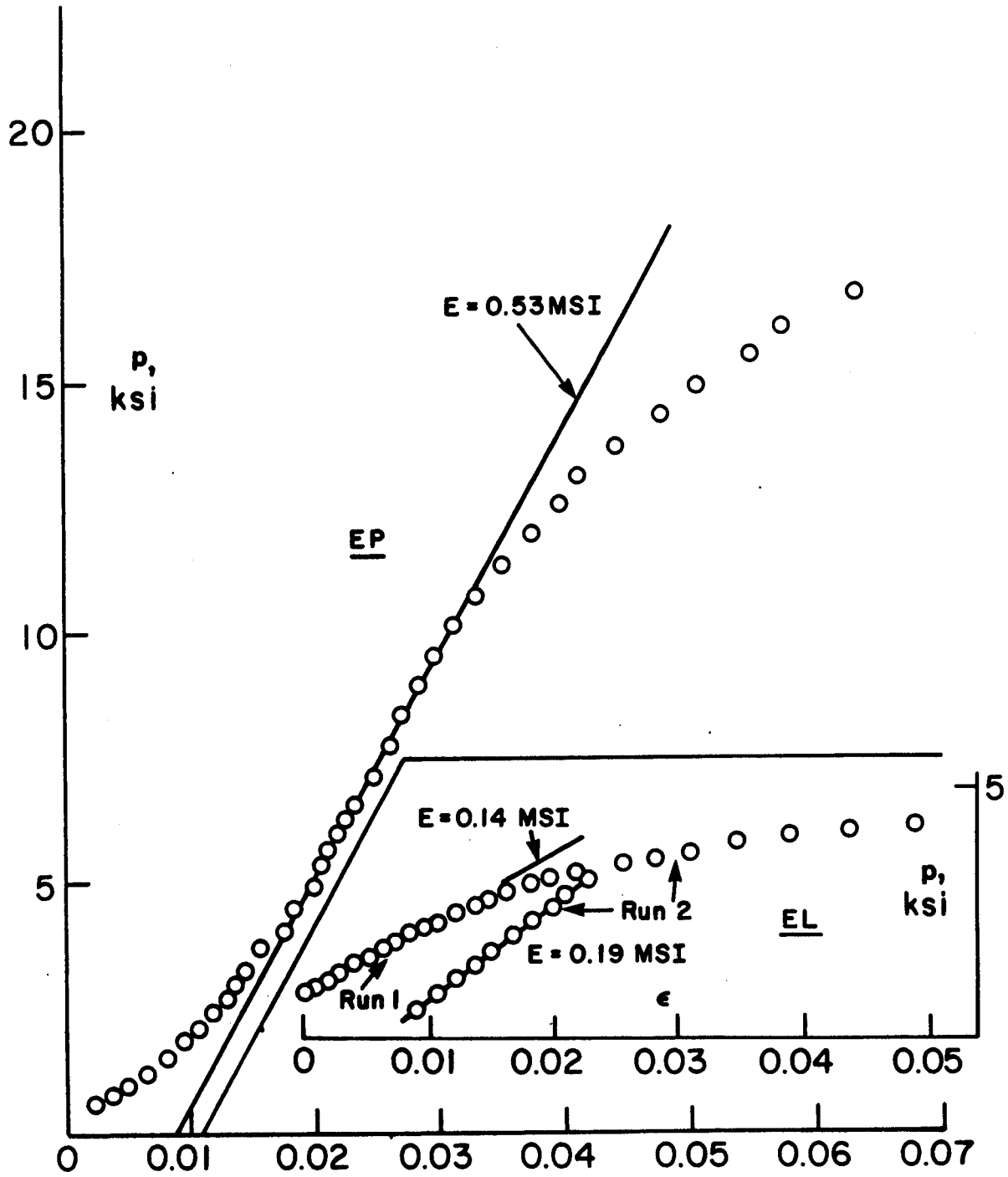

Fig. 20 Pressure-Strain Data from 0.875 Inch Tubes

stack behavior was in the inelastic range. It would appear from extrapolation of the run 2 curve that the supportable pressure of the unpotted array would have approached 5000 psi.

The pressure-strain data for the potted 0.41 inch diameter tubes (Figure 21) reveal a stiffness ratio of 1.6 msi which is nearly three times the value of 0.54 msi for the loose array. However, there are twice as many "vertical walls" in the 0.41 tube stack as in the conduit and 0.875 tube stacks. Consequently, the comparable pressures would have been 22,500 psi maximum and 12,500 psi at initiation of inelasticity. Those values are of the same order as the results for the potted conduit stacks. The curve for the loose array appears to be in an early stage of leveling off at about 15,000 psi. It might be conjectured that the strength would have been of the order of 20,000 psi to 25,000 psi. The potted array strength would have exceeded 45,000 psi, while the initiation of inelasticity occurred at 25,000 psi. If the pressure were to be presumed uniform around each potted tube, the nominal wall stress would have been 142,000 psi which is slightly above the reported yield strength of JBK-75 at 77 K. It also exceeds the CFP stress of 103,000 psi at 22,200 psi pressure if the cable load were accounted for as discussed previously.

The tube curves exhibited little initial nonlinearity in contrast with most of the conduit data.

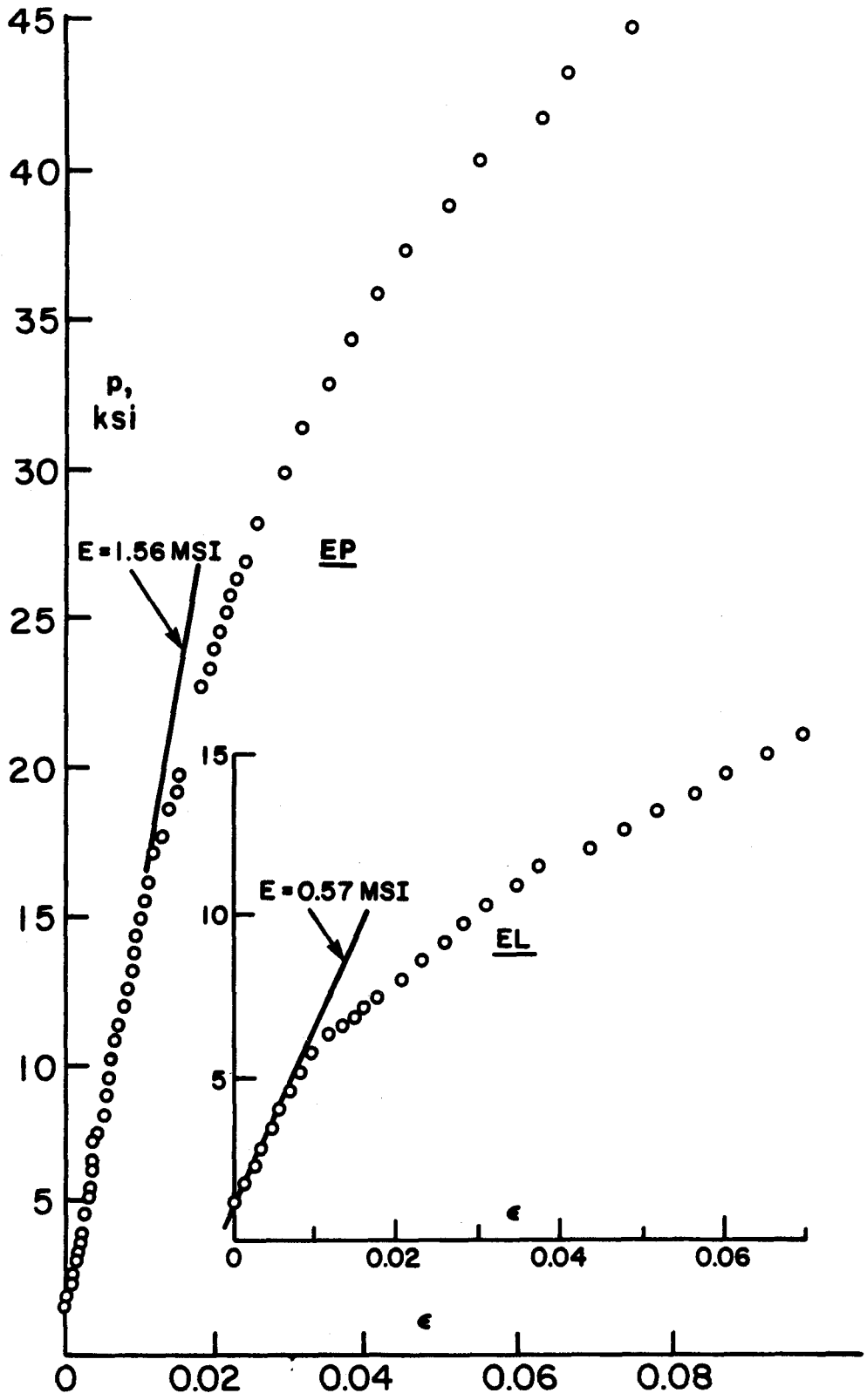

Fig. 21 Pressure-Strain Data from 0.410 Inch Tubes

INTERNAL PRESSURE RESPONSE

High pressure can be produced inside an ICCS conduit during a quench. There has been concern about that effect since a conduit probably would be a square section tube. The prevailing intuitive viewpoint is that the tube would tend toward circularity with consequent large bending stresses and transverse deflections of the walls. However, it has been known for at least half a century that square (and even rectangular) headers in steam generators survive under 150 to 200 atmospheres of internal pressure. In fact, results from the so-called "proportional limit test" that has been used to qualify headers[9], correlated reasonably well with the simple relation $\sigma = pw/2t$, where w is the width of the rectangular section and σ is the proportional limit stress of the wall material. (The effective thickness, t, accounts for holes in the wall).

Tests were performed on Westinghouse conduits by Westinghouse and by ORNL[10–13]. They indicated achievable cryogenic strengths of the order of 1,000 atmospheres. However, load-deflection data were not obtained. Consequently, neither elastic nonlinearity nor the onset of inelasticity could be determined.

A pressure-deflection test was run at room temperature on a length of MIT conduit made from JBK-75. The test arrangement schematic and data appear in Figure 22.

Data from the two dial gauges do not agree well, possibly because the walls of the test specimen (nominally six inches long with capped ends) had unequal initial deflections.

The curves appear to be nonlinear from the start. The two residual deflections (set points) support that inference somewhat since they are smaller than the deflections at the peak of 6,000 psi pressure. The small set values indicate that much higher conduit strengths would be achievable at cryogenic temperature because of the greater material yield strength. However, the deflections could be important because of the greater elastic nonlinearity.

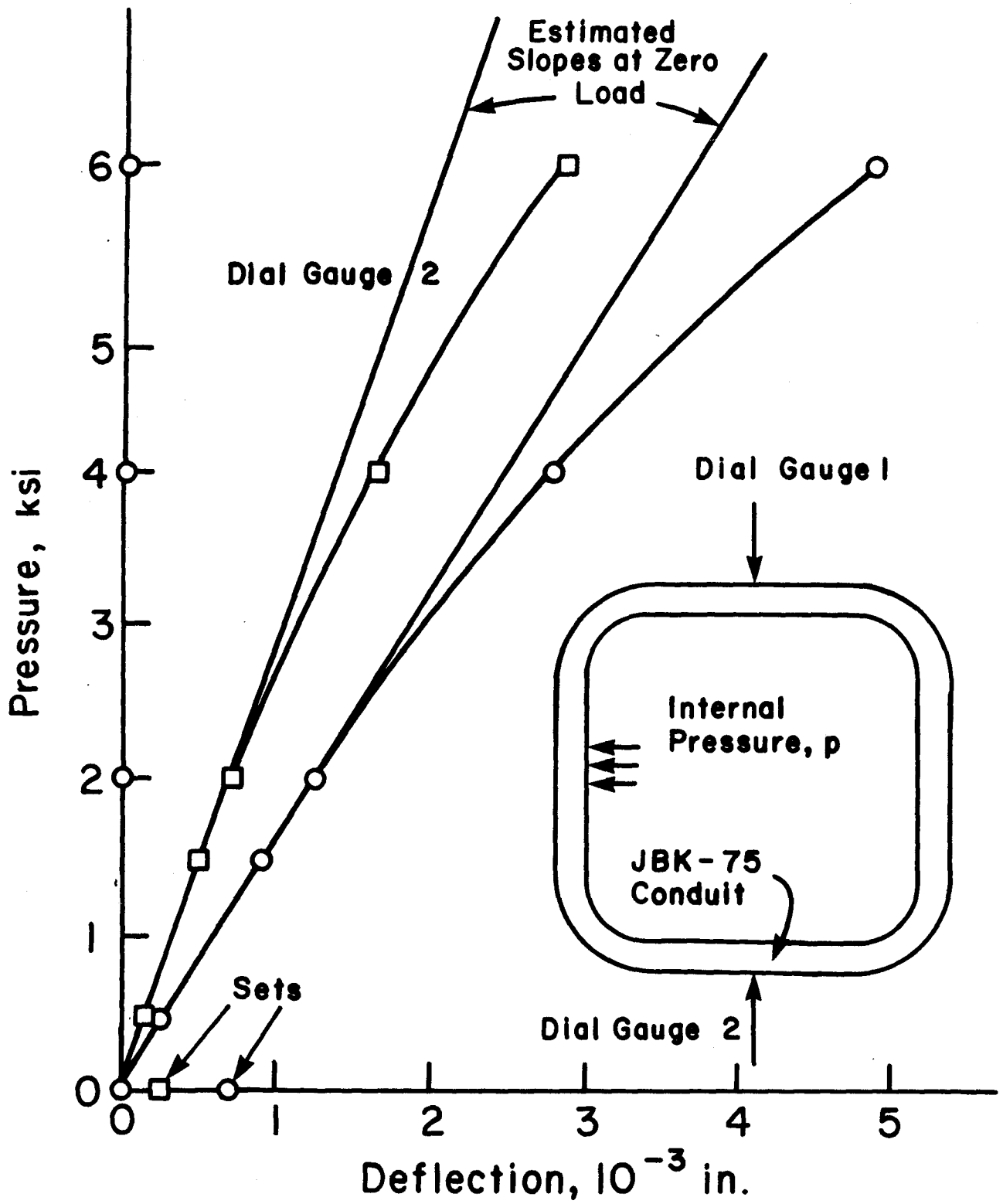

Fig. 22 Conduit Pressure-Deflection Curves

CONCLUSIONS

The exploratory test data indicate the following:

1. A fully wound and potted ICCS coil should be capable of surviving static Lorentz loading greater than 22,000 psi.
2. The presence of corner filler (or potting) undoubtedly is an important factor in achieving that strength.
3. The cable at 32% void fraction appears to support 20% of the pressure applied to the potted and filled conduit.
4. Nonlinear elastic behavior at small loads and (presumably) inelastic behavior at large loads yielded stress-strain curves without a recognizable straight line region. The steepest slope was approximately 0.5 msi. It occurred at 12,500 psi pressure on the stack of filled and potted conduits. A value of 7500 psi was found for the filled and unpotted conduits.
5. The presence of insulation fractures at the corner straight-to-arc transitions indicates high contact pressures at those locations.

RECOMMENDATIONS

The results of the exploratory test program in transverse loading of an ICCS identify the types of data necessary to develop an understanding of the ICCS magnet coil structural behavior. An outline follows of tests recommended to acquire those data. All tests are to be performed at 77 K (possibly supplemented by 300 K tests).

I - TRANSVERSE LOADING

Conduit Elements

1. Yield strength, as formed.
2. Corner fatigue strength (S-N curve).
3. Creep.

Cable Behavior

1. Transverse load-deflection curve as a function of compaction.
2. Permanent deformation as a function of maximum transverse pressure.
3. Creep and stick-slip actions.
4. Internal load distribution of cable under transverse load in conduit.

Conductor Stacks

1. 2×3 stack static load-deflection tests and strength with parameters as follows:
   a. Three controlled lateral restraint stiffnesses (using belleville washers in frame bolts, for example) measuring lateral forces during runs.
   b. Three stiffnesses of potting material (controlled by fillers such as chopped fibers).
   c. Three void fractions with Nb_3Sn cable.
   d. Perform a,b,c for each conduit material after application of activation heat treatment.
   e. Conduct tests on selected combinations of above parameters to determine effect of friction between stack and side restraints.
2. 2×3 stack strength tests on a few efficient combinations from item 1.
3. 2×3 stack fatigue tests on the same combinations selected for item 2.

II - LONGITUDINAL LOADING

Conduit Elements in Tension

1. Measure residual stresses in foot-long piece of conductor by applying strain gauges to activated

length of conduit and then cutting gauged section free.

2. For finished conductor, measure elastic axial stiffness (effective Young's modulus) in tension, using strain gauges if possible.
3. Remove cable from conduit of conductor used in test 2 and determine stress-strain curve into plastic range for conduit alone.
4. Measure cable load-deflection curve, and deduce axial stiffness by cutting away conduit from another length of finished conductor. Continue loading into plastic range.

Conduit Elements in Compression

Repeat above tests under longitudinal compression where possible and compare behavior with tension data.

III - INTERNAL PRESSURE

1. Determine static pressure-deflection curve for empty conduit up to maximum value achievable with laboratory equipment.
2. Apply several cycles of high pressure.

IV - COMBINED LOADS - SCIENTIFIC PROGRAM

1. Fabricate 4×4 array, 40 inches long (for possible cooperative program with Swiss) to be loaded statically under combined axial tension and transverse compression with lateral restraint.
2. Consider including internal pressure.
3. Attempt to acquire fatigue life data.

V - PROTOTYPE TEST

1. Generate a test arrangement to evaluate survivability of a representative prototype coil.

PART II

THEORY

AND COMPARISON WITH EXPLORATORY TEST DATA OF PART I

PRELUDE

Coil in a Case

The following discussion of the general ICCS structural behavior is presented to indicate the types of effects that the theoretical treatments attempted to portray.

The radial peak loading probably would occur on the inner leg of a TF coil. A representative configuration is shown in Figure 23. The radial Lorentz loading, $i \times B$, is maximum on the outer layer and decreases to zero at the innermost layer where the integrated loading is greatest. However, the loading on the conduit walls is not smooth. Neither is the load path within a conductor from the cable to the conduit (Figure 24).

The load within a conductor eventually reaches the inner face where it is transmitted to the next radially-inward conductor. The nature of that load transfer was studied in the theoretical studies.

The integrated Lorentz loading tends to occur in steps, as shown in Figure 25. That behavior cannot be duplicated easily in a mechanically loaded stack. However, the critical layer is the innermost on which the loading is highest. Small details of response within a magnet coil conduit probably would not affect significantly the details of the behavior and, consequently, mechanical loading should yield data of sufficient reliability for coil design.

When the coil is compressed radially, it tends to expand axially and toroidally. The axial expansion may not be restrained. However, the wedging action between adjacent coils (Figure 24) effectively causes significant toroidal constraints at the coil box faces. Consequently, the conductors are loaded in two transverse directions simultaneously.

The transverse loading would depend upon the stiffness of the conductor array. If there were no friction in the coil, then the radial load buildup would be equal to the Lorentz value. If friction is present, then some of the radial loading will be distributed to the case walls in a manner similar to that within a conductor from the cable to the conduit walls (Figure 24).

Conductors adjacent to a shelf would tend to move radially inward past the shelf whereas those seated on the shelf would not if the shelf were rigid. Here also, the interplay between friction and stiffness is a complex problem.

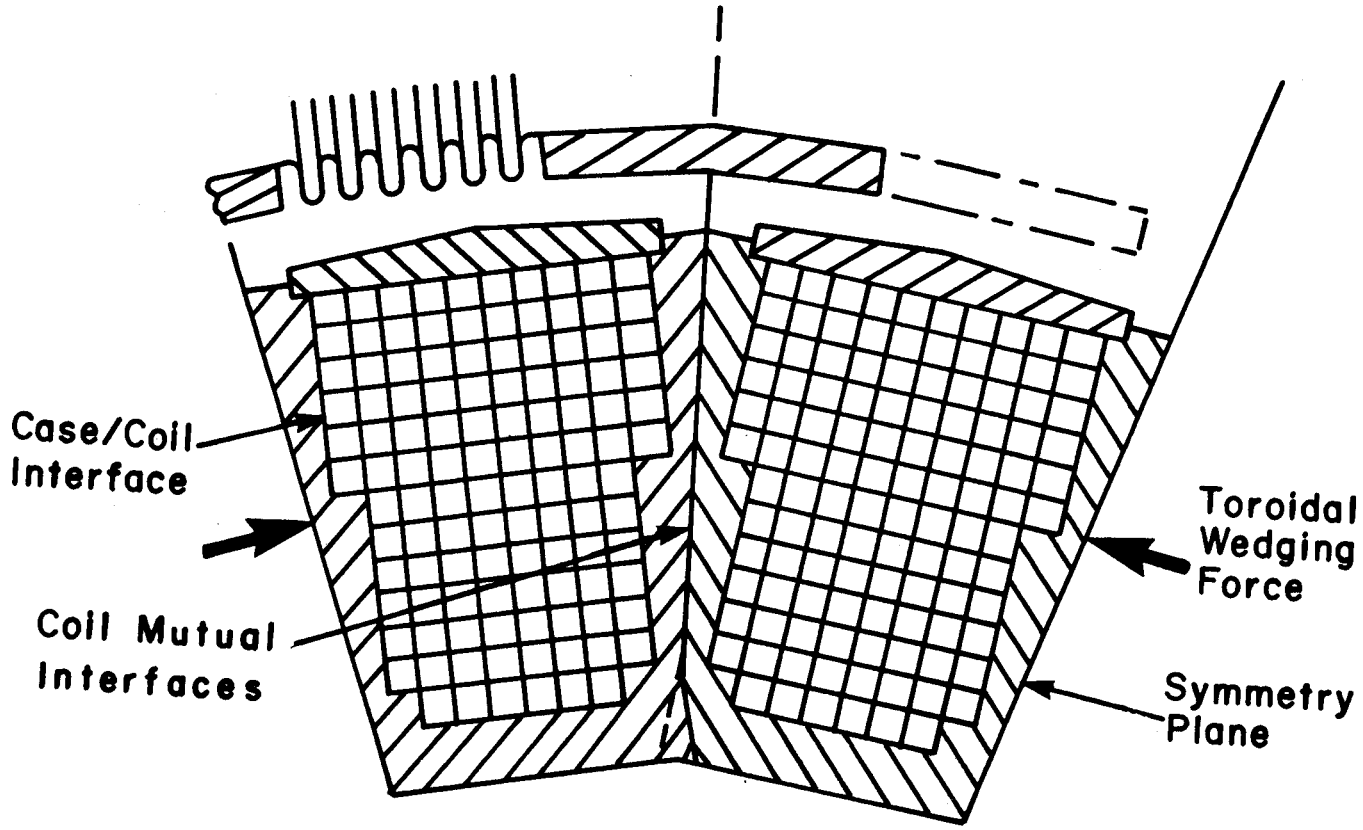

Fig. 23 Section of Typical TF Coil

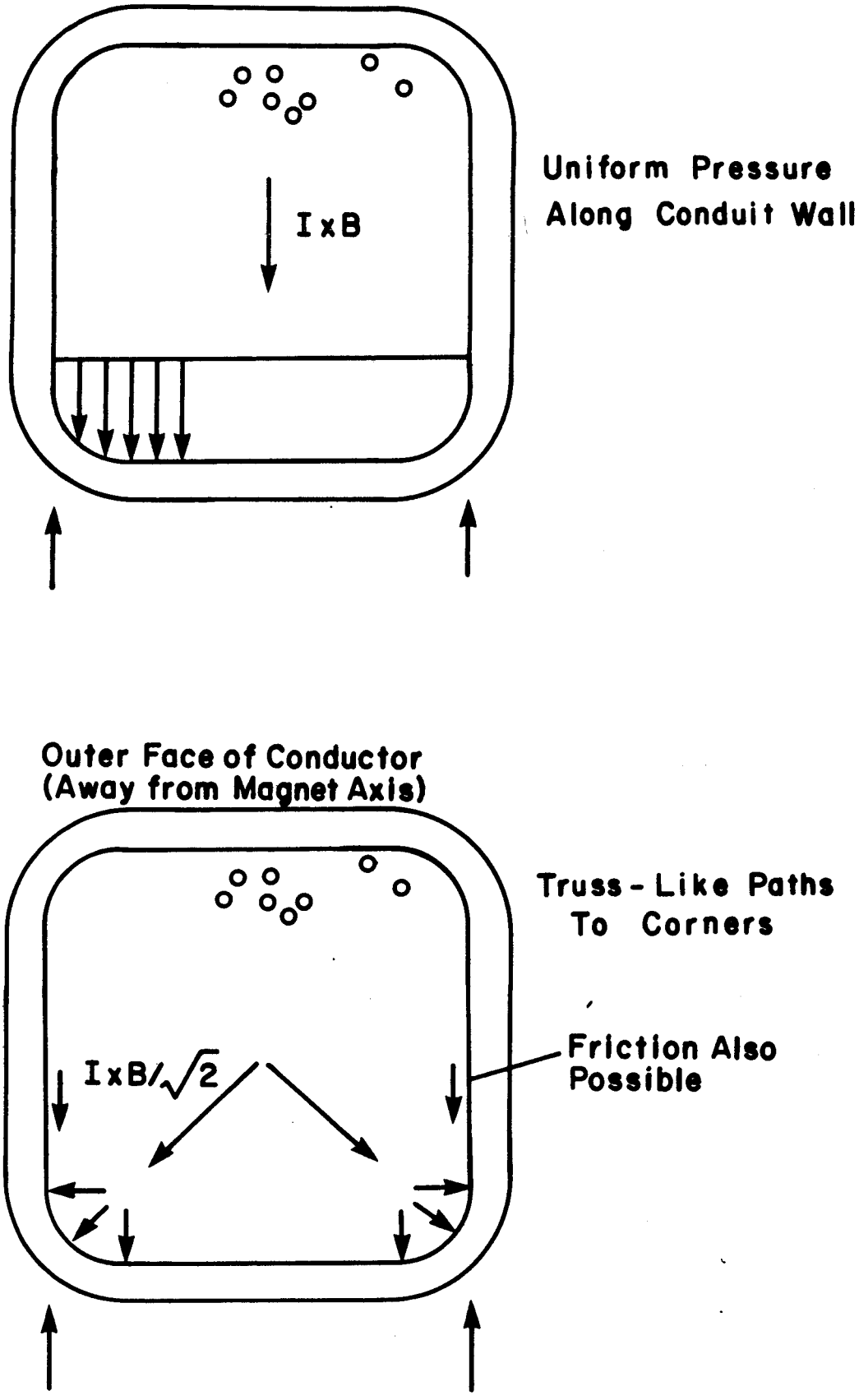

Fig. 24 Possible Cable Lorentz Load Paths Within a Conduit

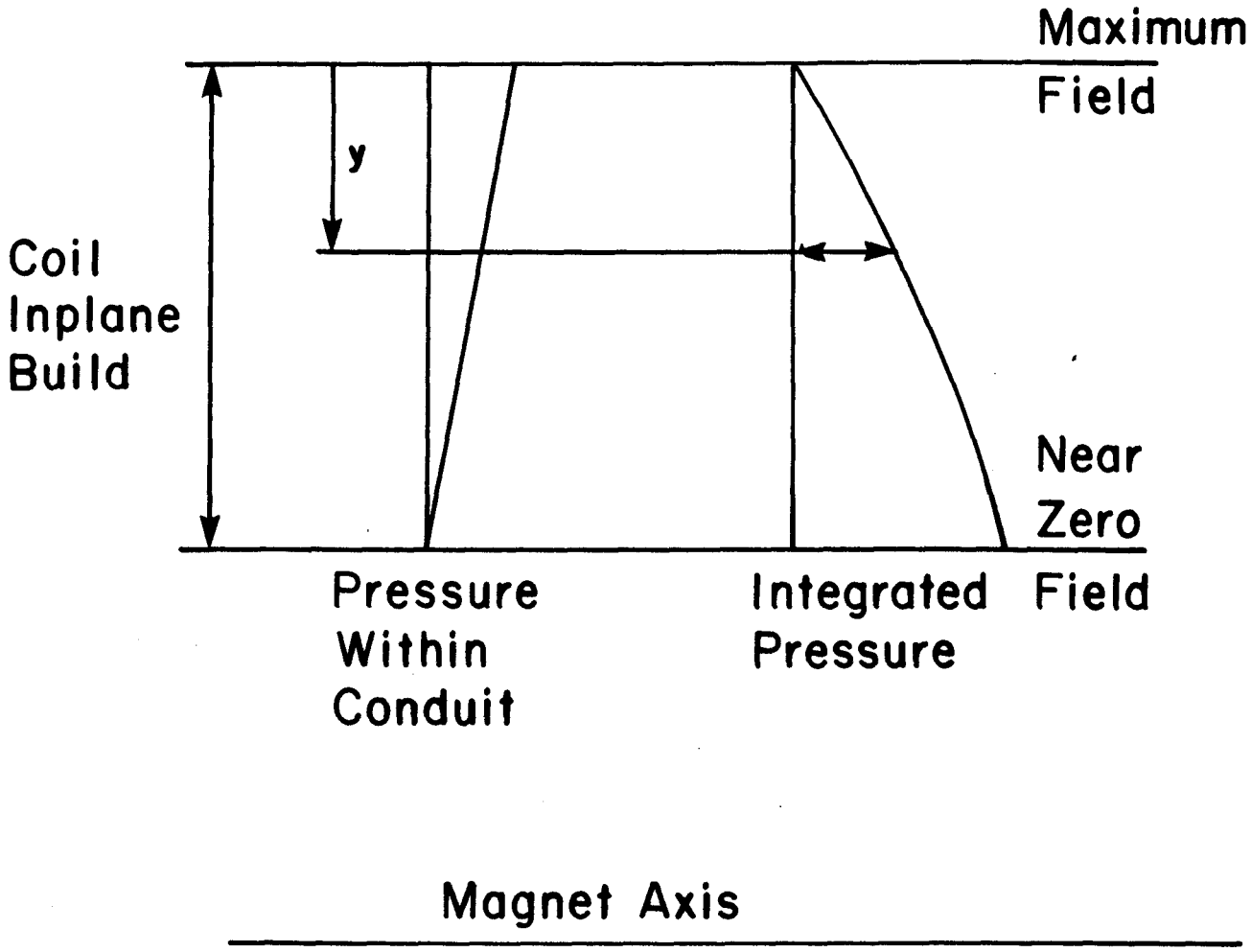

Fig. 25 Local and Integrated Loading on Conduits

Conduit Behavior

The more obvious factors that influence the stiffness, stress distribution and strength of an ICCS are:

1. Cable composition, cable winding details and degree of compaction
2. Conduit cross section shape and dimensions
3. Coil winding details
4. Conduit material
5. Stiffness and thickness of potting material
6. Stiffness and thickness of interturn insulation
7. Stiffness of lateral restraint
8. Coefficient of friction between adjacent conduits
9. Coefficient of friction between conduits and restraining walls

Structures engineering usually is performed on idealized configurations in which there are no defects and all dimensions are nominal. Actual configurations involve departures from the ideal (Figures 6, 24 and 26) for an ICCS coil and conductor.

The materials also should be expected to exhibit defects such as voids, pits, inclusions, folds, cracks, pinholes, and metallurgical and compositional variations. Some of those defects were observed in the specimens tested during the exploratory program.

Defects can affect the load distribution within the coil pack as well as the overall structural strength and stiffness of the pack cross section. They also can lead to variations in strength and stiffness along the coil. The test specimens were too short, and the stacks contained too few conductors, to permit assessment of those effects.

A superconductor will operate in liquid helium at or below 4.5 K. However, array size, specimen load, and test complexity have permitted only 77 K testing throughout the cryogenic phase of the exploratory program. The difference between structural behaviors at those two temperatures is not known.

Corner Structural Behavior

There may be value in examining the corner behavior in a gross way to help understand the structural mechanics. Assume that the array is potted and that one-quarter of the conduit is loaded

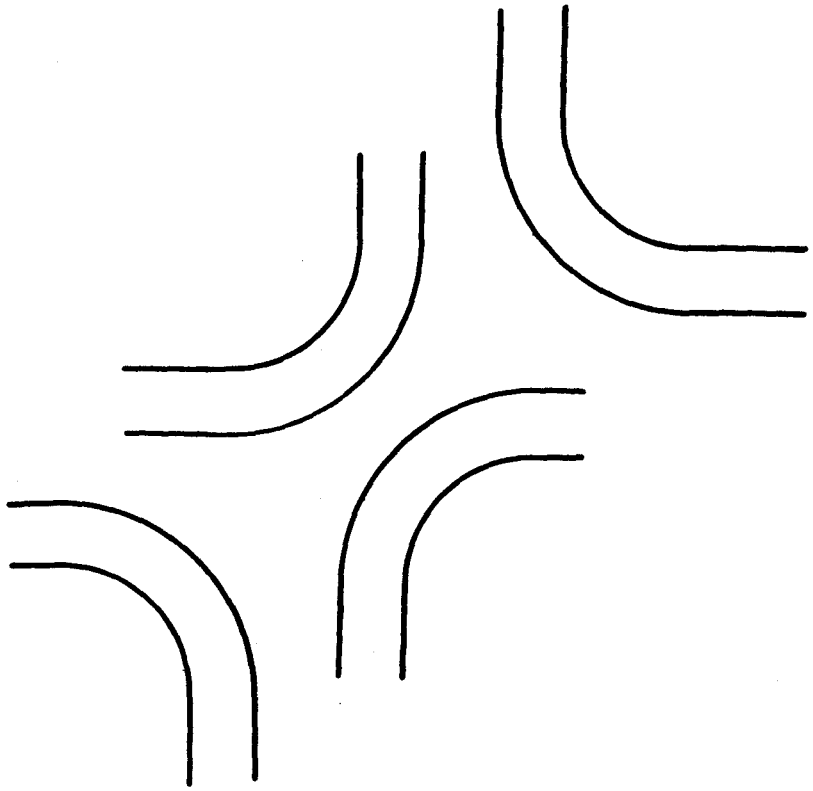

Shown: Relative Displacements of Adjacent Conductors in a Coil

Not Shown: Conductor Cross Section Rotations

Fig. 26 Coil Winding Deviations From Ideal

by equal membrane forces, $N = pW/2$, where p is the design pressure and W is the span over which it acts. Assume also that the corner is supported by an elastic foundation over the 90 degree arc (Figure 27). If the foundation is soft, then the radial pressure $q = N/R$, will react the membrane loads as the corner is pushed into the foundation and there would be no bending of the conduit wall. If the foundation is stiff, the movement of the corner would be less and the radial pressure no longer would be uniform. As a result, bending would be induced in the conduit.

The deformation of the foundation would permit adjacent corners to approach each other. The regions near the tangent points of the straight sides and corner arcs would have the greatest proximity. Distances on the 45 degree lines would be larger. As a result, the strains induced in the filler of an array would not be uniform around the arc. They would be greatest near the tangent points and least at 45 degrees (Figure 28). The magnitude of the local force would be expected to diminish with increases in the thickness of the filler. Also, the bending in the corner regions would tend to reduce the pressure further and to move the actual point of peak pressure toward the 45 degree position (Figure 29). That action would lead to a nonlinear load-deflection characteristic of the coil. The departures from the average radial pressure produce no net force. They cause bending only.

As the corners move together with increasing load, the corner radii decrease; this shifts the tangent points. The structural behavior is nonlinear and, consequently, linear extrapolation of design details (for increased strength and stiffness) is not correct. For example, it is not necessarily true that a 10 percent increase in wall thickness will promote a 10 percent decrease in corner stress.

Another form of nonlinear behavior is the bearing of the conduit corner on the thin layer of potted insulation. At very low loads, the entire flat wall may be assumed effective. However, at loads of the order of 10 percent of design the load paths are confined near the corners causing Hertz contact pressure between adjacent corners. That controls the width of the seating surface and the magnitude of the contact pressure which is not linear with load. The pressure could become high enough to crack the insulation, as was observed during the exploratory tests.

Also, inelastic stresses are nonlinear functions of conduit loads.

The exploratory tests were conducted essentially without friction to avoid restraint of vertical movement by the lateral support frame. That may not be appropriate to a coil in a case. If friction

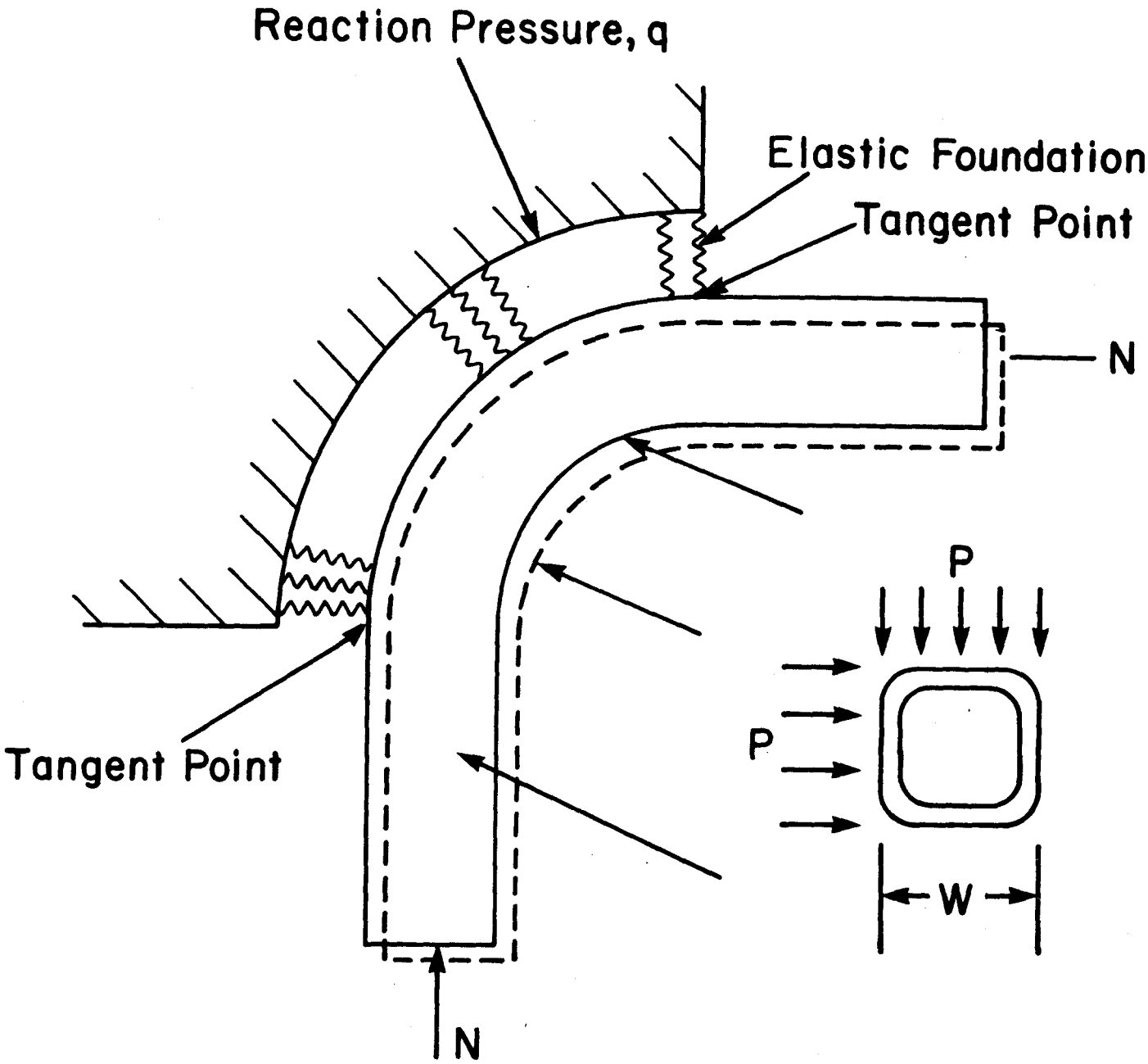

Fig. 27 Representation of Corner Load Reacted by Elastic Foundation

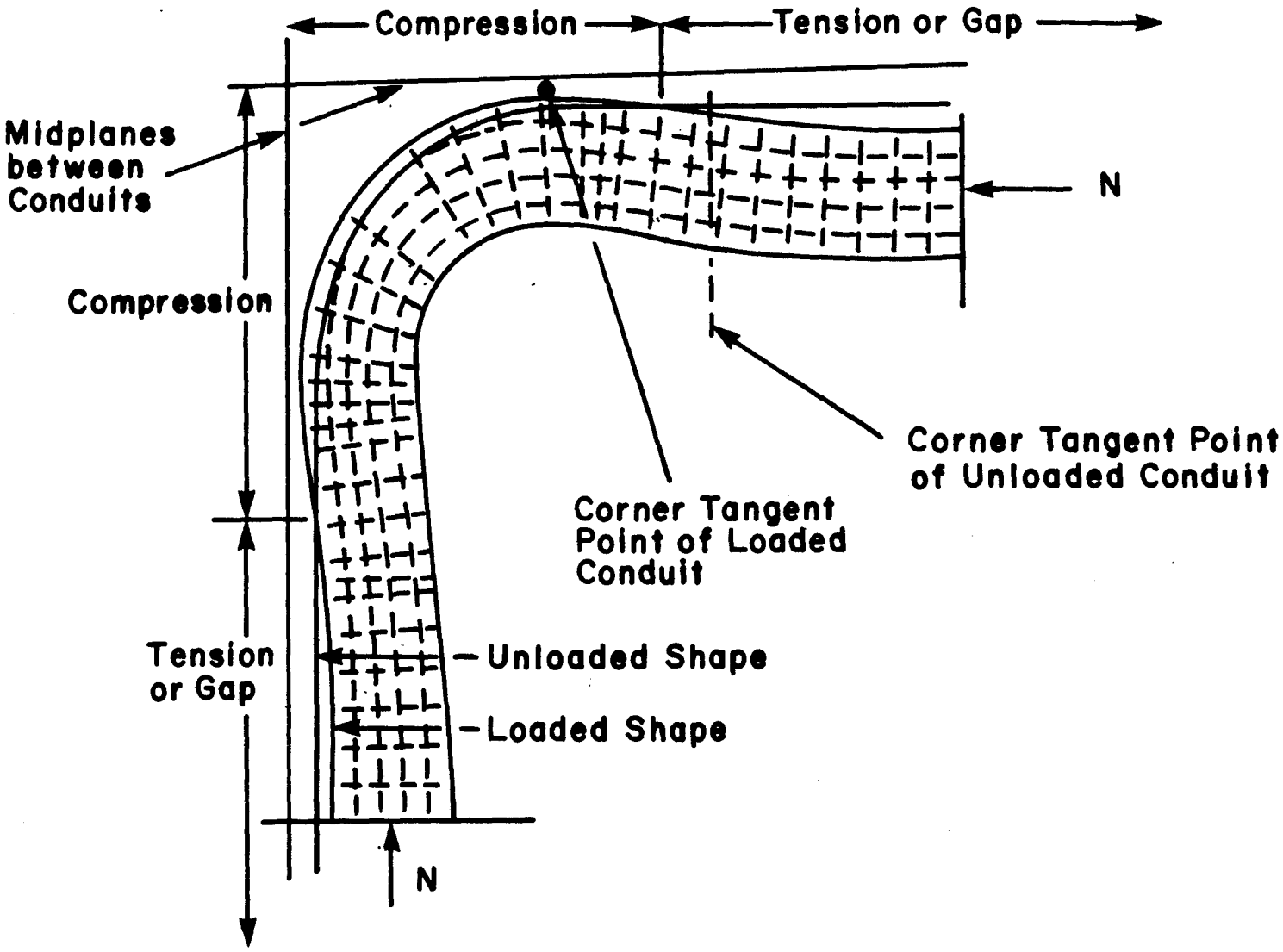

Fig. 28 Corner Movement and Deformation

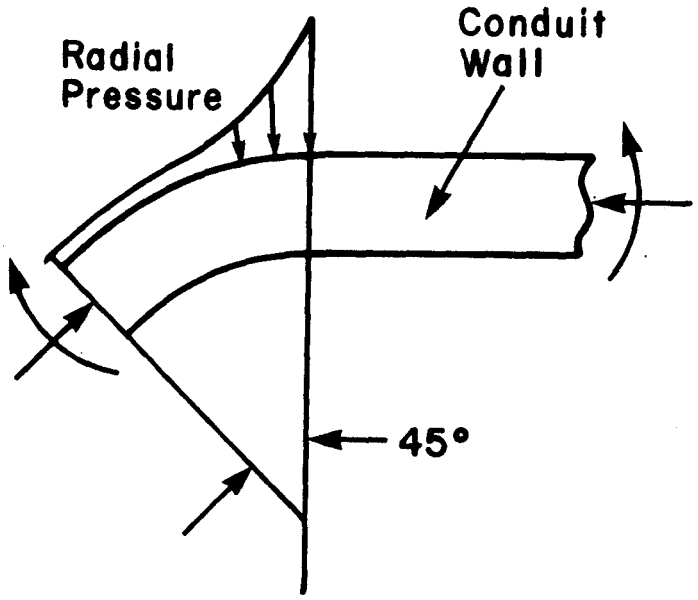

Fig. 29 Conduit and Filler Loads in Corner Region

is present, then the conduits could be subjected to transverse shearing action that could distort the cross section while partially offsetting the integrated pressure acting on the coil pack. The remainder would enter the case side walls.

The lateral restraint from the coil interaction may not be great enough to ensure equality of radial loading and toroidal reaction in a TF coil. Furthermore, toroidal loading is induced in the TF coils by poloidal fields.

Phenomena that may be of secondary concern include long term creep and relaxation in the conduit wall, the potting and the insulators.

FINITE ELEMENT ANALYSES

Introduction

The following finite element analyses depict the general behavior of an ICCS conduit without an internal cable. Effects of lateral restraint, corner fill, material inelasticity, and structural non-linearity are considered. The features of primary interest are the locations and magnitudes of the peak stresses and the effective transverse stiffness of the conduit.

The results are presented in reproductions of the computer printouts. The deflection and stress scales are included.

Shape and Material Properties of Conductor and Potting Epoxy

The geometrical shape of one-quarter of the conductor is shown in Figure 30. The conductor is assumed to be made of stainless steel with the physical properties of

Young's modulus (E) = 30 msi

Poisson's ratio (ν) = 0.3

Yield stress (σ_y) = 140,000 psi

It was also assumed that the stress-strain curve of the material can be represented by

$$\epsilon = (\sigma/E)\,[1 + (3/7)(\sigma/\sigma_y)^7].$$

The potting is done as shown in Figure 31 by epoxy with the physical properties of Young's modulus = 0.6 msi and Poisson's ratio = 0.3, unless otherwise indicated.

Element Discretization

A quarter of the conductor is approximated by plane stress quadratic elements. Except when otherwise specified in the individual cases, the element and node numbers are shown in Figures 32 and 33 for a loose conductor and in Figures 34 and 35 for a potted conductor, respectively. Only a quarter of the conductor is analyzed because it has two planes of symmetry in both load and shape configuration.

Loading Pattern

A uniformly distributed pressure of 7250 lb/in is assumed to act on the top surface of the conductor under working conditions. However, in the case of a loose conductor, this load may be reduced to a concentrated load acting at Node 4 as shown in Figure 33, or it may be distributed

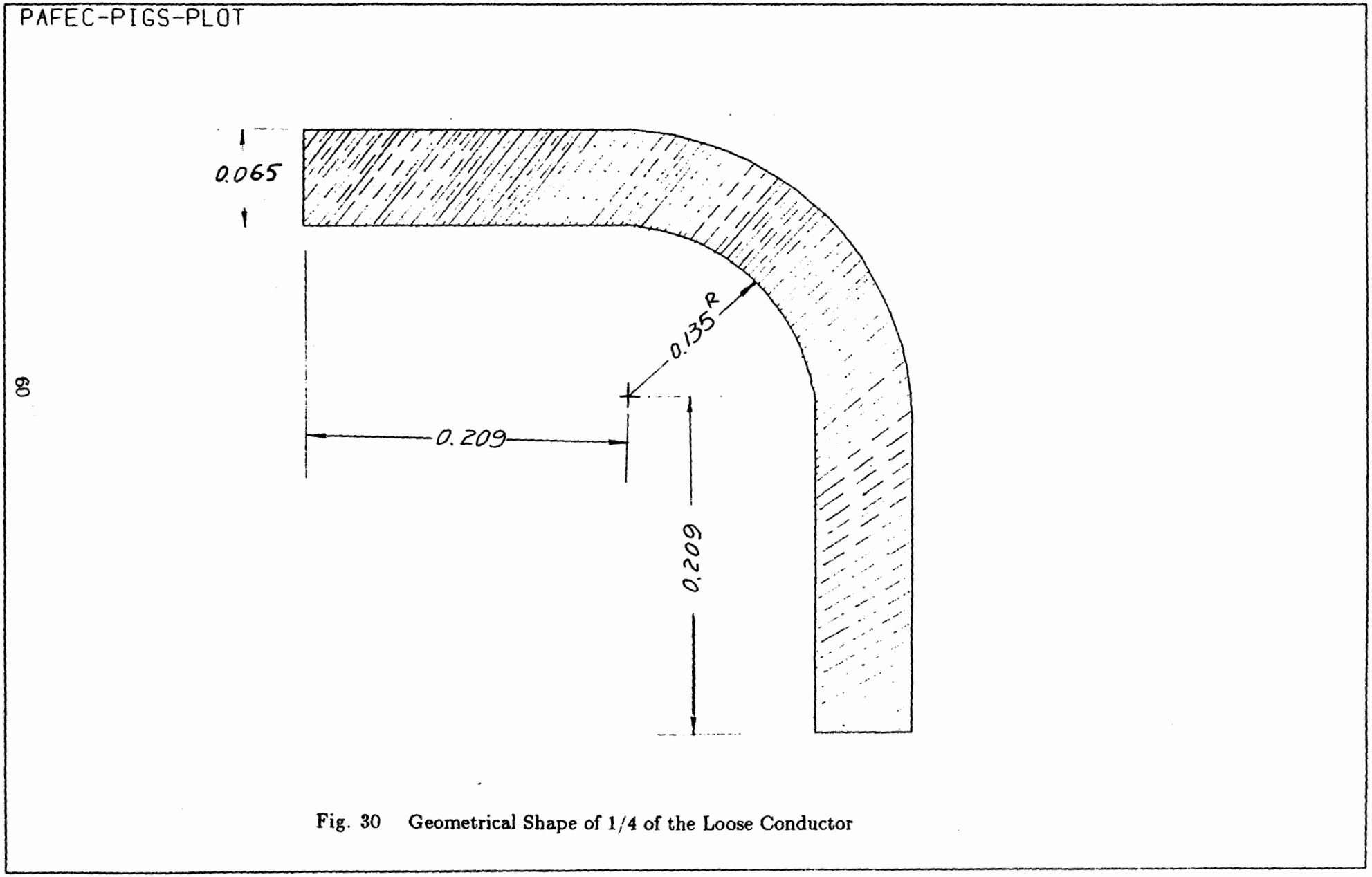

Fig. 30 Geometrical Shape of 1/4 of the Loose Conductor

PAFEC-PIGS-PLOT

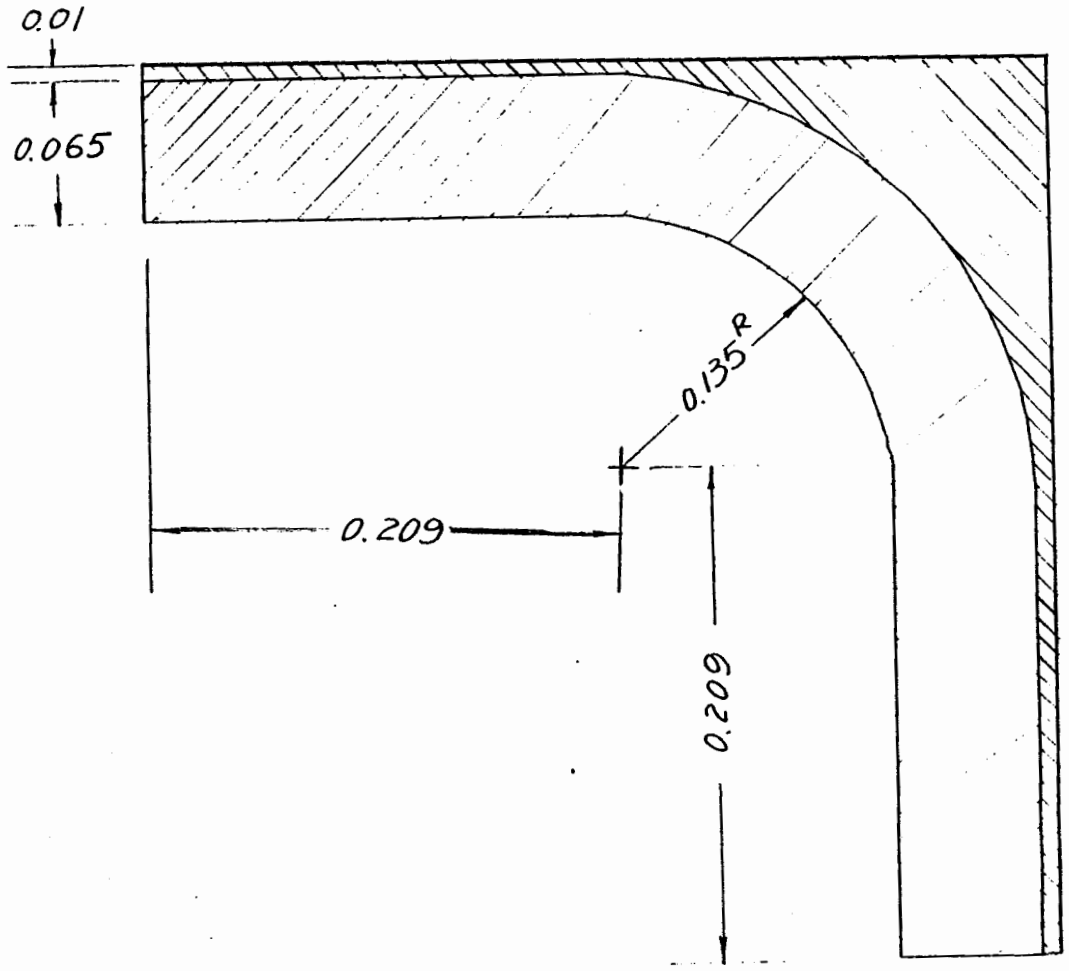

Fig. 31 Epoxy Potting of the Conductor

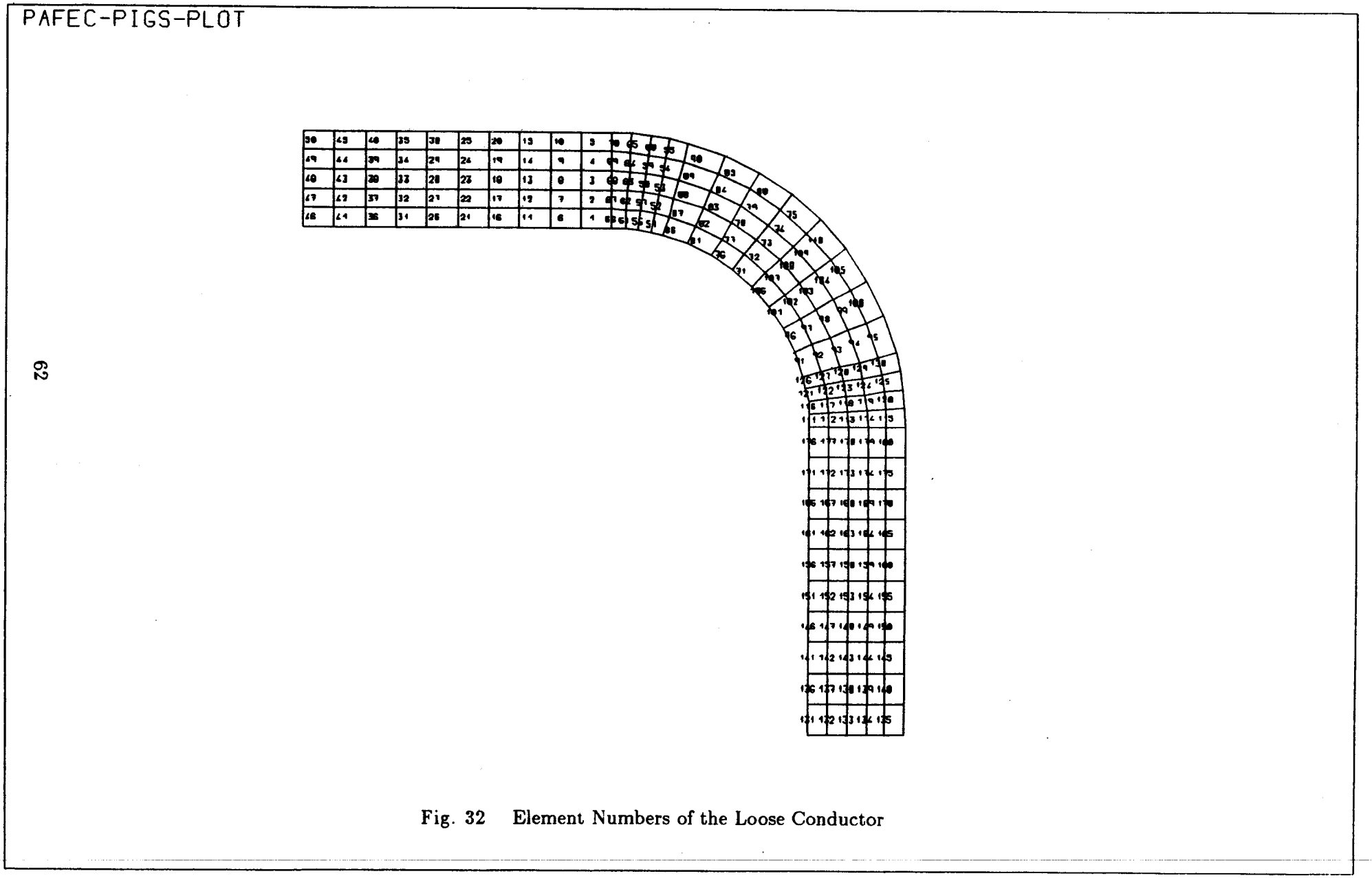

Fig. 32 Element Numbers of the Loose Conductor

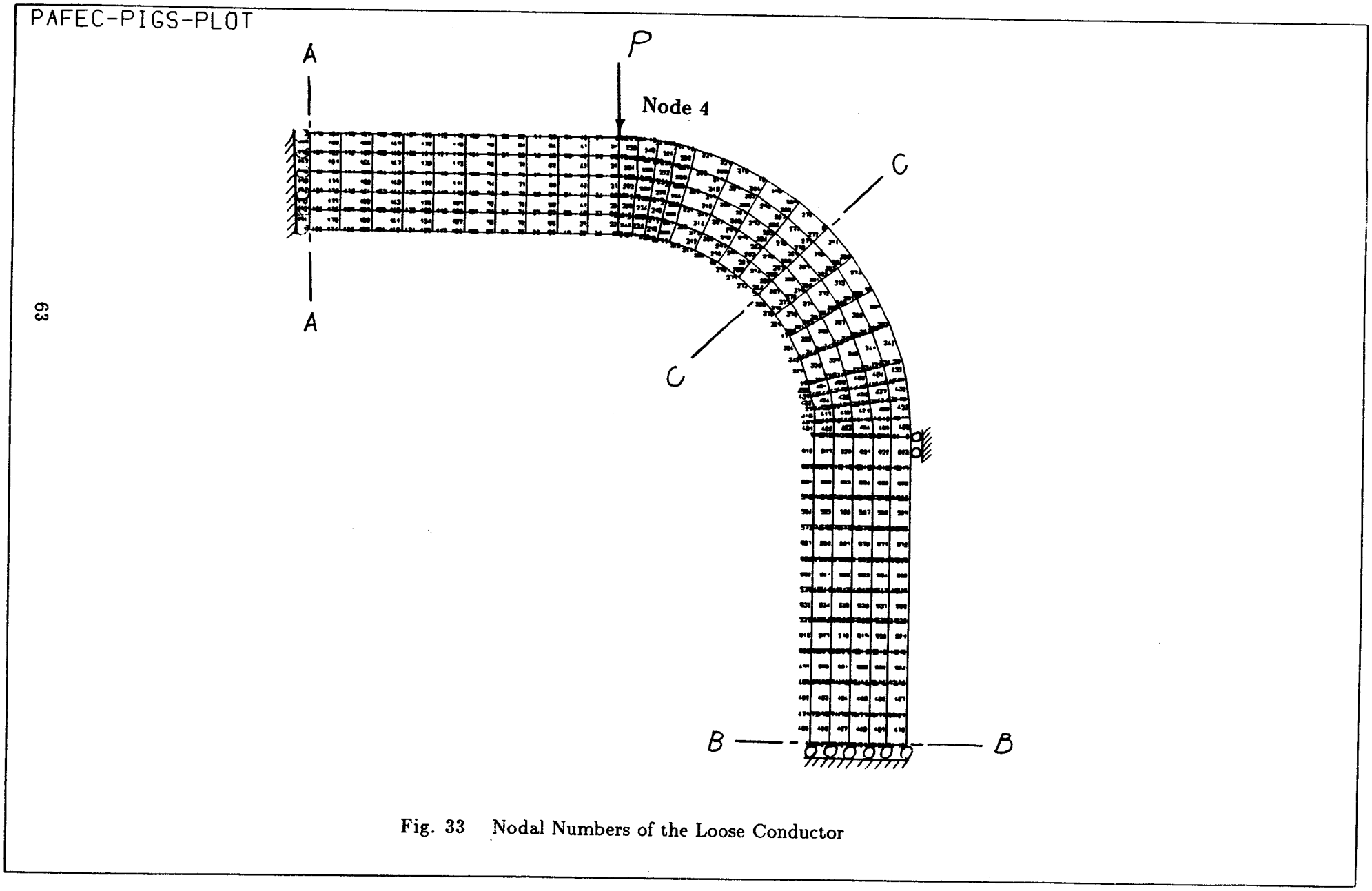

Fig. 33 Nodal Numbers of the Loose Conductor

PAFEC-PIGS-PLOT

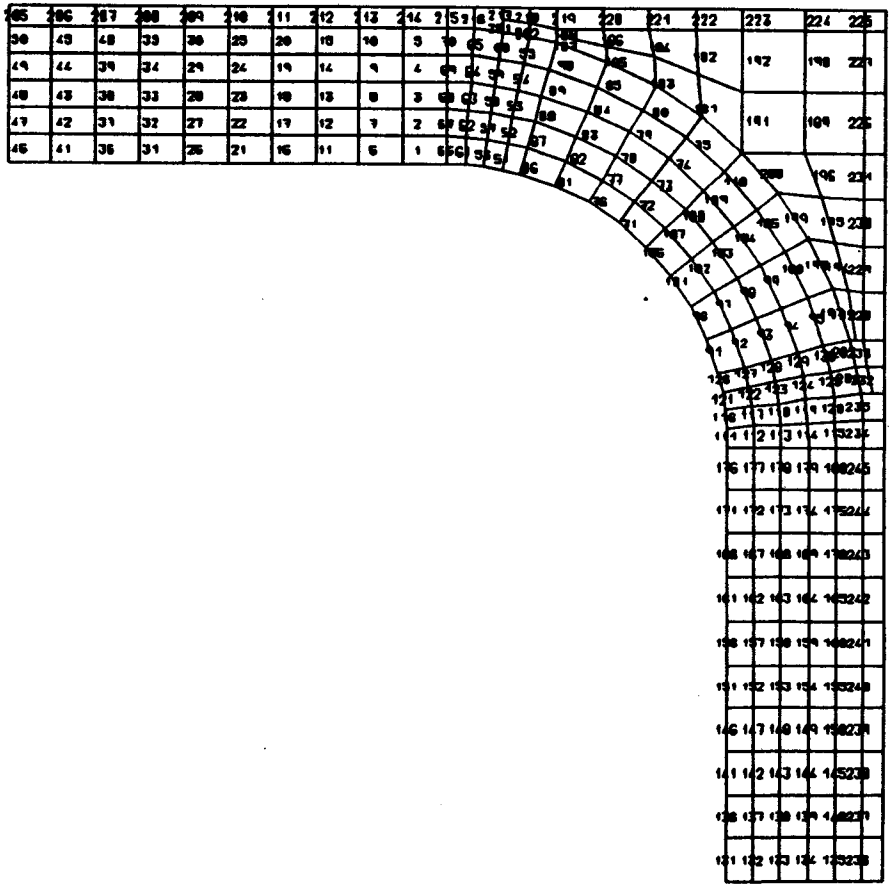

Fig. 34 Element Numbers of the Potted Conductor

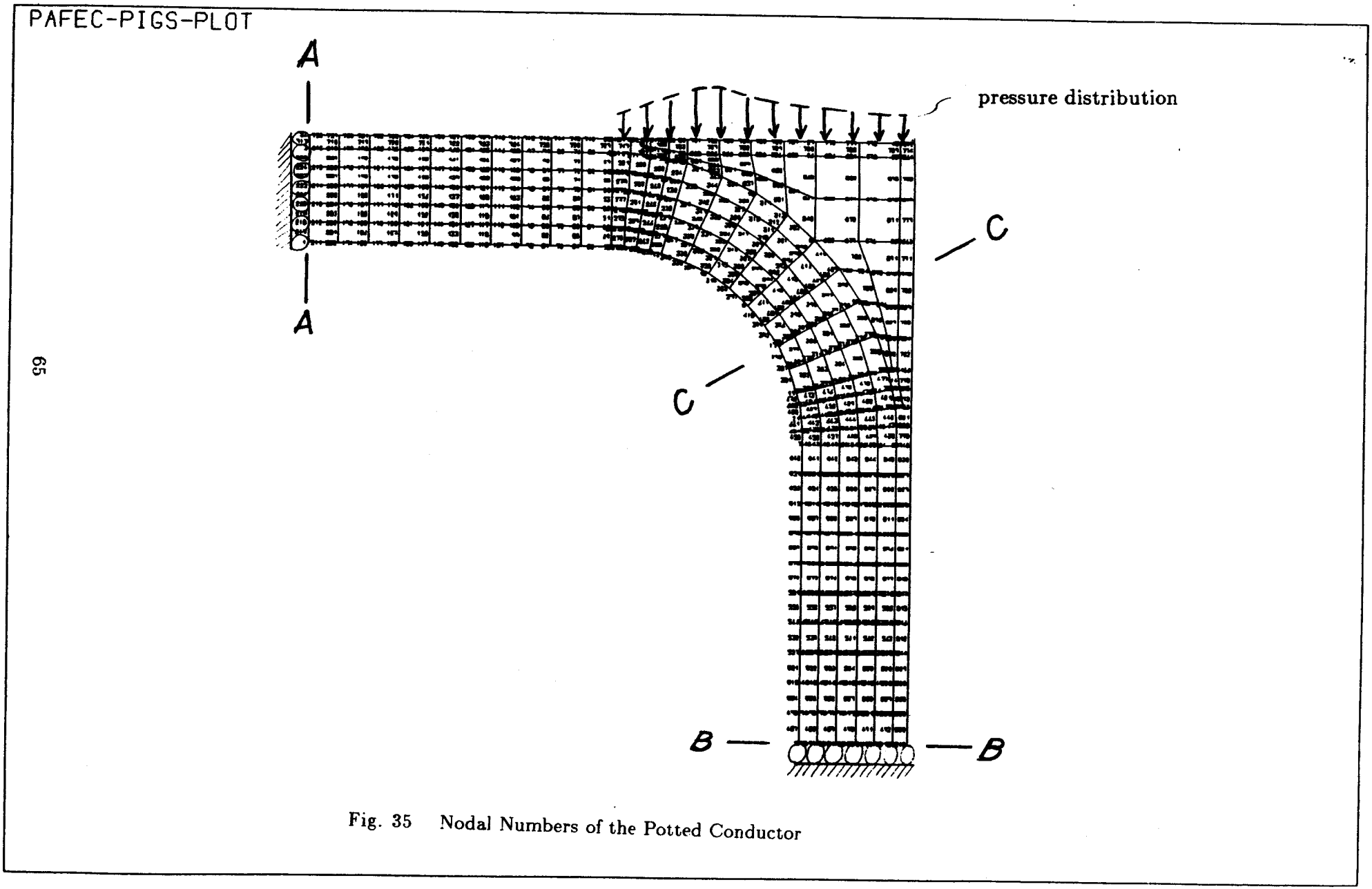

Fig. 35 Nodal Numbers of the Potted Conductor

over a reduced area in the case of a potted conductor, as shown in Figure 35 and enlarged in Figure 36.

When the term "working load" is used in this report, it refers to the loading pattern described in this section.

Displacement Boundary Conditions

The conductor is prohibited to move in the x-direction at Section A-A or in the y-direction at Section B-B, as shown in Figures 33 and 35. The side surfaces are assumed to be partially fixed if rigid side supports are imposed, or a mixed boundary condition of displacement and force may occur in the case of flexible side supports. A more detailed account of boundary conditions will be given, when necessary, in the following analyses.

Elastic - Plastic Analysis of the Loose Conductor

Since rigid side supports will be assumed in this analysis, applied loads reduce to a concentrated load at the transition point between the flat and curved sections of the conductor, as shown in Figure 33. Six load cases were considered. Their magnitudes in pounds are 500, 1000, 1500, 2000, 2500, and 3000, respectively. Table 4 gives a summary of the results of both elastic and plastic analyses.

The force-deformation curve (which can also be converted to the stress-strain curve by dividing both the x and y axes by a scale of 0.409) is shown in Figure 37. This curve is obtained by passing a natural spline through the six calculated data points. Local yielding does not happen until the magnitude of load is over 1000 pounds. Thereafter, the effect of the plastic strains is appreciable.

The equivalent tangent modulus-force curve is obtained by approximating the force-deformation curve with 120 straight line segments and using the slopes of these segments as tangent moduli. The tangent modulus-force curve is plotted in Figure 38. It can be seen that the tangent modulus decreases rapidly after the magnitude of the load increases above 1000 lbs.

The stress variation across the critical section (Section C-C in Figure 33) under the working load (approximately equivalent to a concentrated load of 2965 lbs) is shown in Figure 39. The deformed shape of the conductor is shown in Figure 40.

In the following analysis, the effects of bulge, flexible side supports, and increasing thickness of the conductor on the behavior of the conductor are investigated.

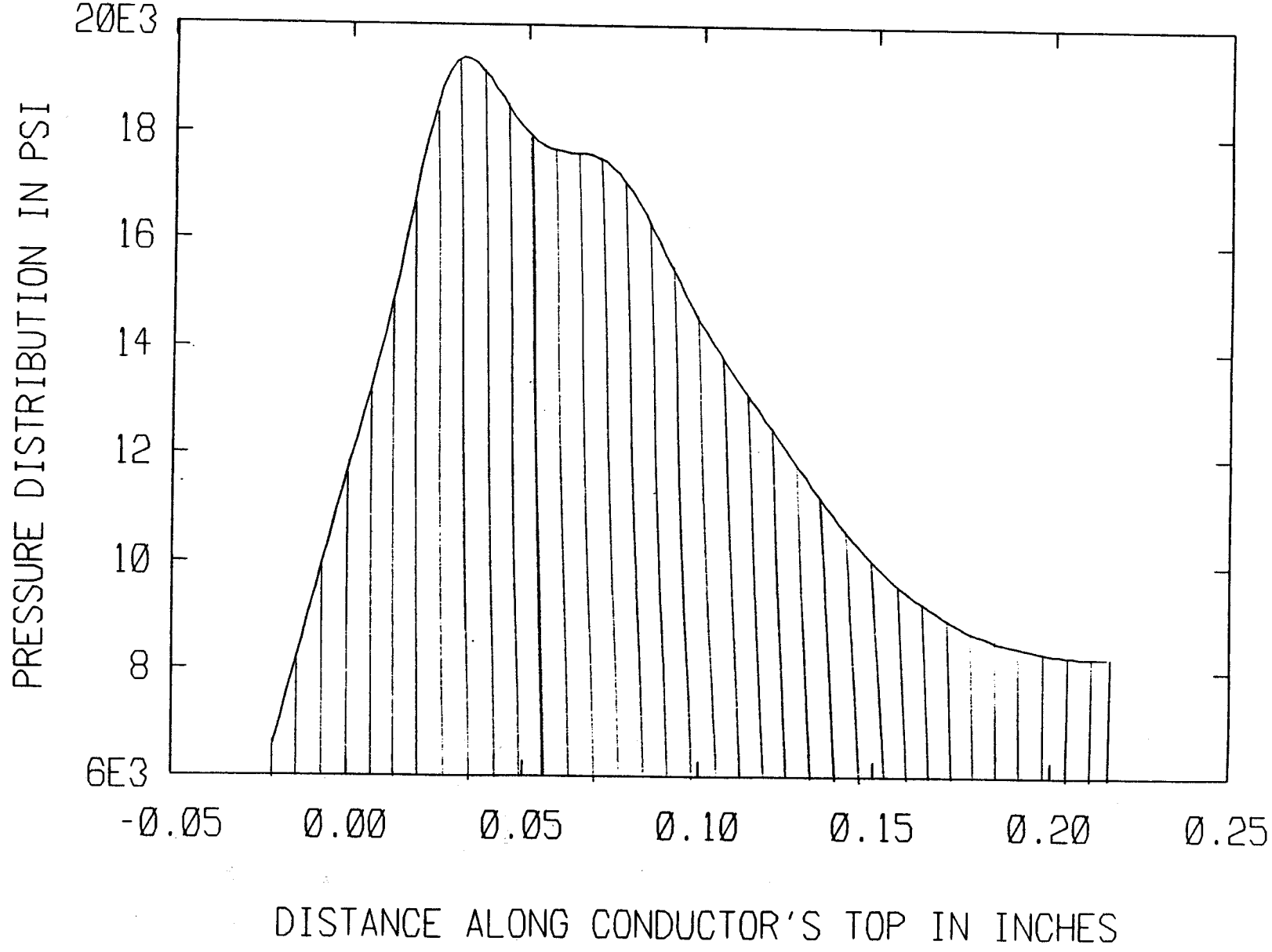

Fig. 36 Load Distribution on Top Surface of the Potted Conductor

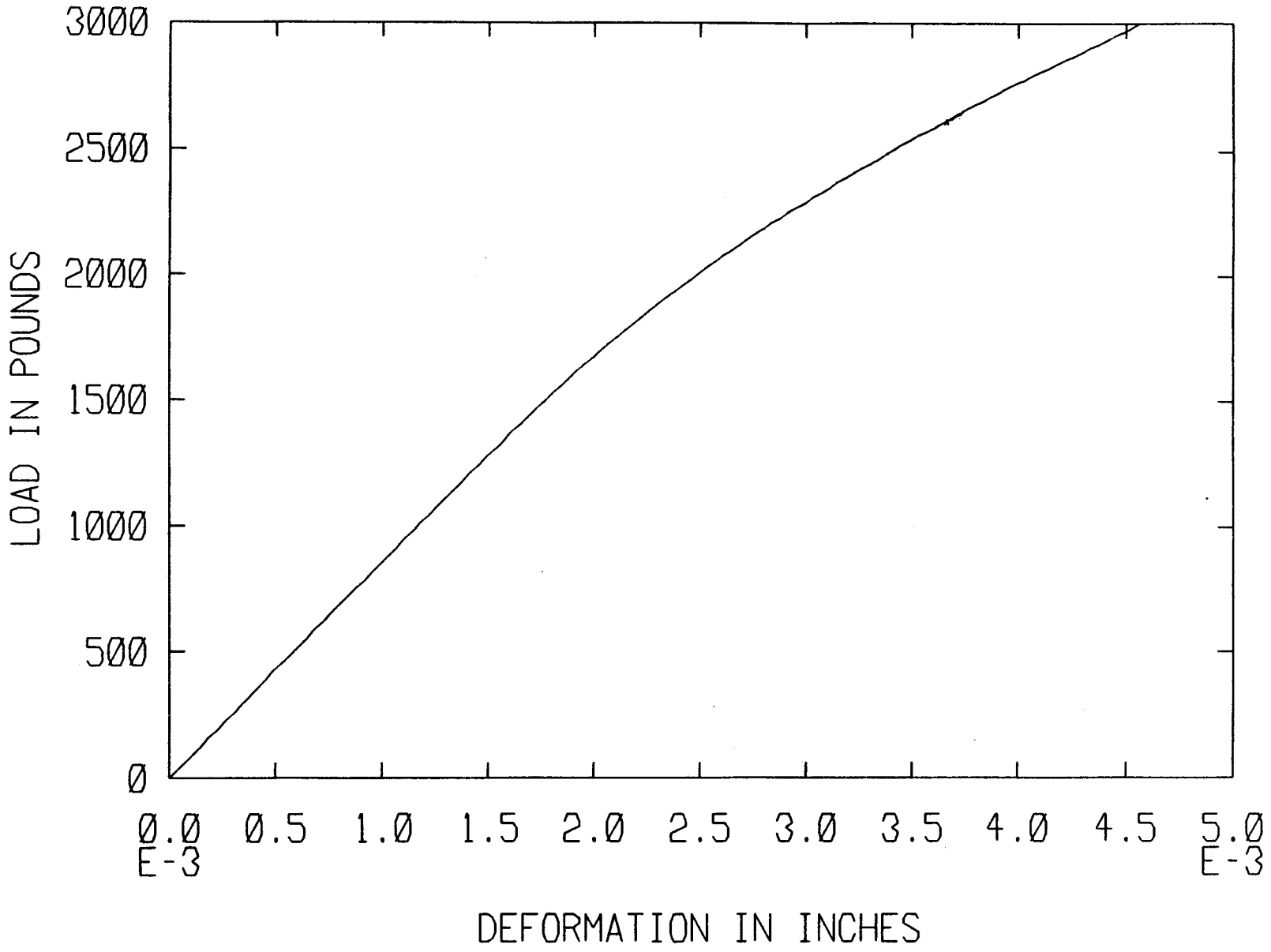

Fig. 37 Force Deformation Curve of the Loose Conductor with Rigid Side Supports

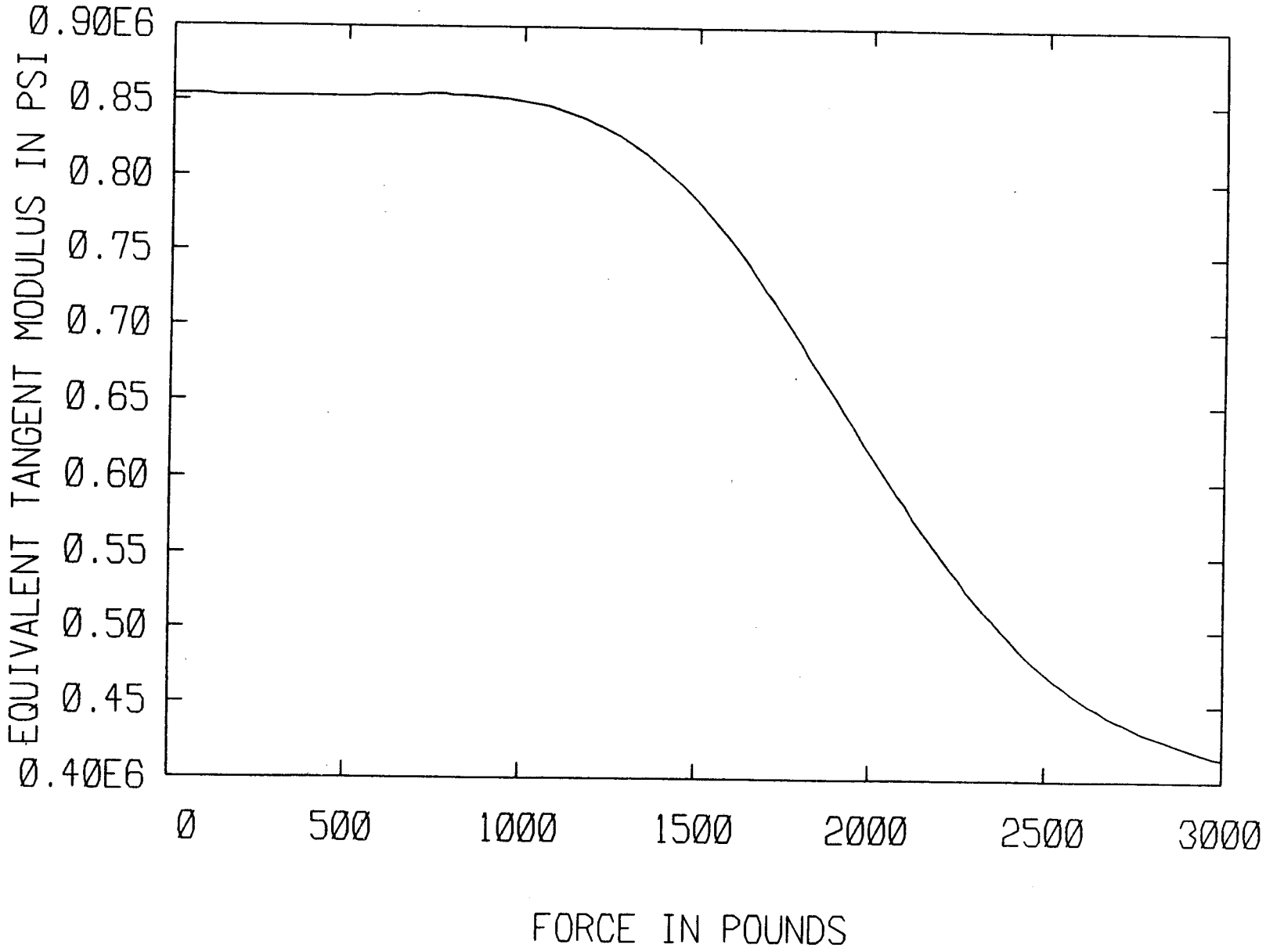

Fig. 38 Equivalent Tangent-Modulus-Force Curve of the Loose Conductor with Rigid Side Supports

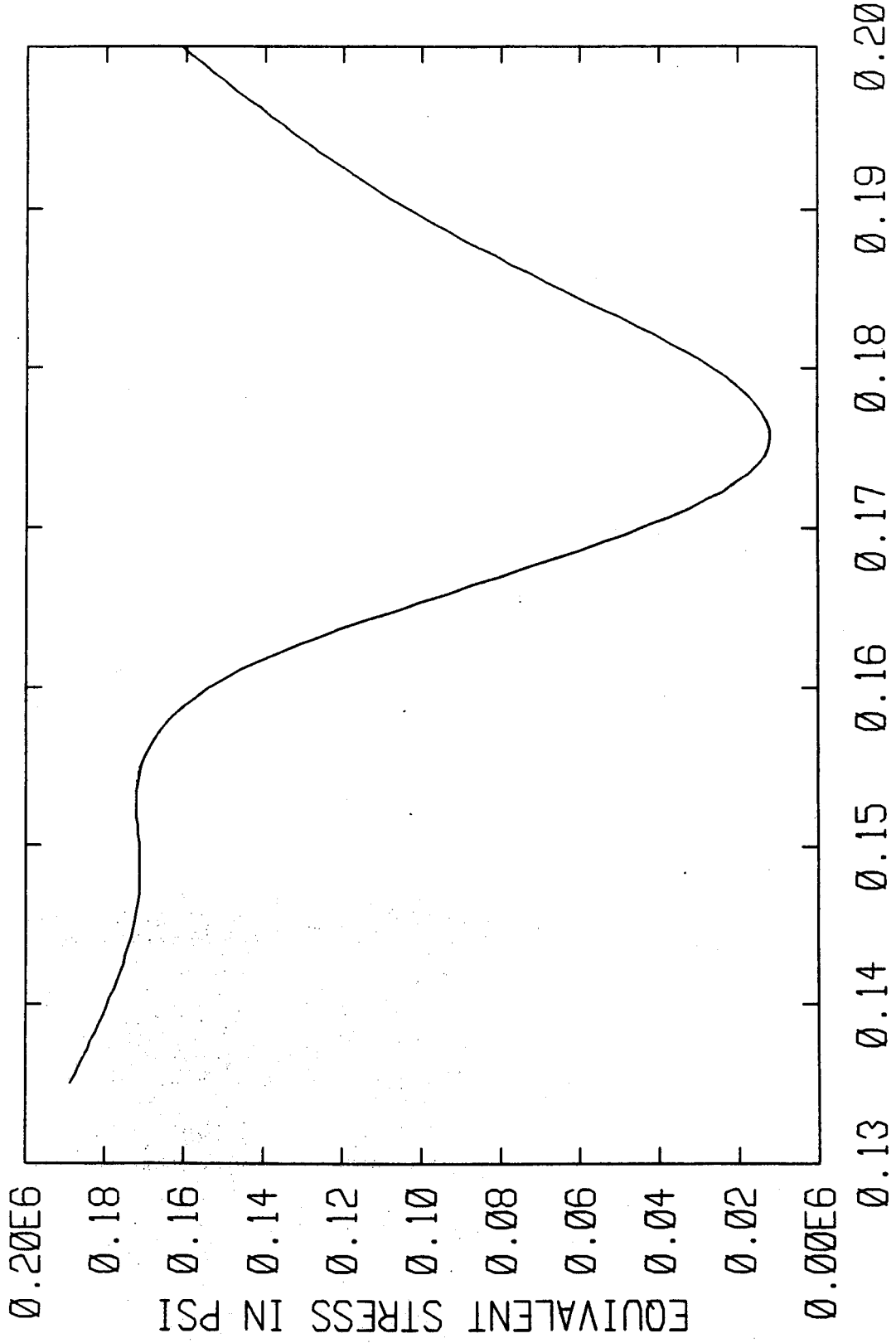

Fig. 39 Variation of Equivalent (Von Mises) Stress Across the Critical Section of the Loose Conductor with Rigid Side Supports

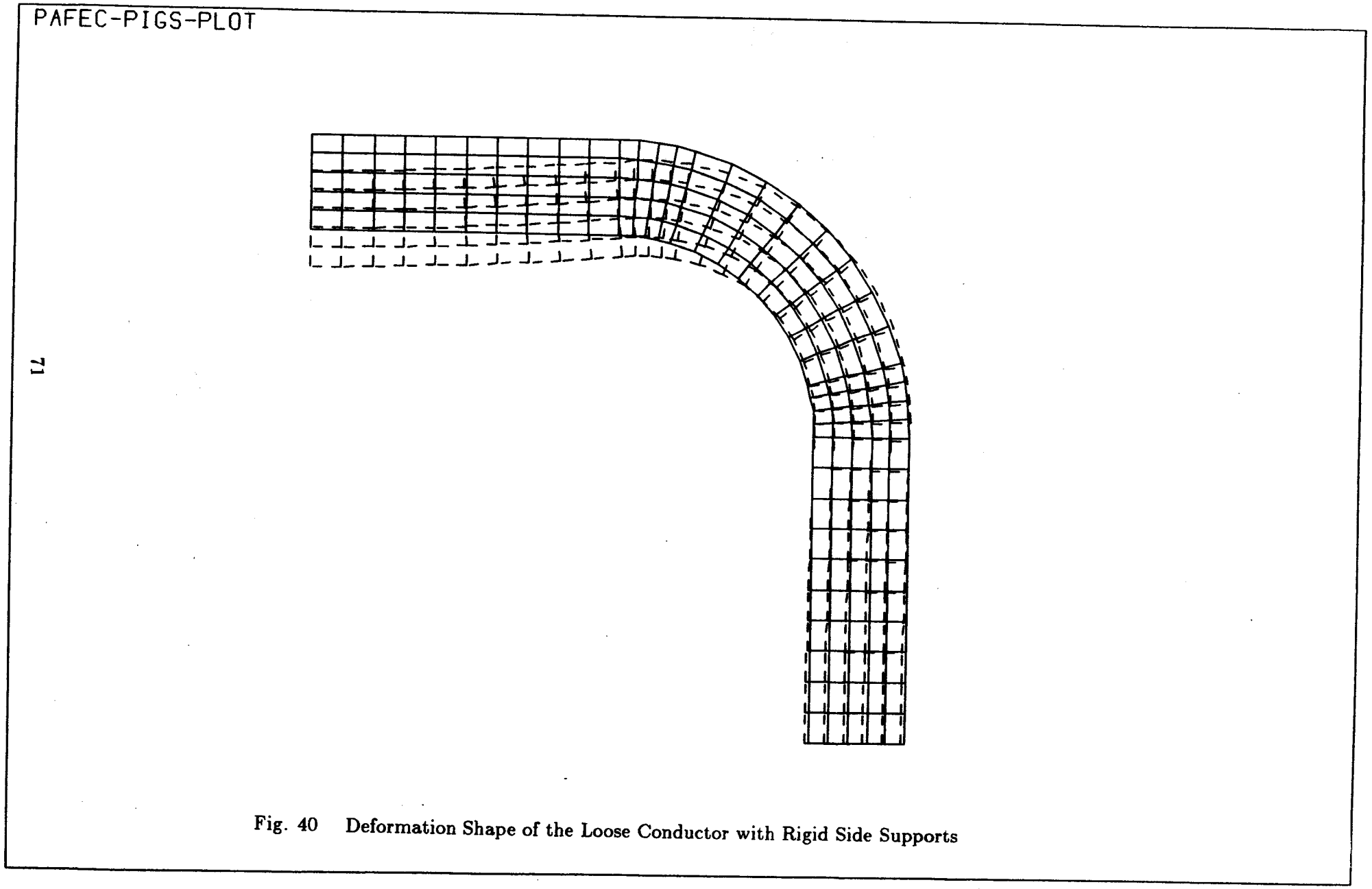

Fig. 40 Deformation Shape of the Loose Conductor with Rigid Side Supports

Table 4. **The Variation of Equivalent Stress and Deformation with Respect to the Applied Load as the Load Increases from Elastic to Plastic Range in the Case of a Flat Conductor with a Concentrated Top Load at Node 4 and Rigid Side Supports at Node 8 and 623, Loose Packing, That Is, No Epoxy, Conductor Only**

(1)	(2)	(3)	(4)	(5)	(6)
	1E+5	1E-3	1E-3	1E+5	1E+5
500	8.5351	0.5858	0.5858	0.405	0.405
1000	8.5077	1.1715	1.1715	0.810	0.810
1500	7.8575	1.7573	1.7669	1.215	1.21
2000	6.1752	2.3430	2.4831	1.62	1.50
2500	4.7138	2.9288	3.4122	2.025	1.65
3000	4.1505	3.5146	4.5690	2.43	1.81

Titles of the columns:

(1) The magnitude in pounds of the concentrated load at node 4 in the opposite y direction.

(2) The equivalent tangent modulus in psi in the y-direction of the conduit calculated by using the loads in column (1) and the deformations in column (4).

(3) The displacement in inches of node 4 in the opposite y-direction calculated by assuming only elastic deformation happens.

(4) The displacement in inches of node 4 in the opposite y-direction calculated by taking both elastic and plastic deformations into consideration.

(5) The elastic stress in psi at the most stressed element.

(6) The equivalent stress in psi at the most stressed element.

Elastic Behavior of a Bulged Loose Conductor

The effect of imperfect shape is investigated here. One of the simplest assumptions about shape imperfection is that the conductor has a symmetrical bulge on its four sides.

A conductor with the same shape and made of the same material as that described above except for a bulge of 1/10 thickness (0.0065 in) at Sections A-A and B-B (Figure 33), is analyzed by using two kinds of elements - plane stress elements and curved beam elements. The mesh of plane stress elements is shown in Figure 41.

When the array of bulged conductors is under compression, a concentrated load will occur initially on the center plane of the individual conductor. However, this load will shift toward the corners of the conductor as its value increases and the conductor deforms. For simplicity, a side load with the same magnitude is assumed to move symmetrically to the 45 degree plane with the applied load whereas no side constraints are considered.

Table 5 and Figure 42 show how the equivalent Young's modulus increases as the load moves along the top surface. These results agree qualitatively with the experimental results in the initial loading period.

The results of the analysis of the bulged conductor with an initial bulge of 0.0065 in. show that at the same load:

(i) The vertical displacement of the point on the upper surface which remains in contact with the adjacent conductor is 25% smaller than the displacement of the similar point on the perfectly flat conductor.

(ii) The maximum bending stress, which occurs at the inner radius of the curved section in the vicinity of the 45 degree plane of symmetry, is about 15 percent less than the maximum bending stress in the perfectly flat conductor.

This happens because the initial conductor imperfection (i.e. the bulge) drives the external concentrated load (by which two adjacent conductors interact) closer to the corner. Thus the overall conductor stiffness is increased and the bending moment acting in the curved section is reduced.

Effect of Flexible Side Supports on the Elastic Behavior of Loose Conductor

In the analysis of the perfectly flat conductor, an assumption of rigid side supports was made. However, this assumption is rarely valid and flexibility of the side supports has to be considered.

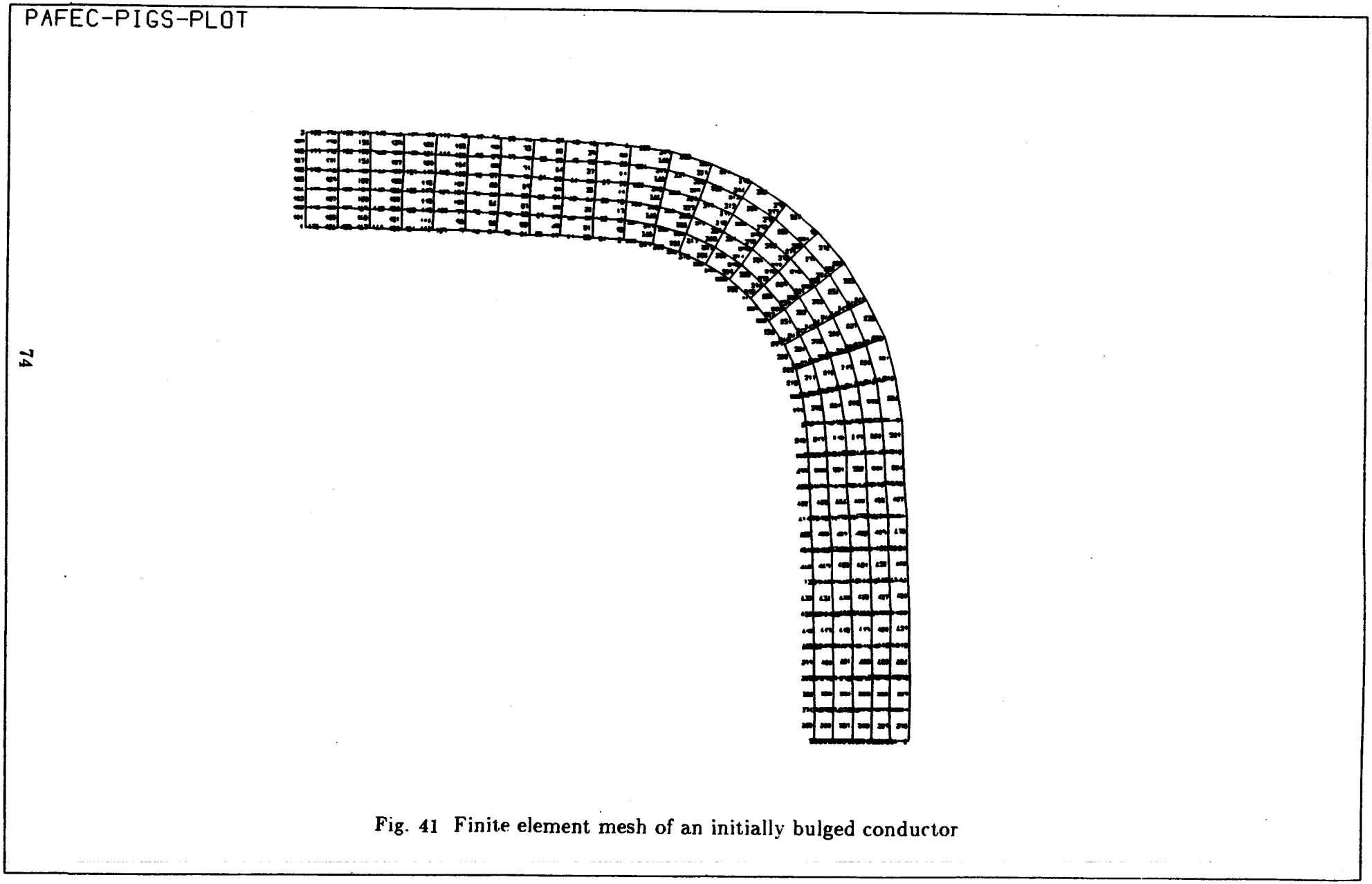

Fig. 41 Finite element mesh of an initially bulged conductor

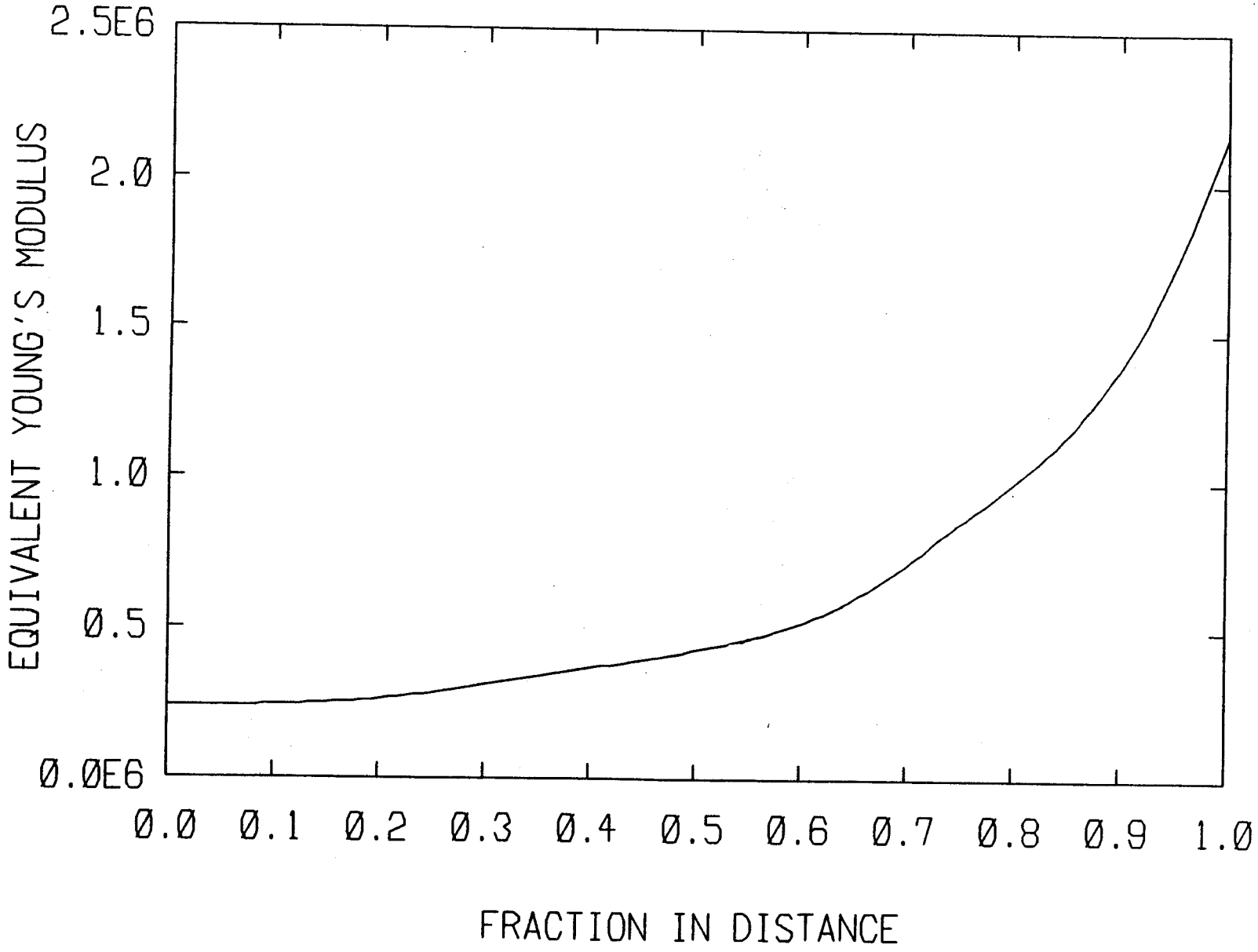

Fig. 42 Change of Equivalent Young's Modulus as the Applied Load Moves Along the Top Surface of the Bulged Conductor

Table 5. **The Variation of Equivalent Young's Modulus of the Bulged Conductor as the Concentrated Load Shifting From its Plane of Symmetry Towards the Corner Along its Bulged Top Surface. A Comparison of the Results is Made by Using Two Kinds of Elements - Plane Stress Elements and Curved Beam Elements**

Location of the Applied Load as a Fraction of Distance From Plane of Symmetry to Where Curvature Changes	Model	Young's Modulus in 1E5
0	Plane Stress	2.403
	Beam	2.394
1/4	Plane Stress	2.876
1/3	Beam	3.312
1/2	Plane Stress	4.331
	Beam	4.214
2/3	Beam	6.356
3/4	Plane Stress	8.618
0.943	Plane Stress	16.701
0.953	Beam	17.737
1	Plane Stress	21.685
	Beam	21.654

The flat conductor with a fixed concentrated load of 2965 lbs (working load) acting at the corner node (the point where the straight top surface and the circular surface of the conductor meet) was assumed supported by springs with the same spring constant on its sides. The spring constant of the springs was varied and the behavior of the conductor was investigated.

Table 6 and Figure 43 show the results of this investigation. Several important aspects are summarized below:

(i) The value of the equivalent Young's modulus changes almost by a factor of five as the spring constant increases from zero to infinite.

(ii) When the spring constant falls between 10,000 lbs/in and 10,000,000 lbs/in, the equivalent Young's modulus of the conductor is strongly affected by the slight variation of the rigidity of the side supports, while out of this range (both below 10,000 lbs/in and above 10,000,000 lbs/in) a threshold of equivalent Young's modulus is almost independent of the rigidity of side supports. This is shown in Figure 43.

(iii) The point in the middle of the side (originally bulging out when the side supports are soft) bends in when the spring constant exceeds 525,000 lbs/in, as indicated in both Table 6 and Figure 44. Thereafter, there is a rapid decrease in contact area (corresponding to a rapid decrease in the number of springs in the model used) and the problem becomes a Hertz contact problem.

As a matter of interest, the side support of the experimental set-up was analyzed by a strength-of-materials approach, and an equivalent spring constant was obtained. The value of 79,900 lbs/in/spring was reached by treating the side supports as a combination of extensional bars and a simply-supported beam, while the value of 92,650 lbs/in/spring was reached by assuming a combination of extensional bars and a clamped beam. The calculated results seem to agree with the experimental results.

The finite element discretization of this analysis is shown in Figure 45.

The above analysis shows how the variation of the stiffness of the side supports can affect the behavior of the conductor. It is highly desirable that in the actual design a thorough study of the supporting system be made and stiffness estimated before a precise analysis of the conductors begins.

Table 6. **The Variation of Equivalent Young's Modulus of the Flat Conduit with Respect to the Spring Constants of the Side Supports Assuming That a Concentrated Working Load is Constantly Acting at Node 4 and Only Elastic Deformation is of Concern**

(1)	(2)	(3)	(4)	(5)
	1E+5	1E-3	1E-3	1E-3
0	1.74216	17.047	22.350	25.610
1E2	1.75131	16.928	22.120	25.435
1E4	2.69542	10.983	10.772	16.771
7.99E4	4.81232	6.1589	1.8448	9.7318
9.265E4	4.96524	5.9717	1.5385	9.4572
1E5	5.04286	5.8816	1.3954	9.3250
5.25E5	6.46831	4.5845	0.0071	7.3950
1E6	6.96378	4.2563	-0.1471	6.8971
1E7	8.19672	3.6165	-0.4560	5.9175
1E8	8.56899	3.4608	-0.4931	5.6743
1E9	8.62068	3.4395	-0.5288	5.6431
1E19	8.62812	3.4372	-0.5328	5.6396
Infinite	8.62812	3.4372	-0.5328	5.6396

Titles of the columns:

(1) The magnitudes of spring constants in pounds/inch of the side supports in the x-direction (that is, KX).

(2) The equivalent Young's modulus in psi of the flat conduit in the y-direction.

(3) The displacement in inches of node 4 (where the level top surface and circular corner surface meet) in the opposite y-direction calculated by assuming only elastic deformation happens under a concentrated load of 2965 pounds acting at node 4.

(4) The displacement in inches of node 10 (which is in the middle of side surface) in the positive x-direction calculated under the same assumptions as in (3).

(5) The displacement in inches of node 3 (which is in the middle of the top surface) in the opposite y-direction calculated under the same assumptions as in (3).

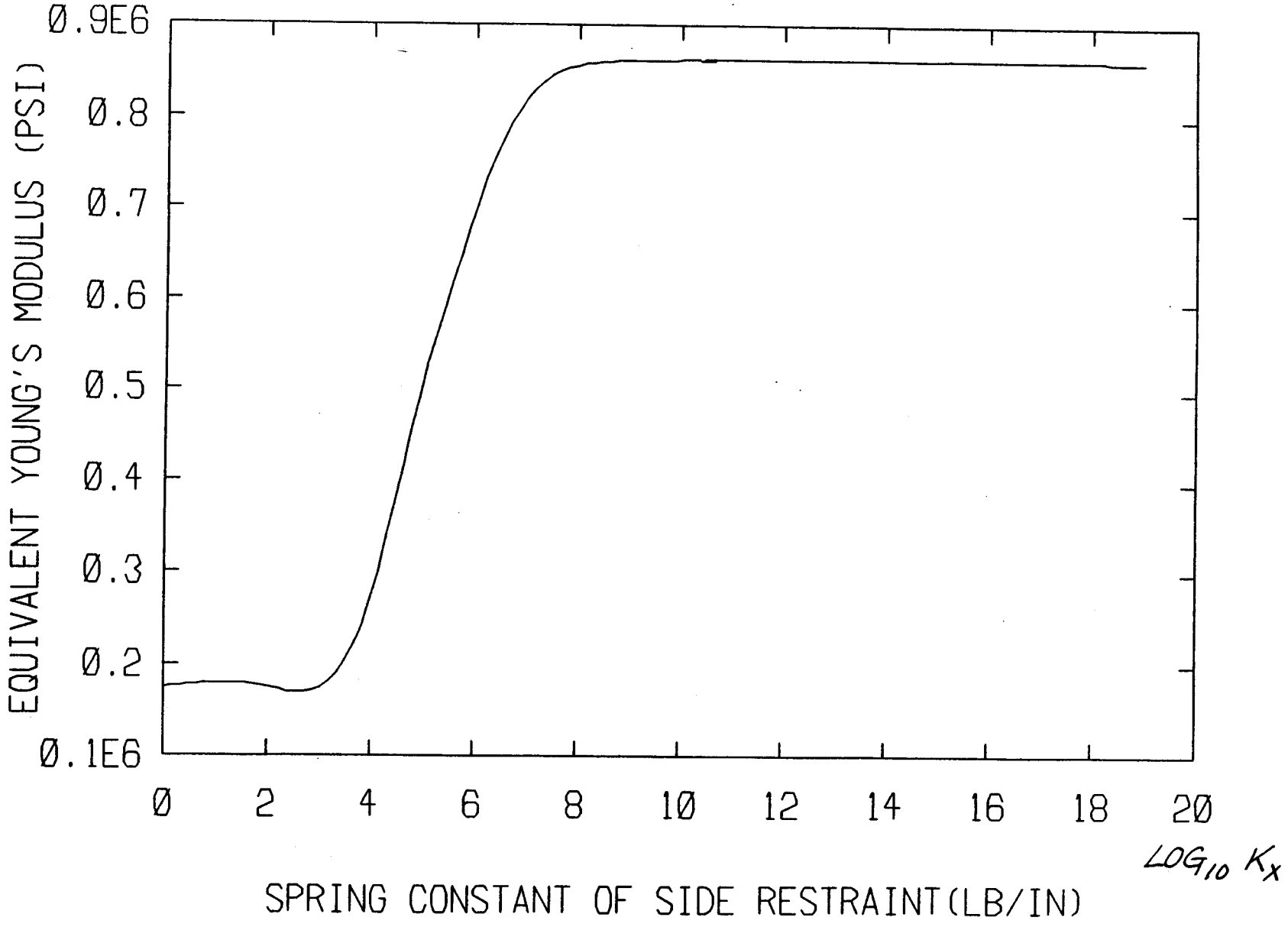

Fig. 43 Variation of Equivalent Young's Modulus with Respect to Spring Constant of Side Restraint

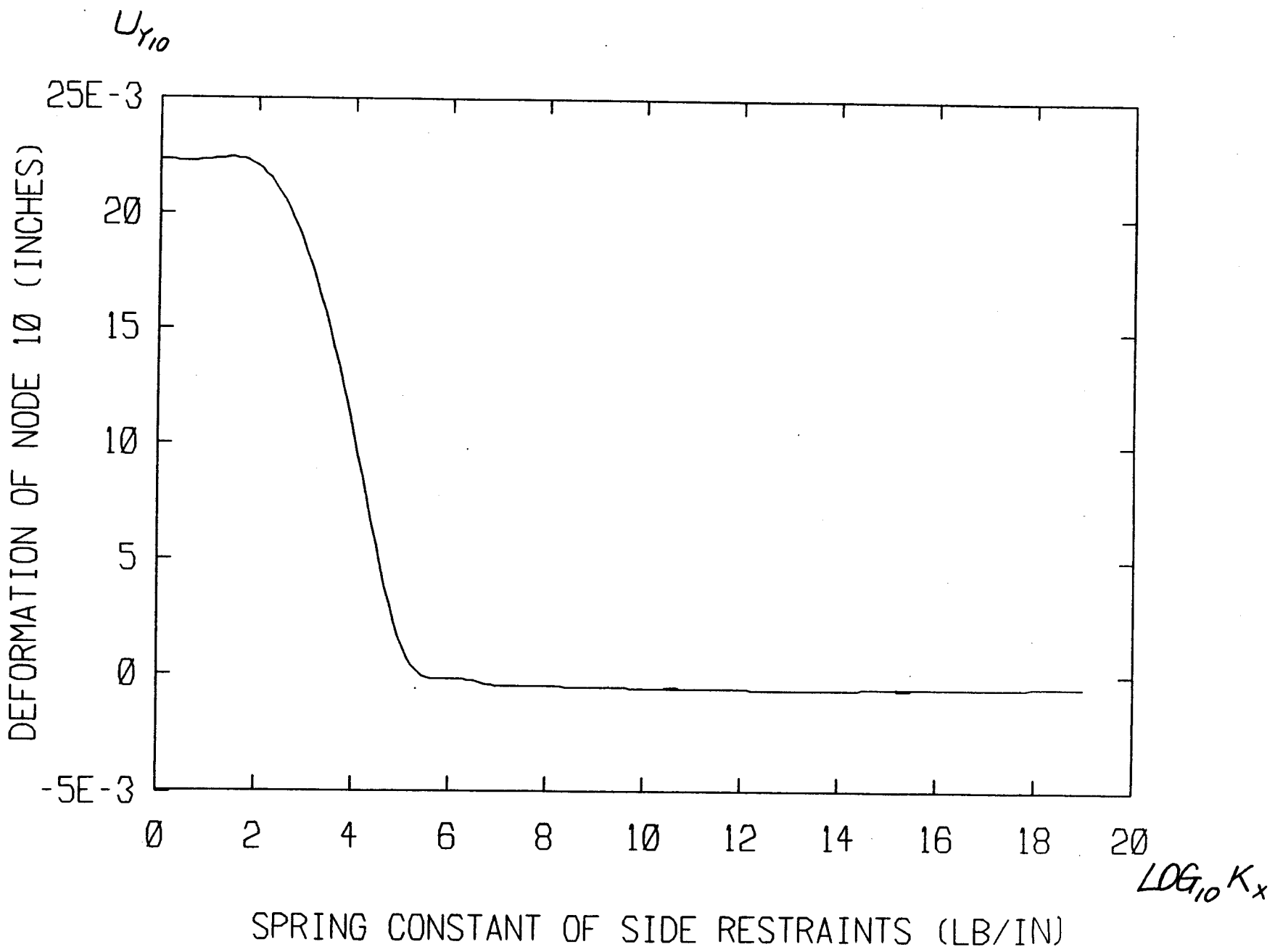

Fig. 44 Influence of the Spring Constant on Deformation of the Node in the Middle of Conductor's Sides

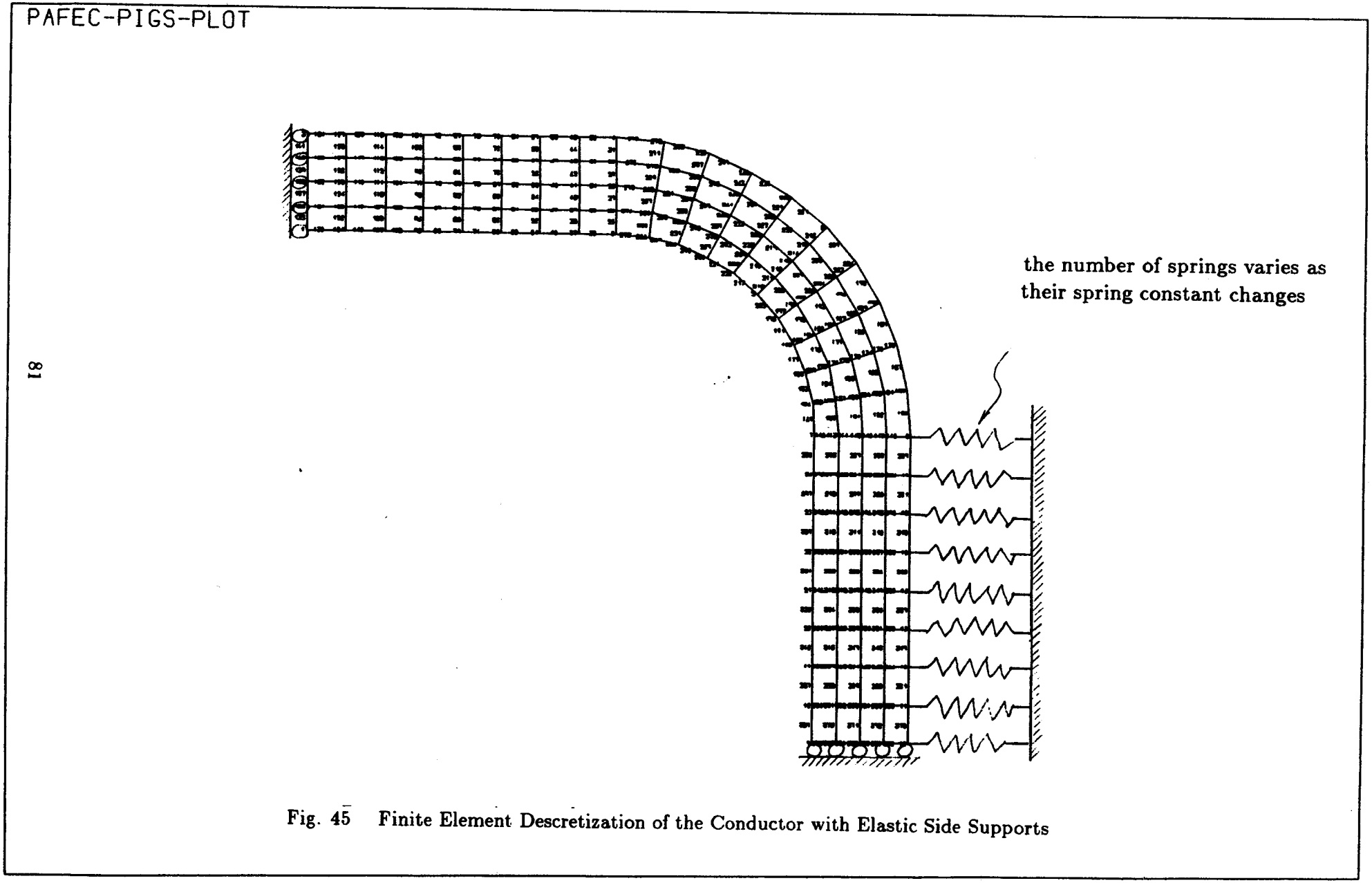

Fig. 45 Finite Element Descretization of the Conductor with Elastic Side Supports

In general, an analysis based on the assumption of rigid side supports would indicate a larger stress but a smaller deformation.

Reanalysis of Loose Conductor with Flexible Side Supports

As mentioned above, the conductor cannot be analyzed without considering the flexibility of the side supports. As a case of interest, the behavior of a conductor was studied under experimental loads and with an experimental set-up. Since the side support of the experimental set-up is a thick beam which is tightened by two bolts, we assume that the equivalent spring constant is between that of the combination of a simply-supported beam held by two tension bars and the combination of a clamped beam held by two tension bars, but closer to the former. Therefore, as an approximation, we take 60% of the stiffness of the former and 40% of the latter and come out with $K_x = 1.73 \times 10^7$ lb/in.

The conductor was analyzed under the same force and displacement boundary conditions as above, except that each side was assumed to be supported by 204 springs instead of being partially fixed. As indicated in Table 7, if the spring constant is below 52,500 lb/in, the conductor will bulge out and a separation between the side support and conductor itself will not occur. Therefore, a steel block with an equivalent spring constant of 17.3×10^6 lb/in and with no Poisson's ratio is used instead of those 204 springs. This not only enables us to do the elastic - plastic analysis (since a spring element would not yield), but also gives an improved result. The finite element model of this analysis is shown in Figure 46.

The results of the analysis are shown in Table 7 and can be summarized as follows:

By comparison to the results obtained by assuming rigid side supports, we find:

(i) The magnitudes of the deformations decrease under the same load.

(ii) The magnitudes of the critical stresses decrease slightly under the same load.

(iii) From (i), the magnitudes of the equivalent tangent moduli decrease under the same load.

Figures 47, 48, and 49 show these contrasts. Figure 50 shows the deformation shape of the conductor for this analysis.

If only the strength of the conductor is of concern, the effect of elastic side supports seems to be negligible. Assuming rigid side supports will yield a more conservative design. However, if the displacement of the conductor is critical, the stiffness of the side supports should be evaluated

Table 7. **The Variation of Equivalent Tangent Modulus of the Flat Conduit with Respect to the Magnitudes of a Concentrated Load at Node 4 Assuming that the Side Support has a Total Equivalent Spring Constant of 1.73E7 Pounds/Inch, the Thickness of the Conduit is 0.0605 Inches and the Yielding Stress of the Conduit is Taken to be 140 ksi**

(1)	(2)	(3)	(4)
	1E+5	1E-3	1E+5
500	6.4350	0.7739	0.388
1000	6.3525	1.5478	0.775
1500	6.1067	2.3232	1.16
2000	5.3059	3.2079	1.47
2500	3.8514	4.2852	1.63
3000	3.1156	5.7880	1.77

Titles of the columns:

(1) The magnitude of a concentrated load in pounds at node 4 in the opposite y-direction.

(2) The equivalent tangent modulus in psi of the flat conduit in the y-direction.

(3) The displacement in inches of node 4 in the opposite y-direction calculated by elastic and plastic analysis under the concentrated load specified in column (1)

(4) The equivalent stress in psi at the most stressed element under the specified load in column (1).

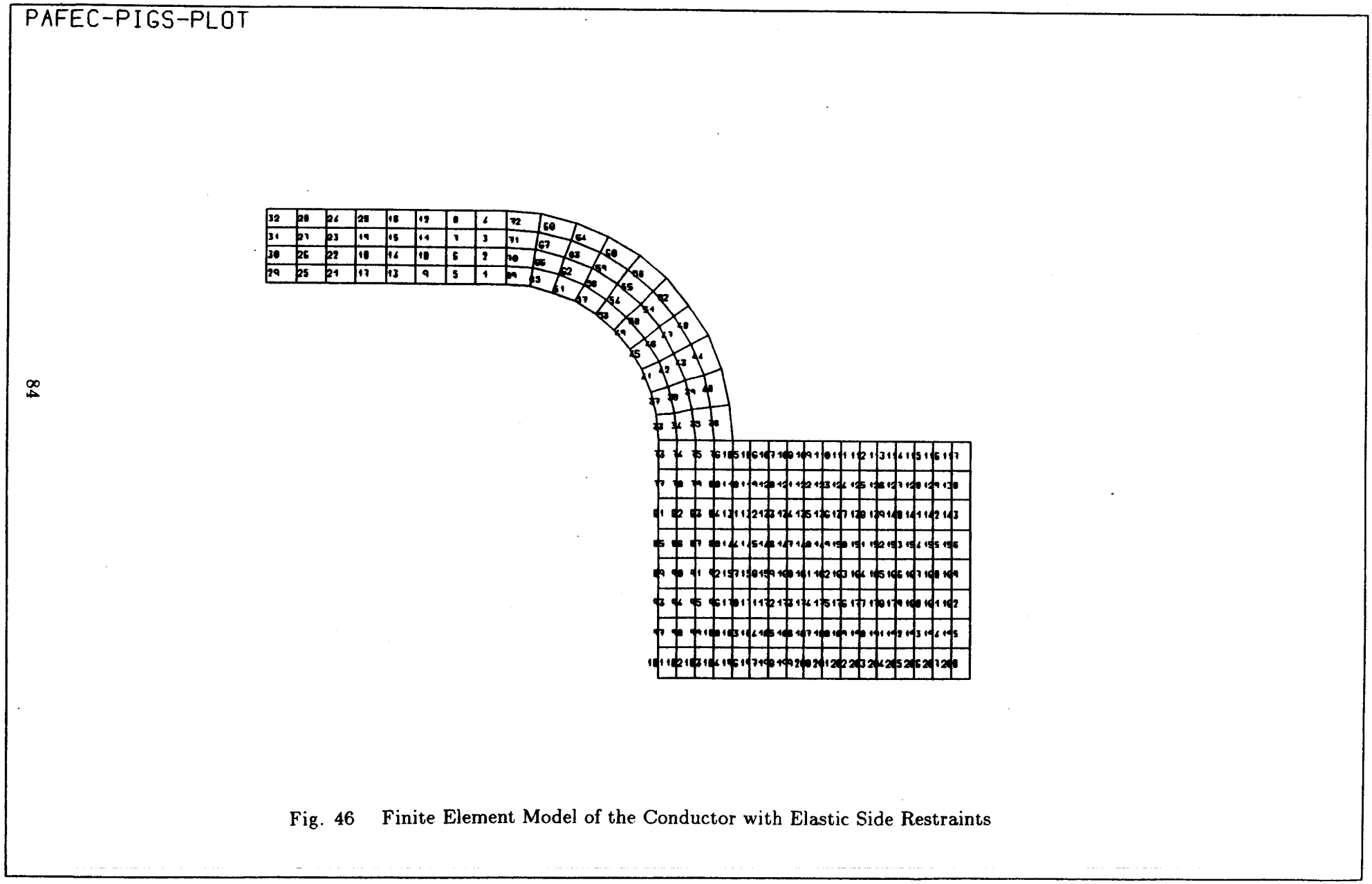

Fig. 46 Finite Element Model of the Conductor with Elastic Side Restraints

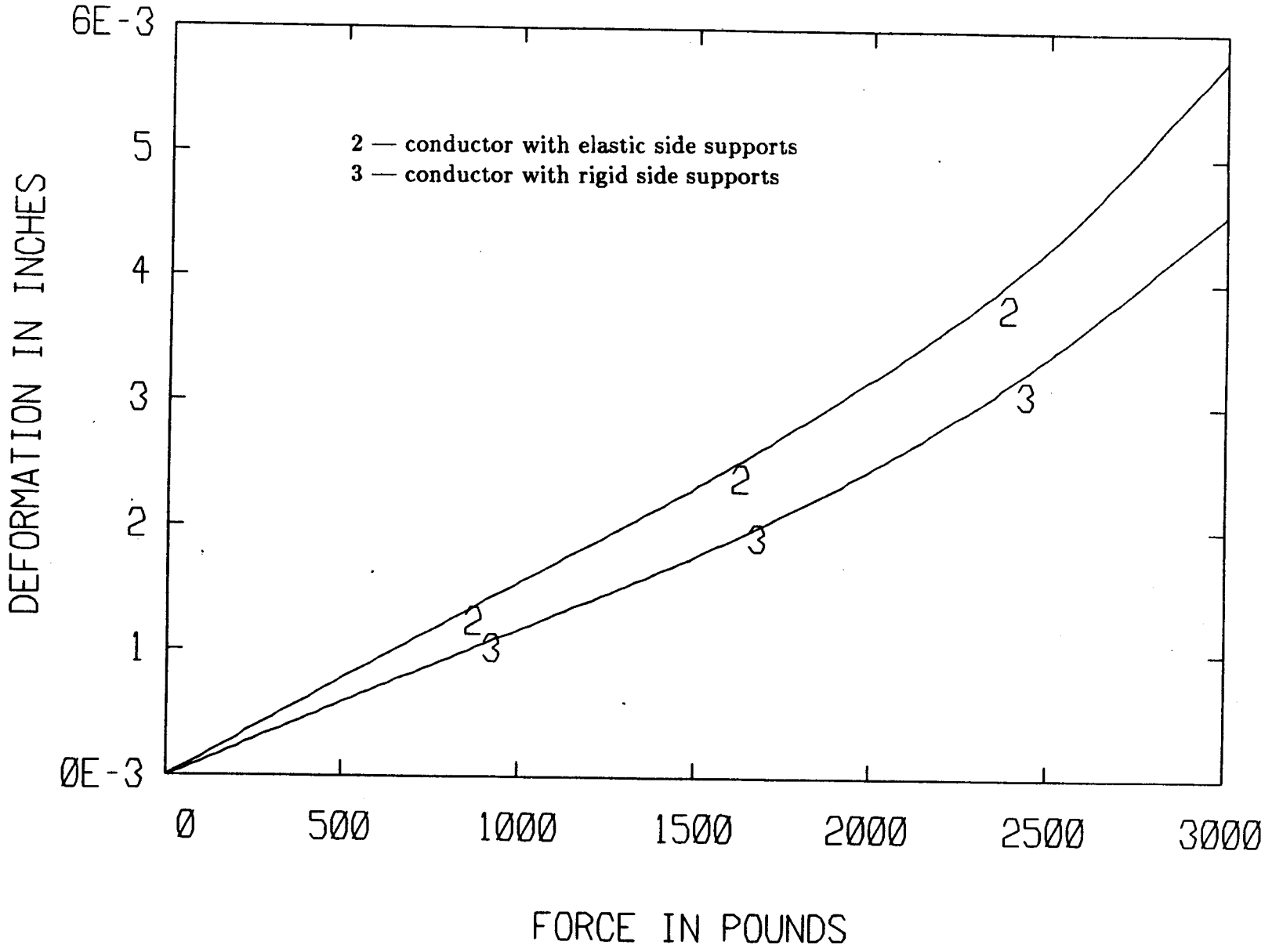

Fig. 47 Effect of Elastic Side Supports on Deformation

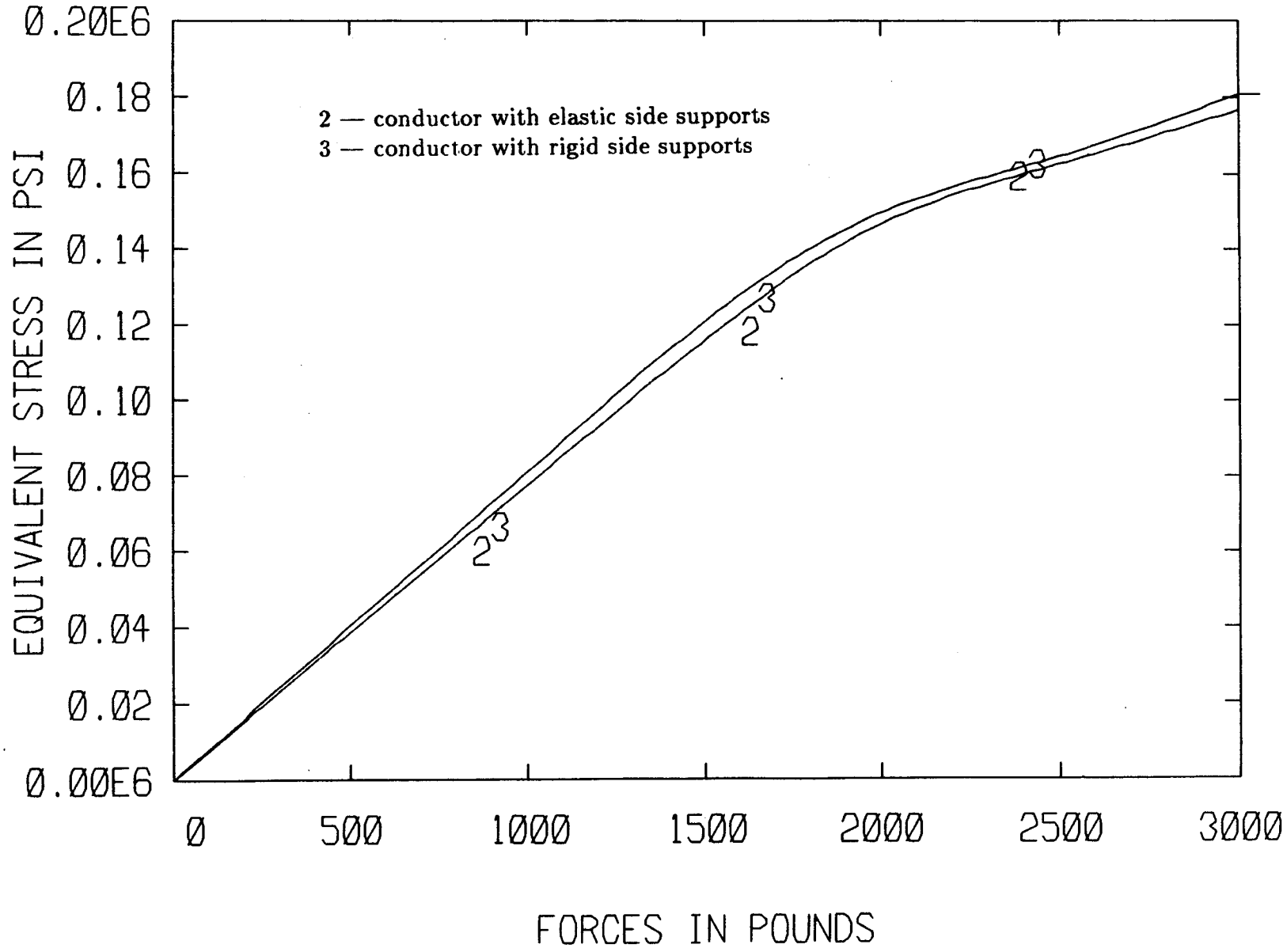

Fig. 48 Effect of Elastic Side Supports on Equivalent Stress

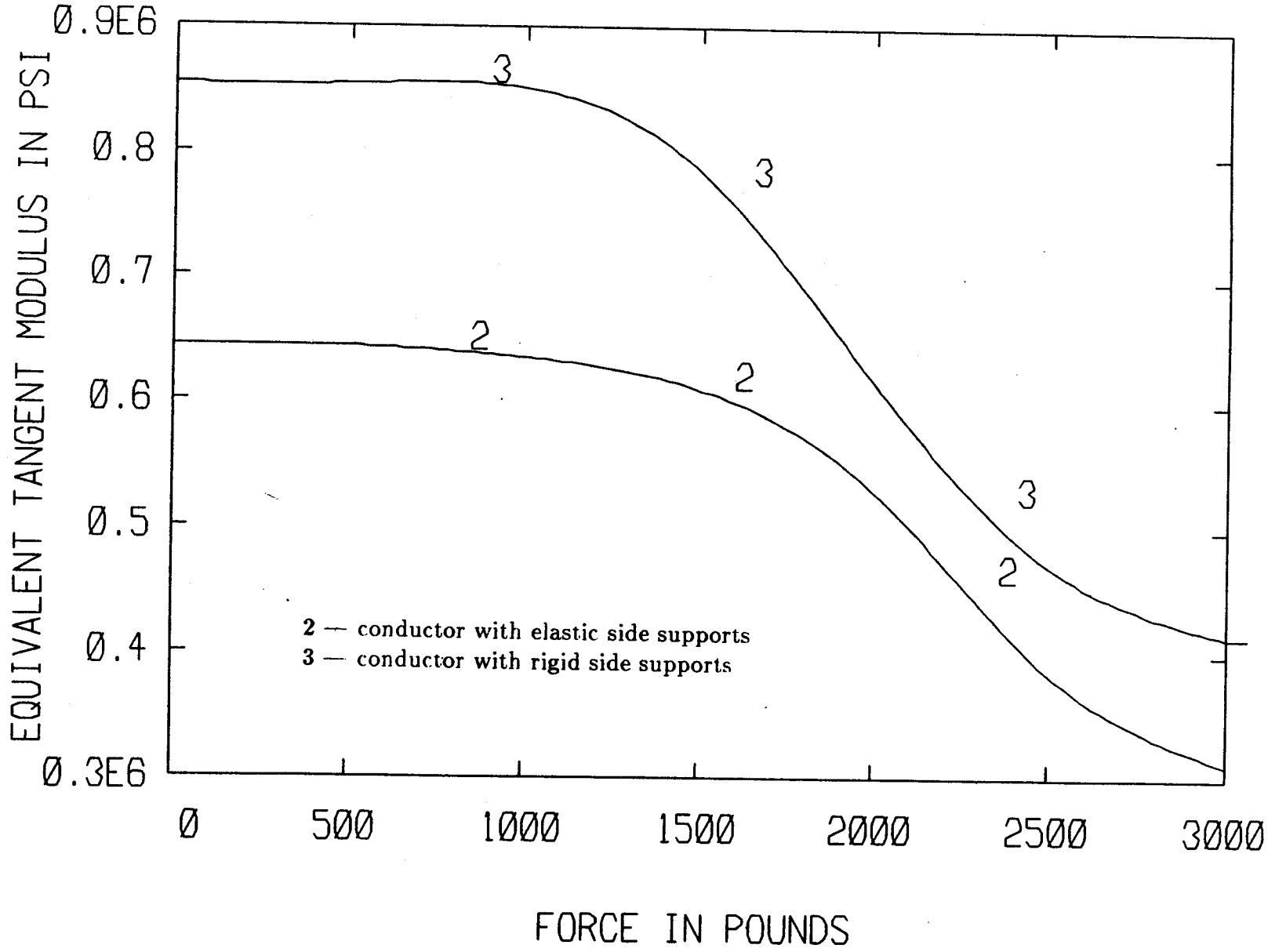

Fig. 49 Effect of Elastic Side Supports on Modulus

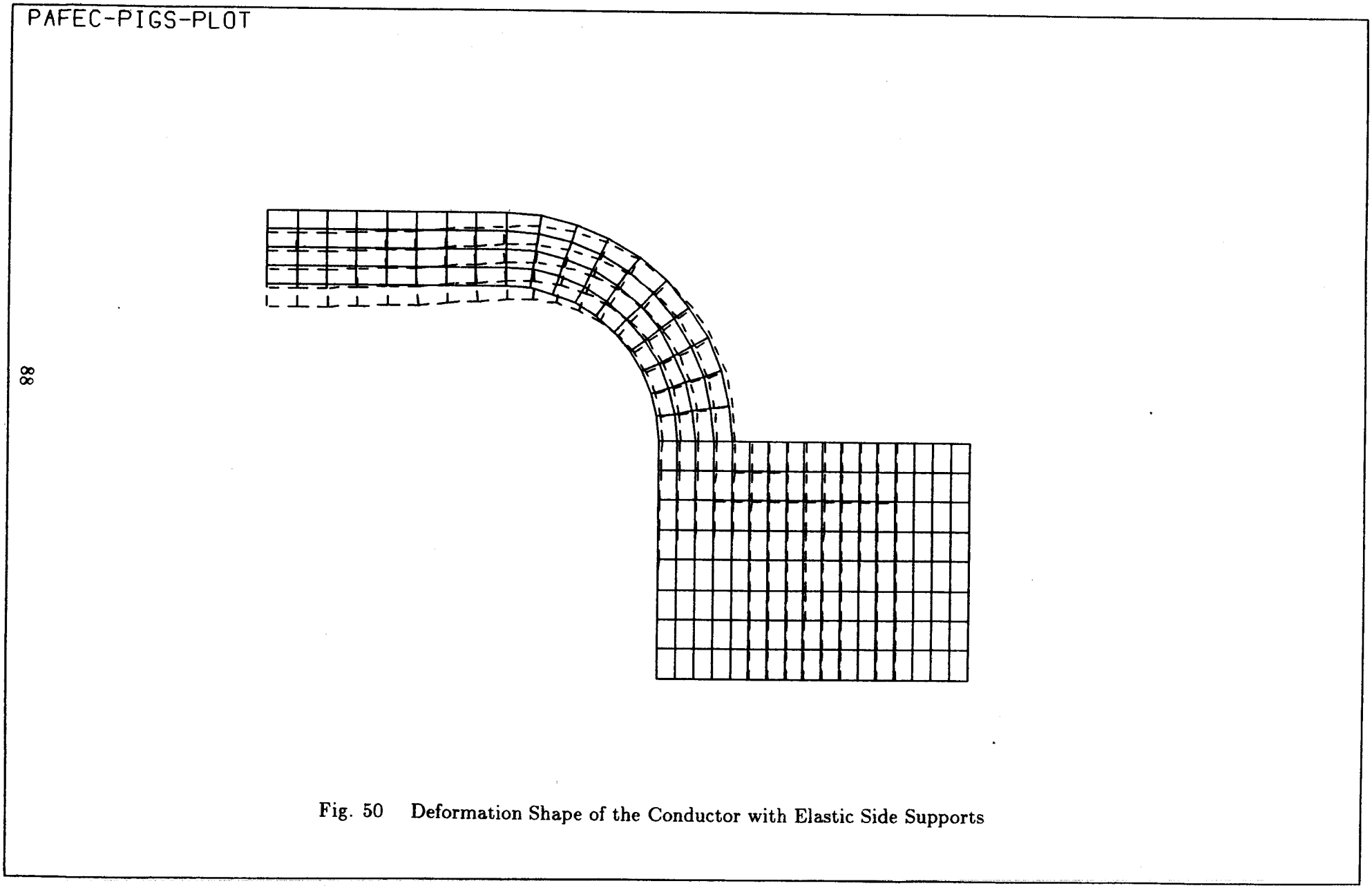

Fig. 50 Deformation Shape of the Conductor with Elastic Side Supports

carefully.

Effect of Increasing Thickness of Loose Conductor

As was shown, the maximum equivalent stresses exceed the yield stress of the stainless steel and the inelastic behavior of the material has to be considered. This is an undesirable feature from the viewpoint of structural design.

It was proposed to increase the conduit thickness to counteract this disadvantage. A study of the conductors with five different thicknesses under a concentrated corner load (at Node 4, Figure 33) of 500 lb was undertaken. Under this load all conductors with different thicknesses behaved within the elastic range. As described previously, the conductor is supported with steel blocks with an equivalent spring constant of 17.3×10^6 lb/in on both sides. The results are depicted in Figures 51, 52, and 53.

From these figures it might be safe to say that:

(i) If the thickness of the conductor increases by a factor of two, both critical stresses (Section C-C in Figure 33) and deformation at the corner node (Node 4) reduce to less than one-half of their original values.

(ii) The equivalent Young's modulus of the conductor is almost a linear function of its thickness.

Analysis of Potted Conductor with Rigid Side Supports

In the earlier calculation, only the bare conductor was analyzed. However, it was found that potting the conductor with epoxy produced a great change in the loading pattern and, consequently, in the behavior of the conductor.

With rigid side supports, the working loads were found to be distributed over a certain portion of the top surface, as was already shown in Figure 36. As elastic analysis indicates that the maximum equivalent stresses are reduced to around 65% of those of a loose conductor and there is no incidence of yielding.

Figure 54 shows the deformed shape of the conductor superimposed on its original shape. The deformation of the loaded area is found to be uniform and has a magnitude of 0.001708 inches in the opposite y-direction under the working load. An equivalent Young's modulus based on this deformation is 1.78 msi, which is more than twice that of a loose conductor (Table 7).

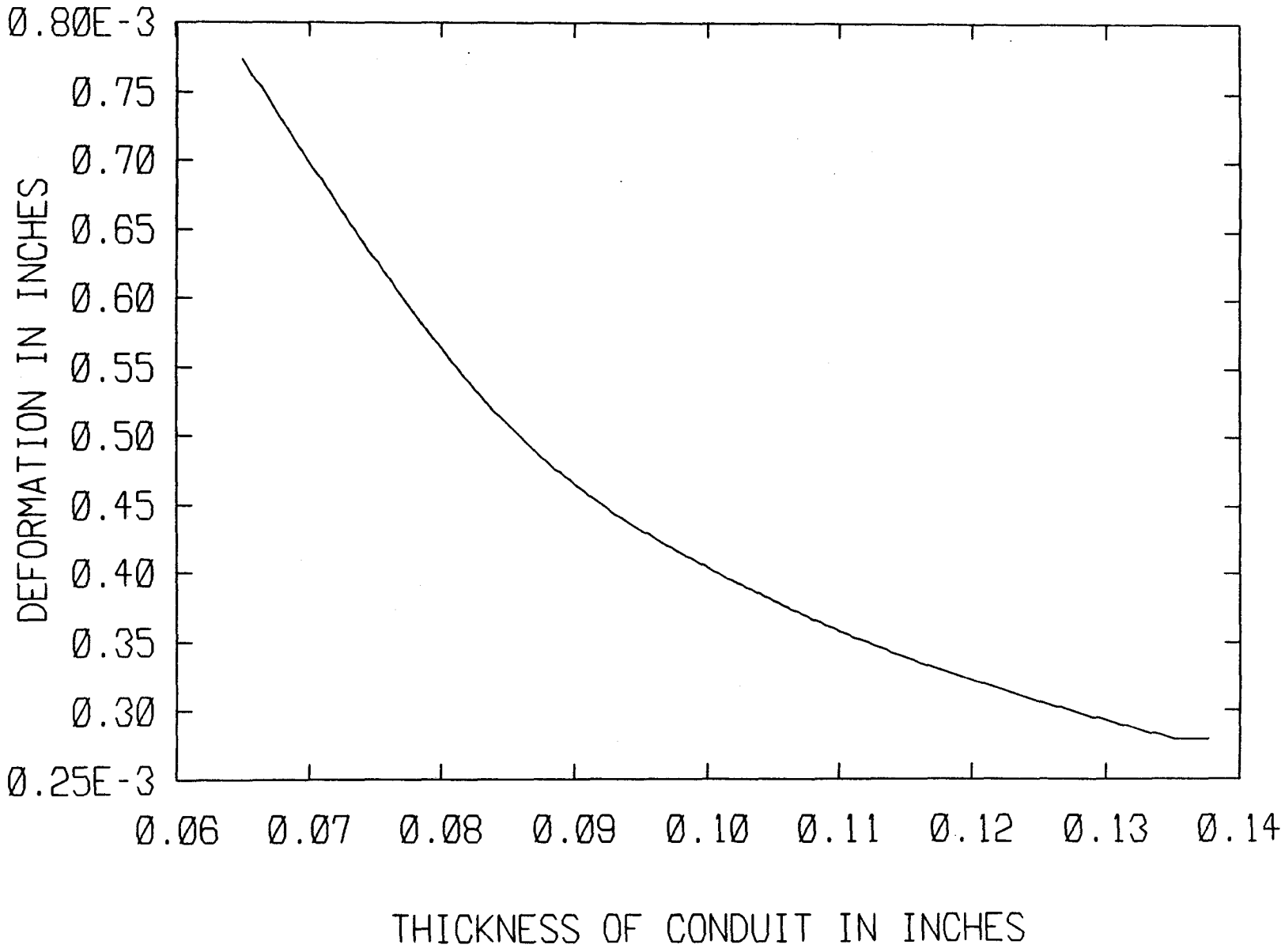

Fig. 51 Thickness Effect on Deformation of Node 4 Under a Concentrated Load of 500 Pounds at the Same Node

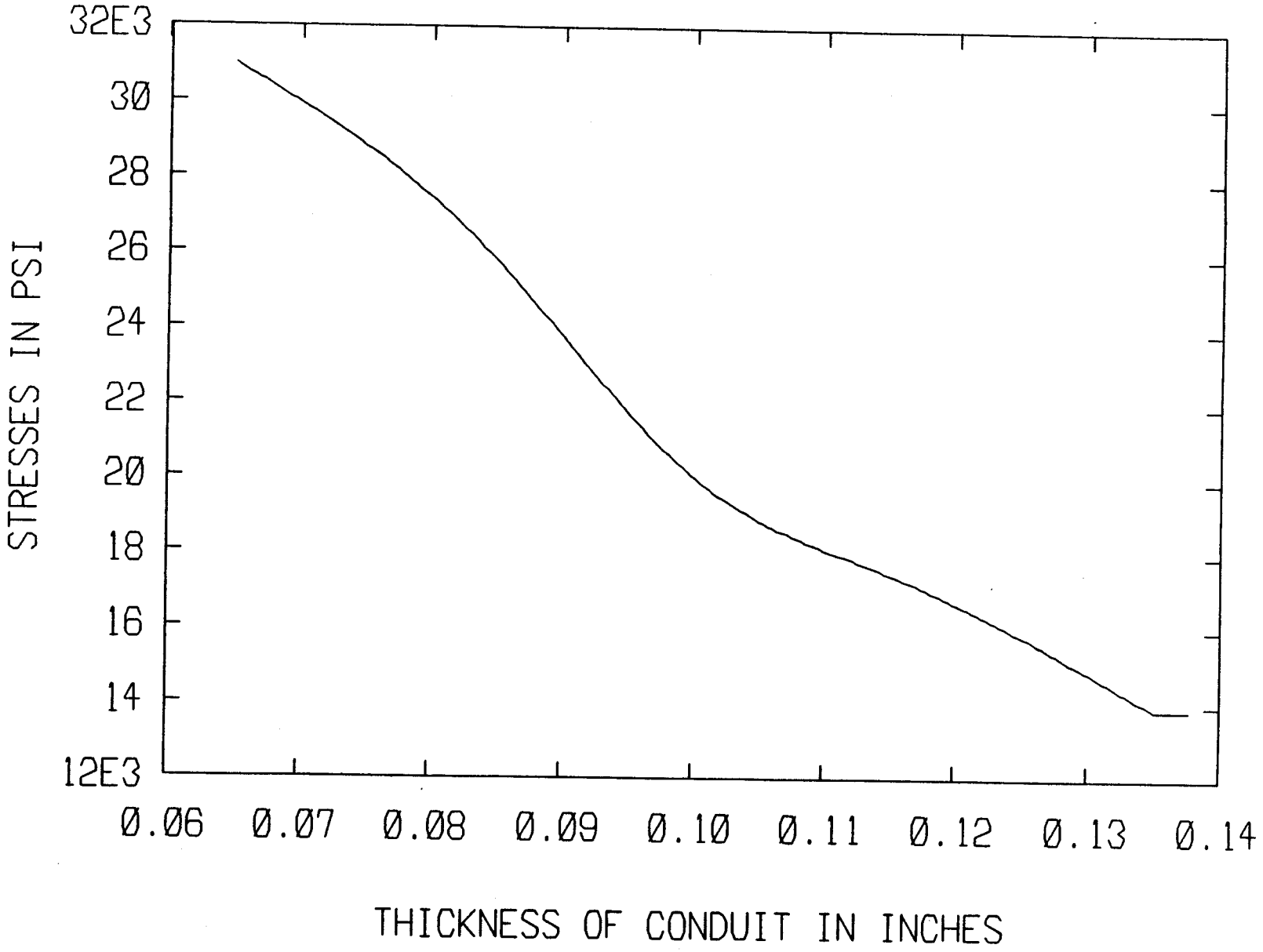

Fig. 52 Thickness Effect on Principal Stress at Critical Section Under a Concentrated Load of 500 Pounds

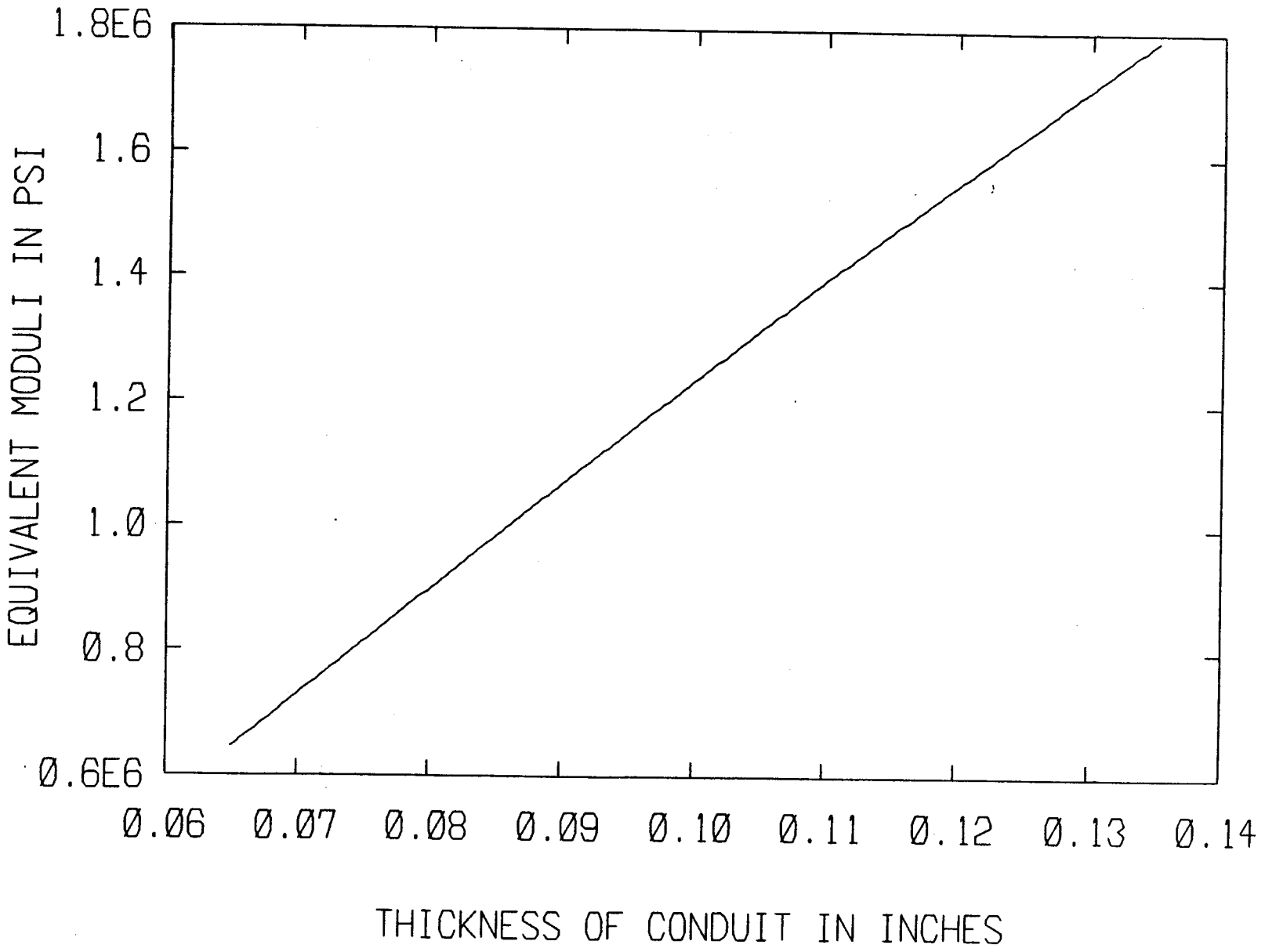

Fig. 53 Thickness Effect on Equivalent Modulus

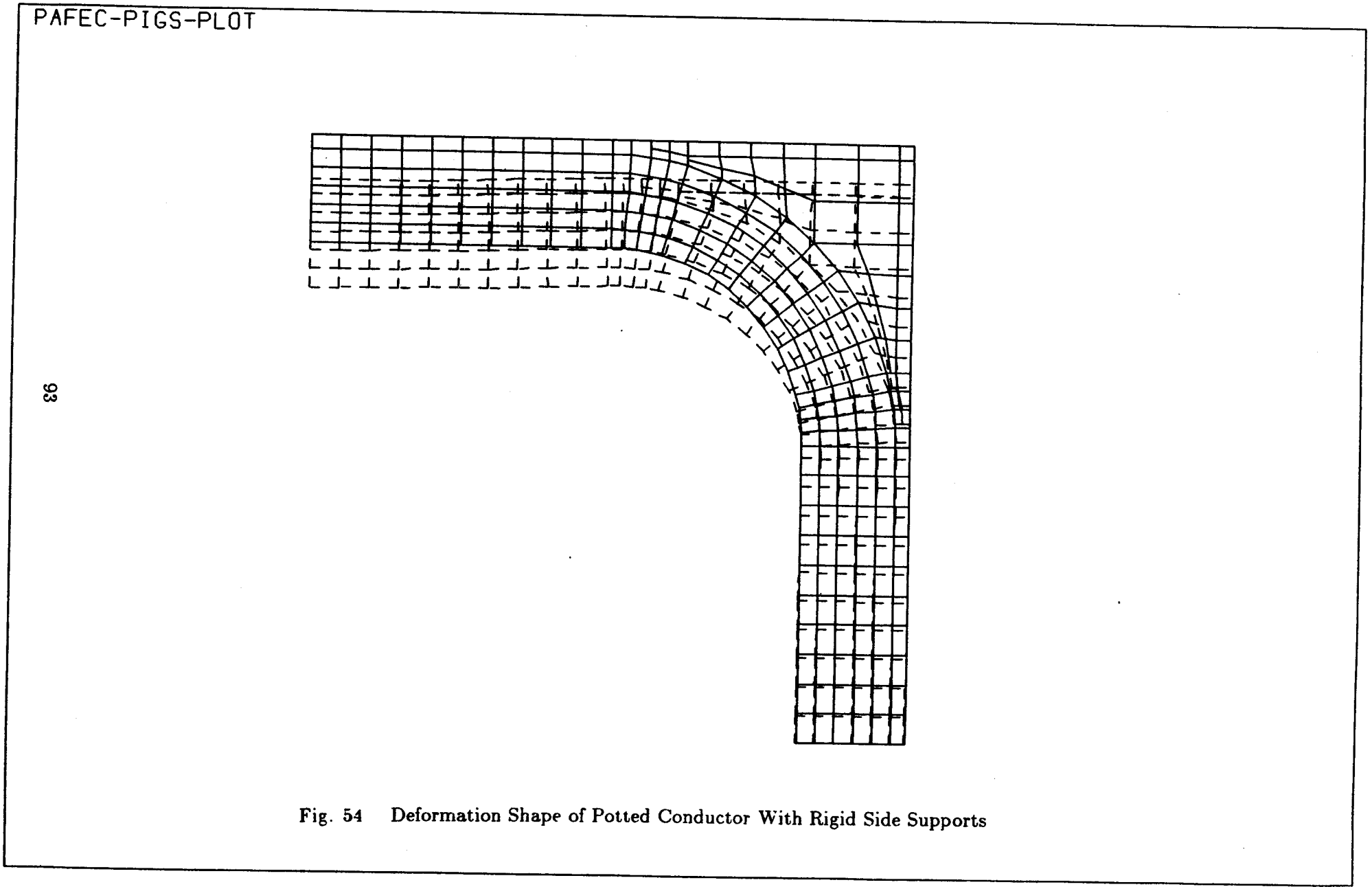

Fig. 54 Deformation Shape of Potted Conductor With Rigid Side Supports

The maximum principal stress contours, the minimum principal stress contours and the Von Mises stress contours of this analysis are shown in Figures 55, 56, and 57, respectively. It is evident from these figures that the critical section has changed from Section C-C in Figure 33 for a loose conductor to that for a potted one in Figure 35.

The largest minimum principal stress is found to be 0.125×10^6 psi. Figure 58 shows the principal stress distribution across the critical section.

As seen in this analysis, the epoxy potting not only insulates, but also has the following effects on the behavior of the conductor:

(i) It serves to break the concentrated load down (as in the case of a loose conductor) and redistributes it more evenly across the loaded area, thus reducing the magnitude of the peak load and, consequently, the magnitudes of the critical stresses.

(ii) For the same reason, the maximum deformation is also reduced and as a result the equivalent Young's modulus of the conductor increases.

(iii) Since the loading pattern is changed by potting, the maximum principal stresses occur in different places from that of the loose conductor.

Effect of Stiff Insulation

In this analysis, the Young's modulus of the insulation (the epoxy) is increased from 0.6 msi to 3 msi. The side supports are assumed rigid.

The maximum principal stress contours, the minimum principal stress contours, and the Von Mises stress contours of this analysis are shown in Figures 59, 60, and 61, respectively.

The deformation of the loaded area is again uniform and has a magnitude of 0.000905 inches in the opposite y-direction. By dividing the working pressure with the strain calculated from this deformation, an equivalent Young's modulus of 3.36 msi for the potted conductor is obtained. The deformed shape is shown in Figure 62.

The use of an insulation material with a higher Young's modulus has two advantages:

(i) Both the loading and its peak are shifted towards the corners, as shown in an enlarged view in Figure 63. The bending stresses are therefore greatly reduced and so are the principal stresses.

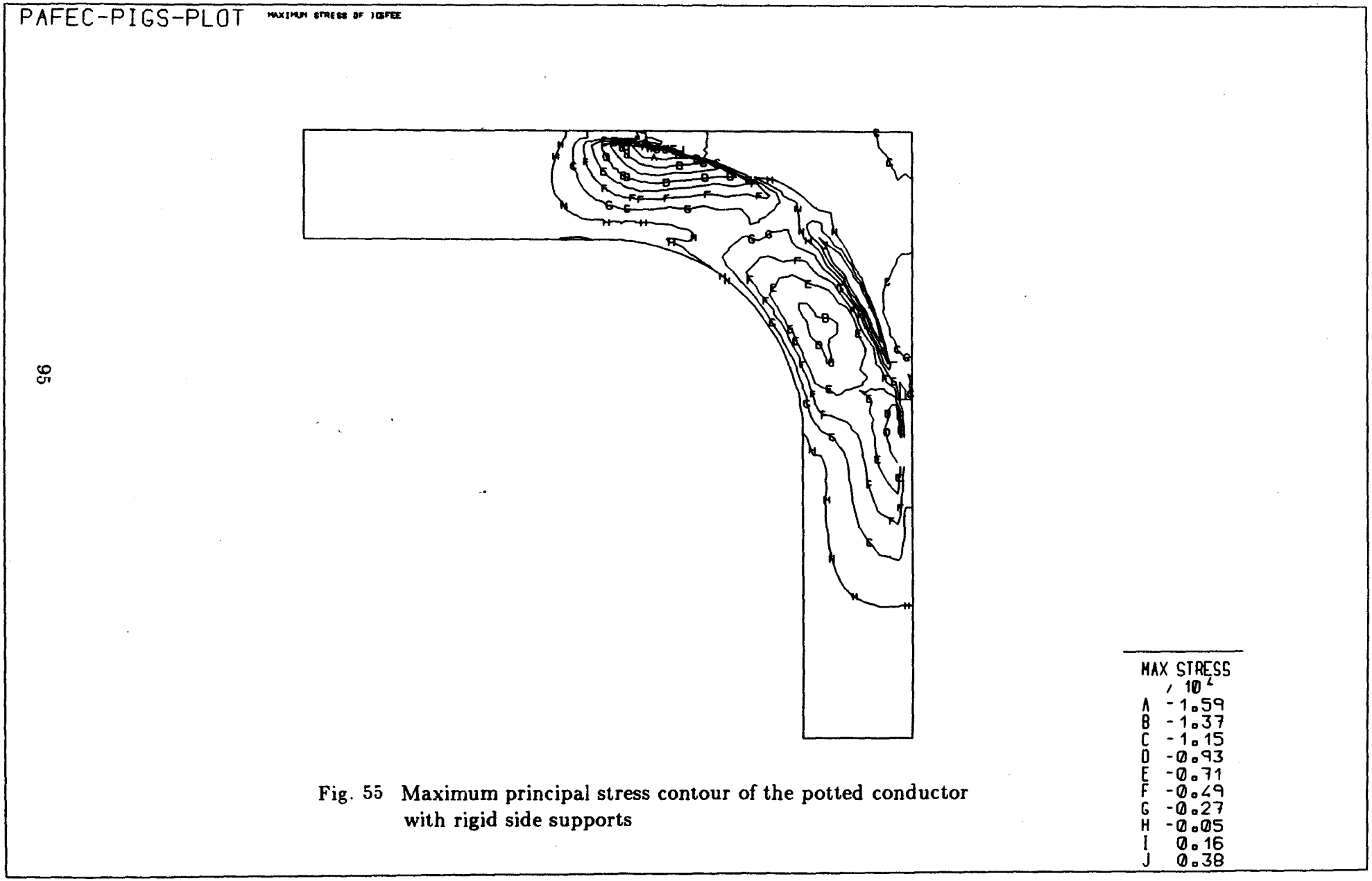

Fig. 55 Maximum principal stress contour of the potted conductor with rigid side supports

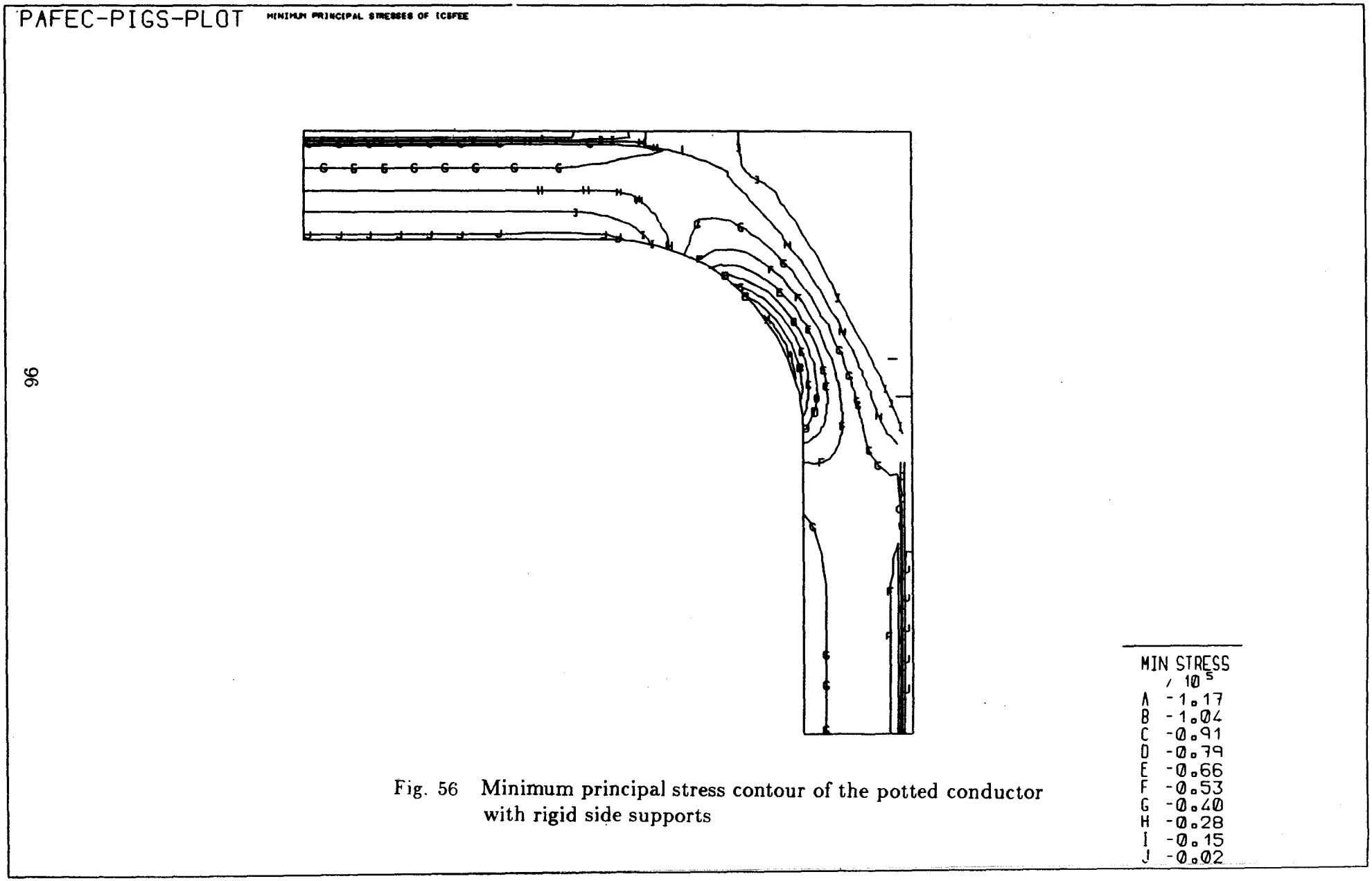

Fig. 56 Minimum principal stress contour of the potted conductor with rigid side supports

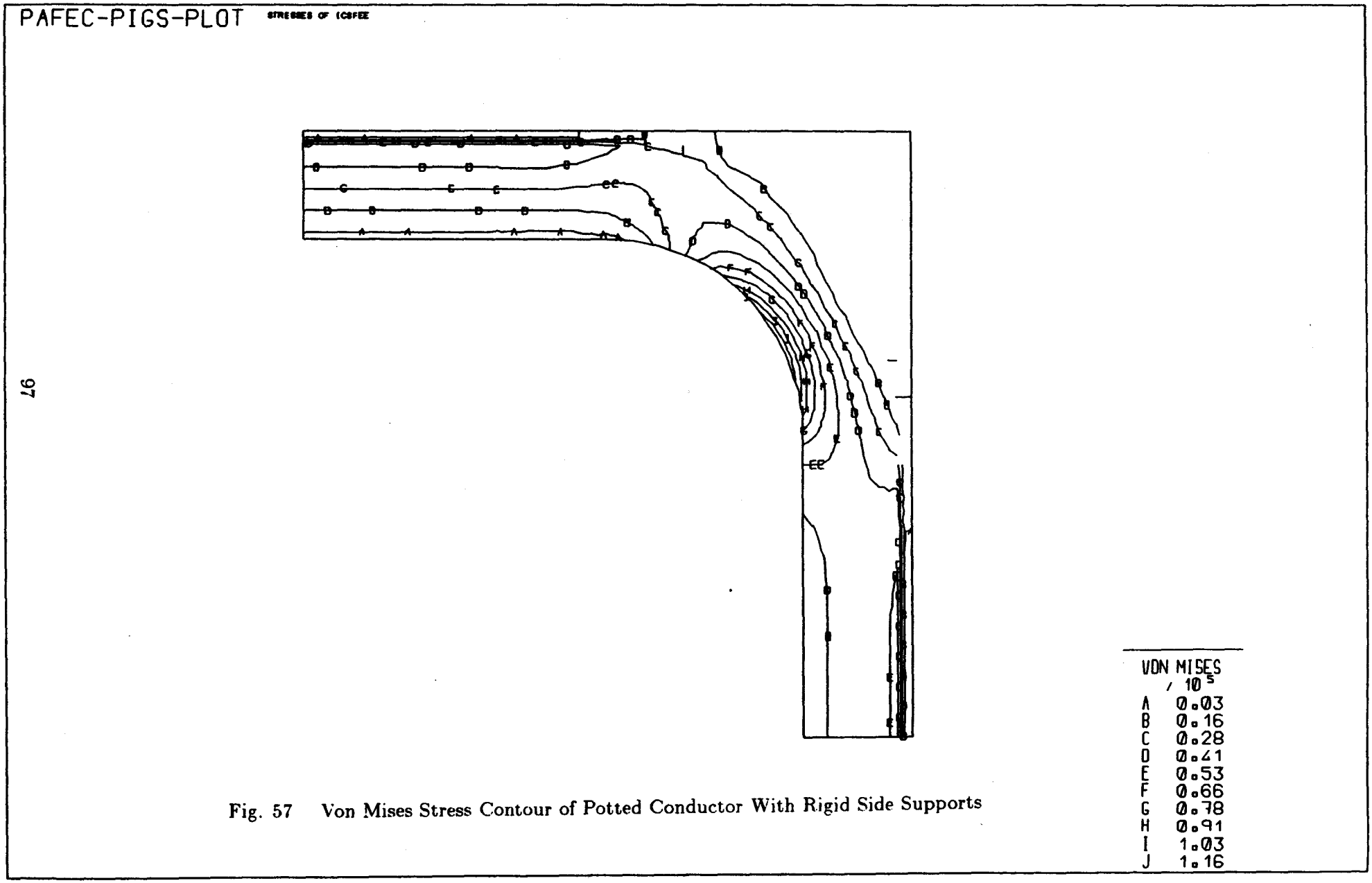

Fig. 57 Von Mises Stress Contour of Potted Conductor With Rigid Side Supports

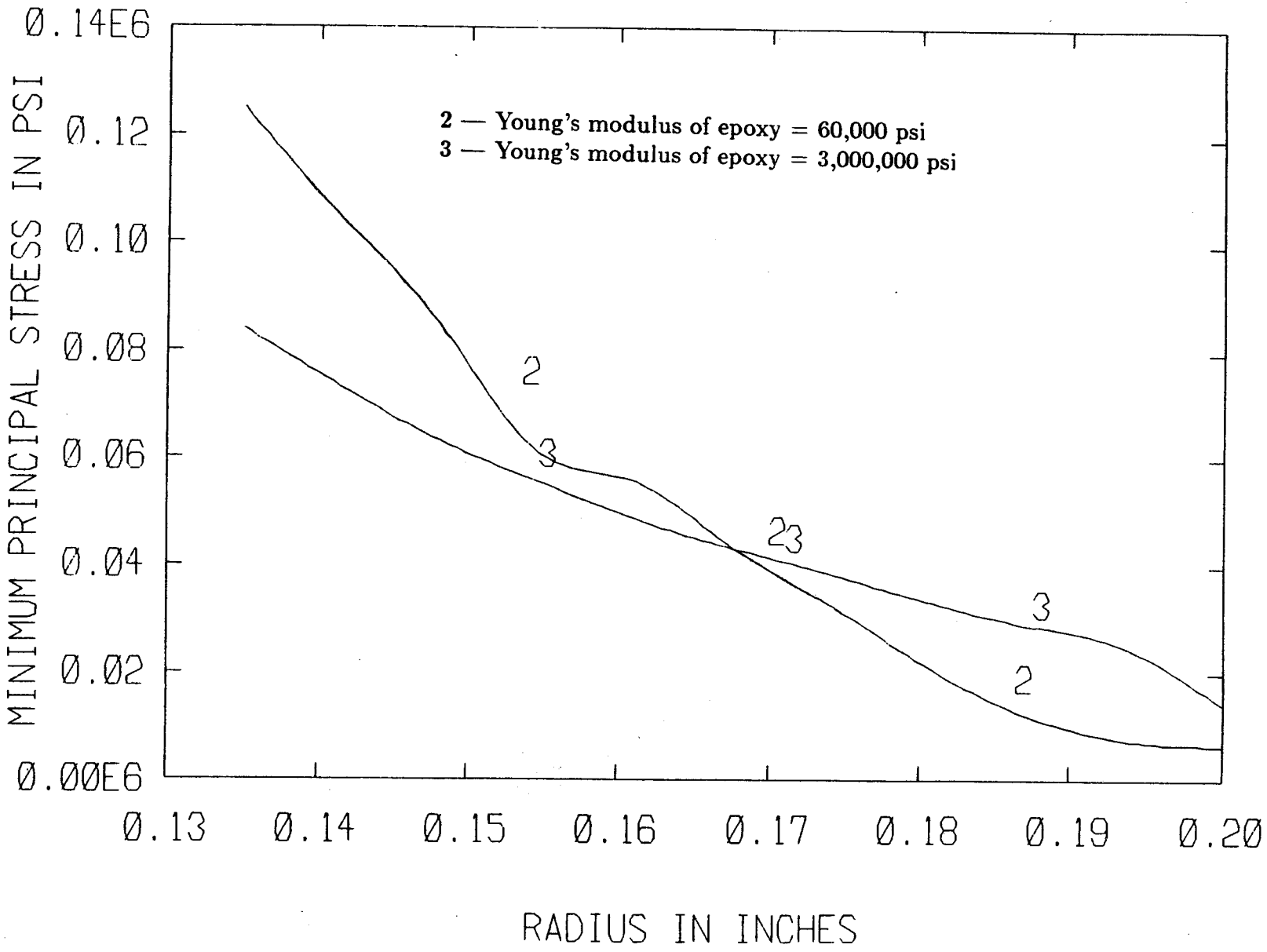

Fig. 58 Variation of Minimum Principal Stress Across Critical Section of Potted Conductor

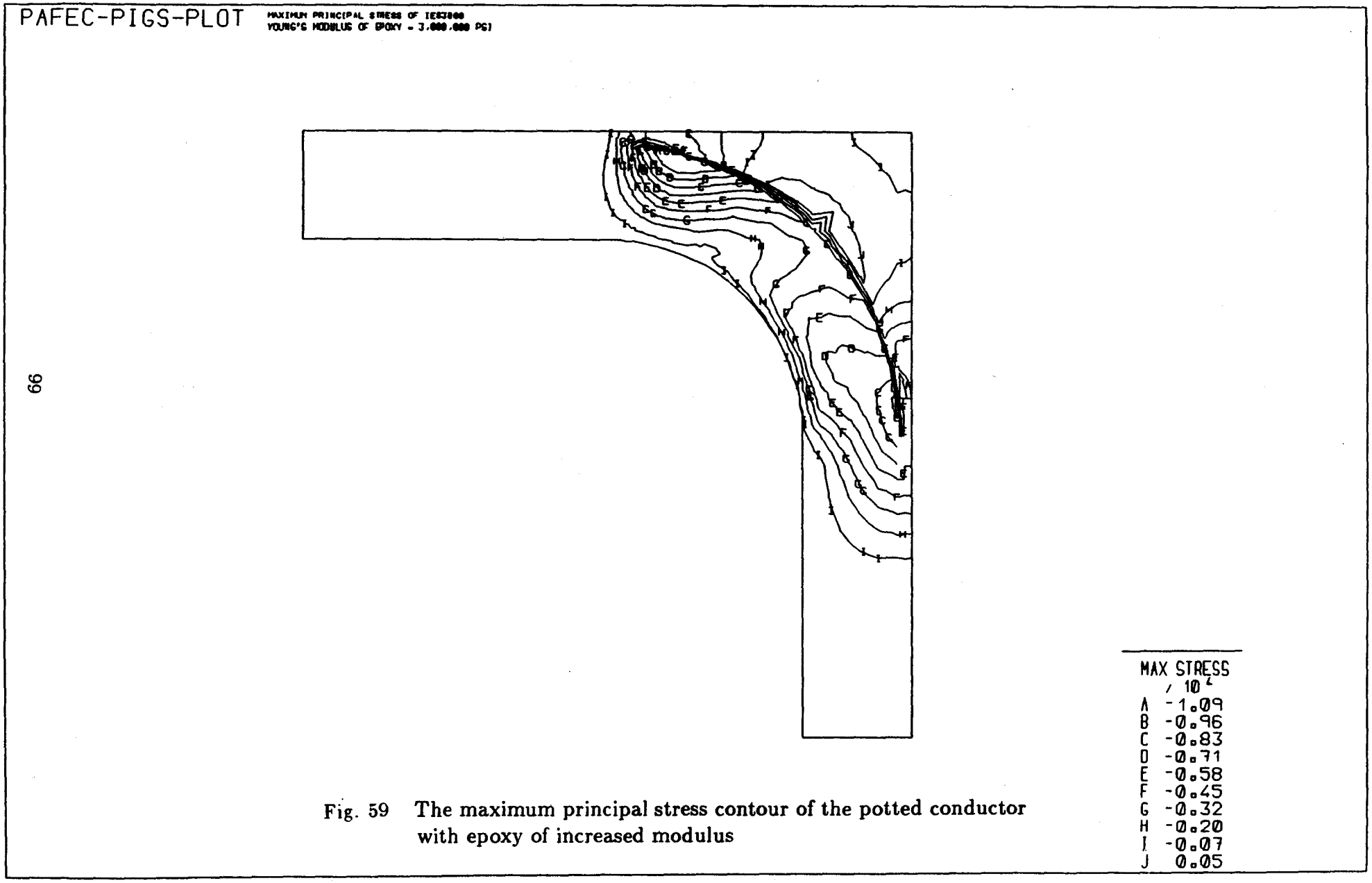

Fig. 59 The maximum principal stress contour of the potted conductor with epoxy of increased modulus

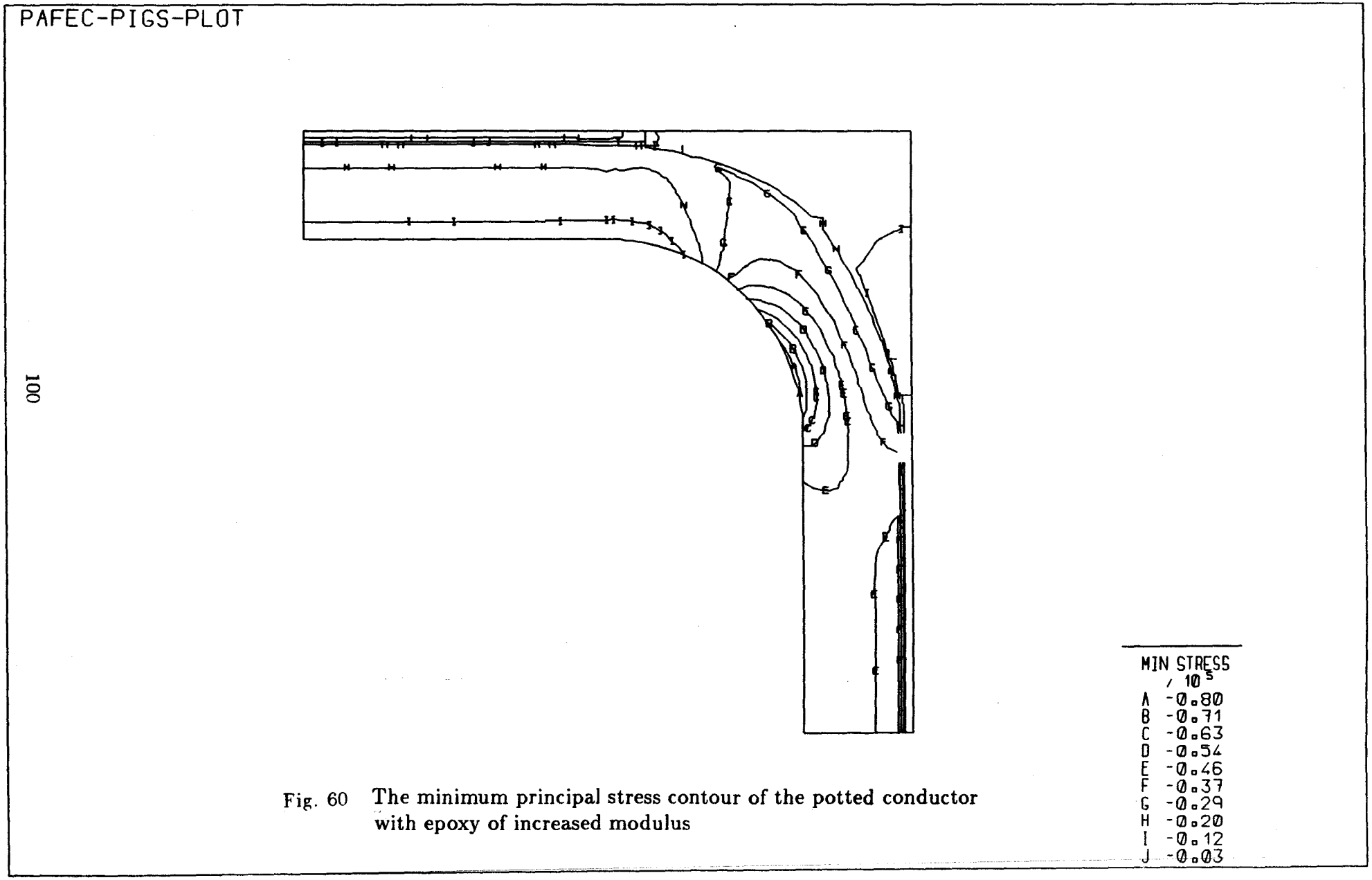

Fig. 60 The minimum principal stress contour of the potted conductor with epoxy of increased modulus

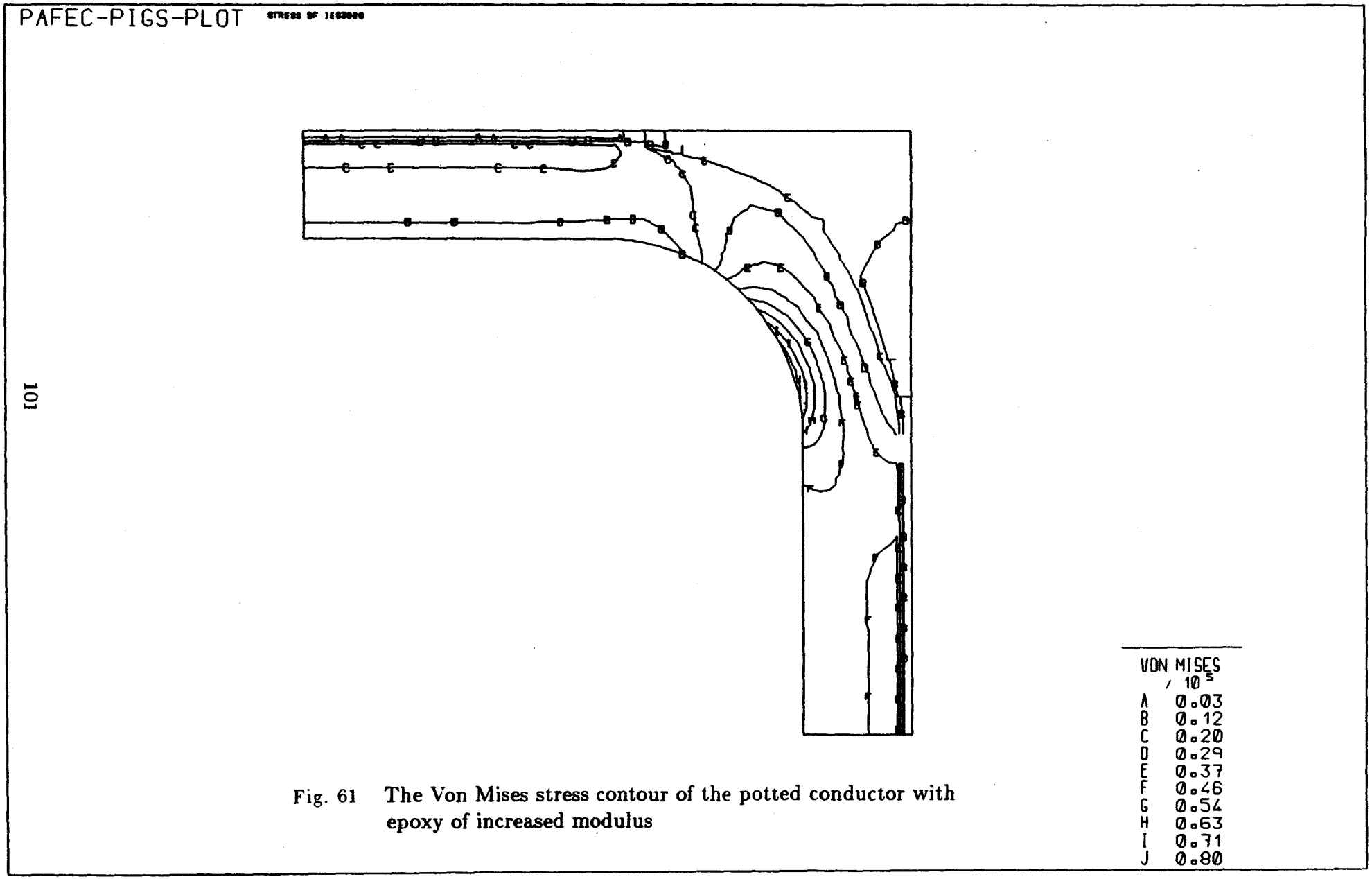

Fig. 61 The Von Mises stress contour of the potted conductor with epoxy of increased modulus

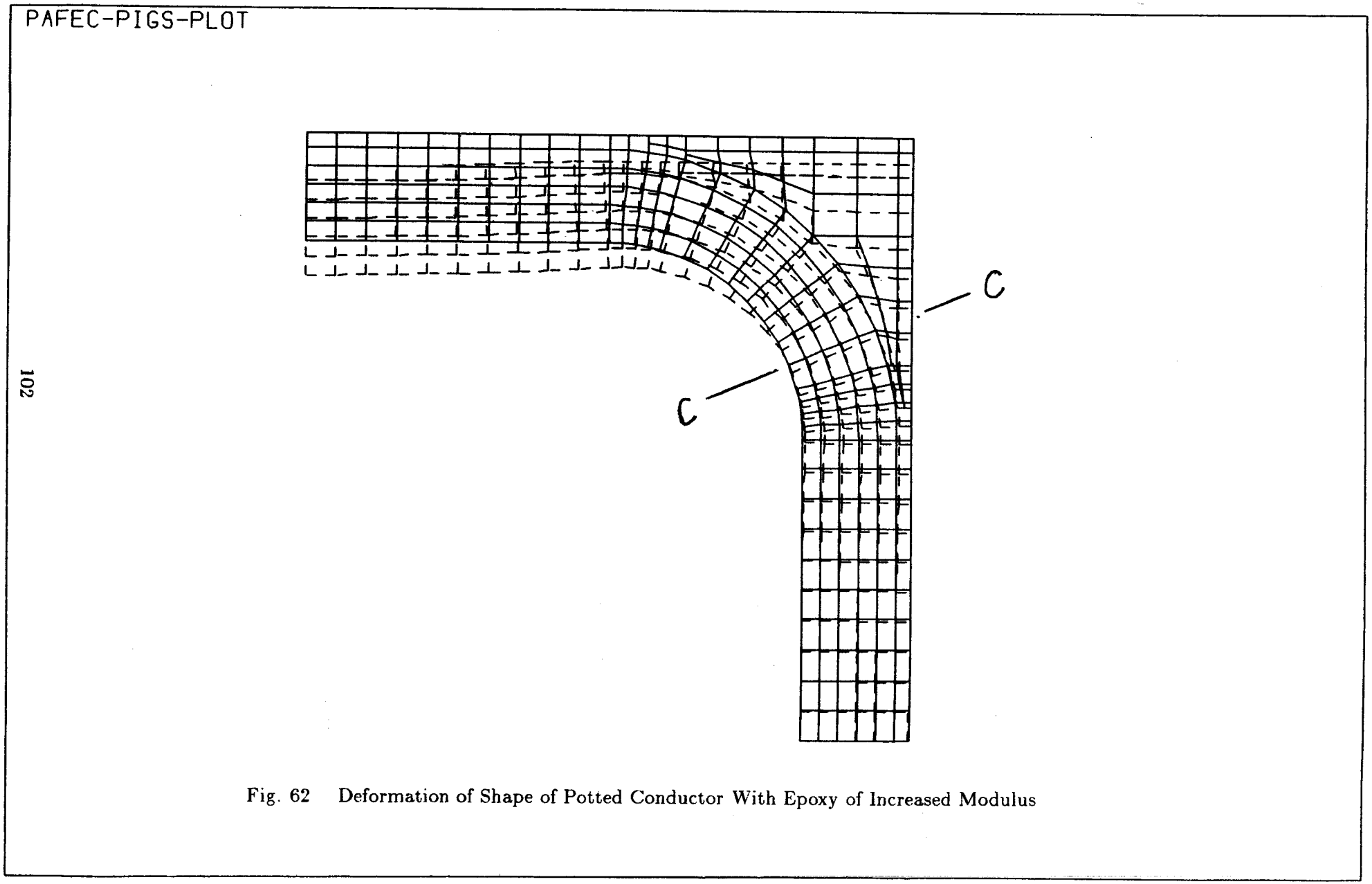

Fig. 62 Deformation of Shape of Potted Conductor With Epoxy of Increased Modulus

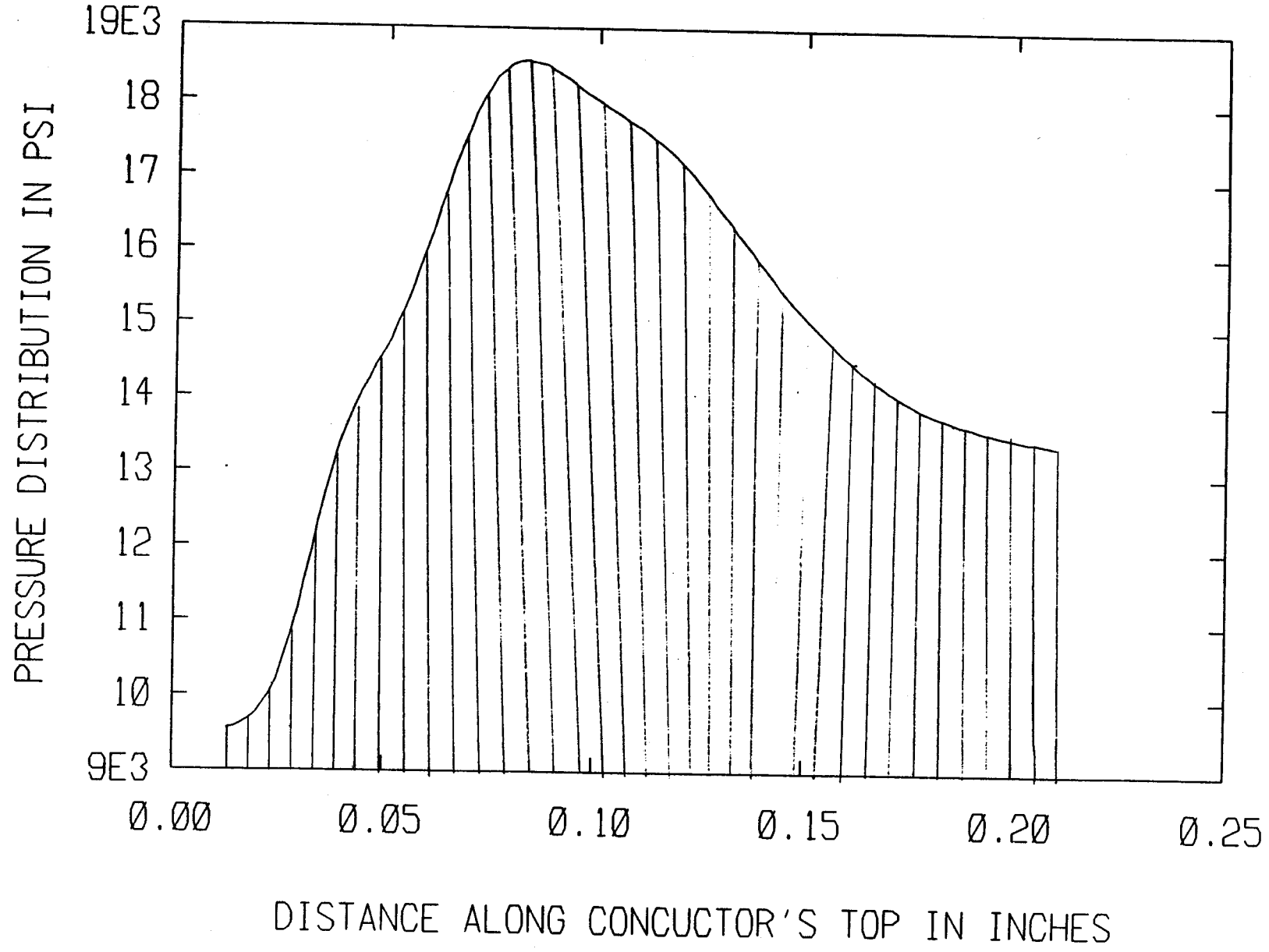

Fig. 63 Load Distribution on Top Surface of Potted Conductor With Insulation of Increased Young's Modulus

(ii) The deformation is also reduced due both to the fact that the conductor is in a more compressive mode and to the increase in the Young's modulus of the epoxy.

The position of the critical section, as shown in Figure 62, is also shifted to a lower plane compared with that of the previous section. The largest minimum principal stress is 0.841×10^5 psi (Table 8). The variation of the minimum principal stress across this section is shown in curve 3 of Figure 58 which shows a more even distribution of the stress. This curve, together with Figure 63, provides the evidence to support the statement made in (ii) of this section that the conductor is in a more compressive mode than that of the previous section.

Effect of Increased Potting Thickness

The thickness of the epoxy is increased from 0.01 inch to 0.02 inch in the middle of the plane of the conductor (Figure 31). The side supports are again assumed rigid.

The loading produces a uniform deformation of 0.001976 inch in the opposite y-direction of the area it acts on. The minimum principal stress occurs at the critical section, c, of Figure 64 and its largest value is 0.13×10^6 psi.

The minimum principal stress contours, the maximum principal stress contours, and the Von Mises stress contours are shown in Figures 65, 66, and 67, respectively. Basically, increasing the thickness of the epoxy produces little effect on either the magnitudes of the deformations or those of the critical stresses.

Reanalysis of Potted Conductor with Flexible Side Supports

The conductor was reanalyzed as above, but with flexible side supports with a stiffness equal to that of the experimental setup. The loading pattern is very similar to that in Figure 36. The results are higher deformations and slightly lower critical stresses, as for a loose conduit.

The critical values of the results are given in Table 9, while the deformation shape and stress contours are given in Figure 68 and Figures 69 - 71, respectively.

Conclusions

The behavior of the conductor under a working pressure of 7250 psi with different supporting and potting systems is summarized in Table 9. The following conclusions are drawn:

(1) The elasticity of side restraints increases the magnitudes of deformations, but has little effect on decreasing the magnitudes of critical stresses.

Table 8. **Stresses Across the Critical Section**

(1)	(2)	(3)	(4)	(5)
0.135	0.186E6	0.188E6	0.125E6	0.841E5
0.142	NA	NA	0.103E6	0.723E5
0.1479	).170E6	NA	0.855E5	0.633E5
0.1512	NA	0.170E6	NA	NA
0.1547	NA	NA	0.609E5	0.555E5
0.1606	0.149E6	NA	0.561E5	0.491E5
0.1675	NA	0.866E5	0.436E5	0.433E5
0.1743	0.150E5	NA	0.323E5	0.383E5
0.1803	NA	NA	0.217E5	0.335E5
0.1838	NA	0.656E5	NA	NA
0.1871	0.831E5	NA	0.123E5	0.290E5
0.1938	NA	NA	0.762E4	0.247E5
0.2	0.161E6	0.166E6	0.661E4	0.141E5

Titles of columns:

(1) Radius in inches.

(2) Equivalent stress in psi at nodes across the critical section of the loose, rigidly side-supported conductor.

(3) Equivalent stress in psi at nodes across the critical section of the loose, elastically side-supported conductor.

(4) Same as in (4) except the Young's modulus of epoxy is increased to 3,000,000 psi.

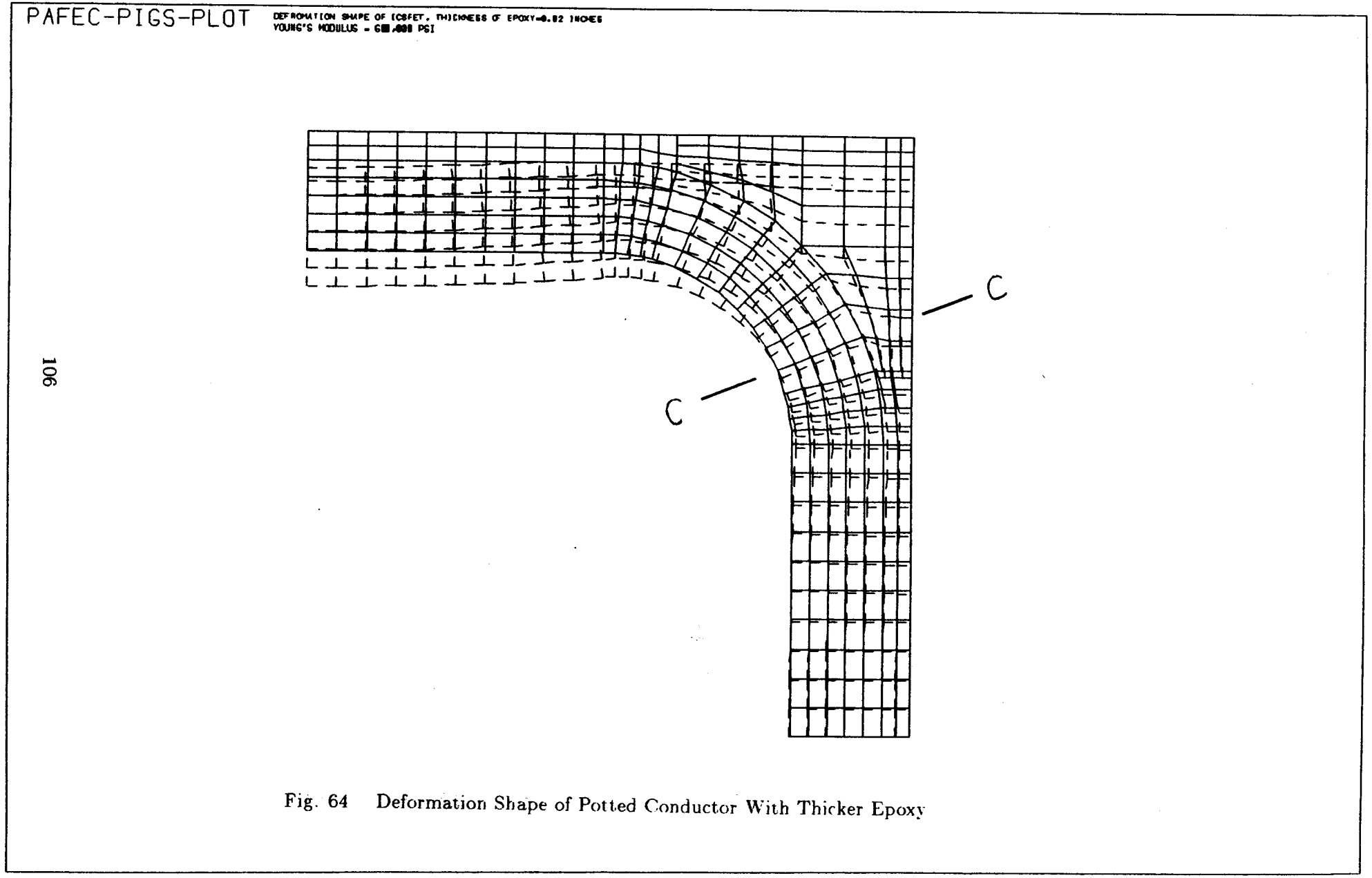

Fig. 64 Deformation Shape of Potted Conductor With Thicker Epoxy

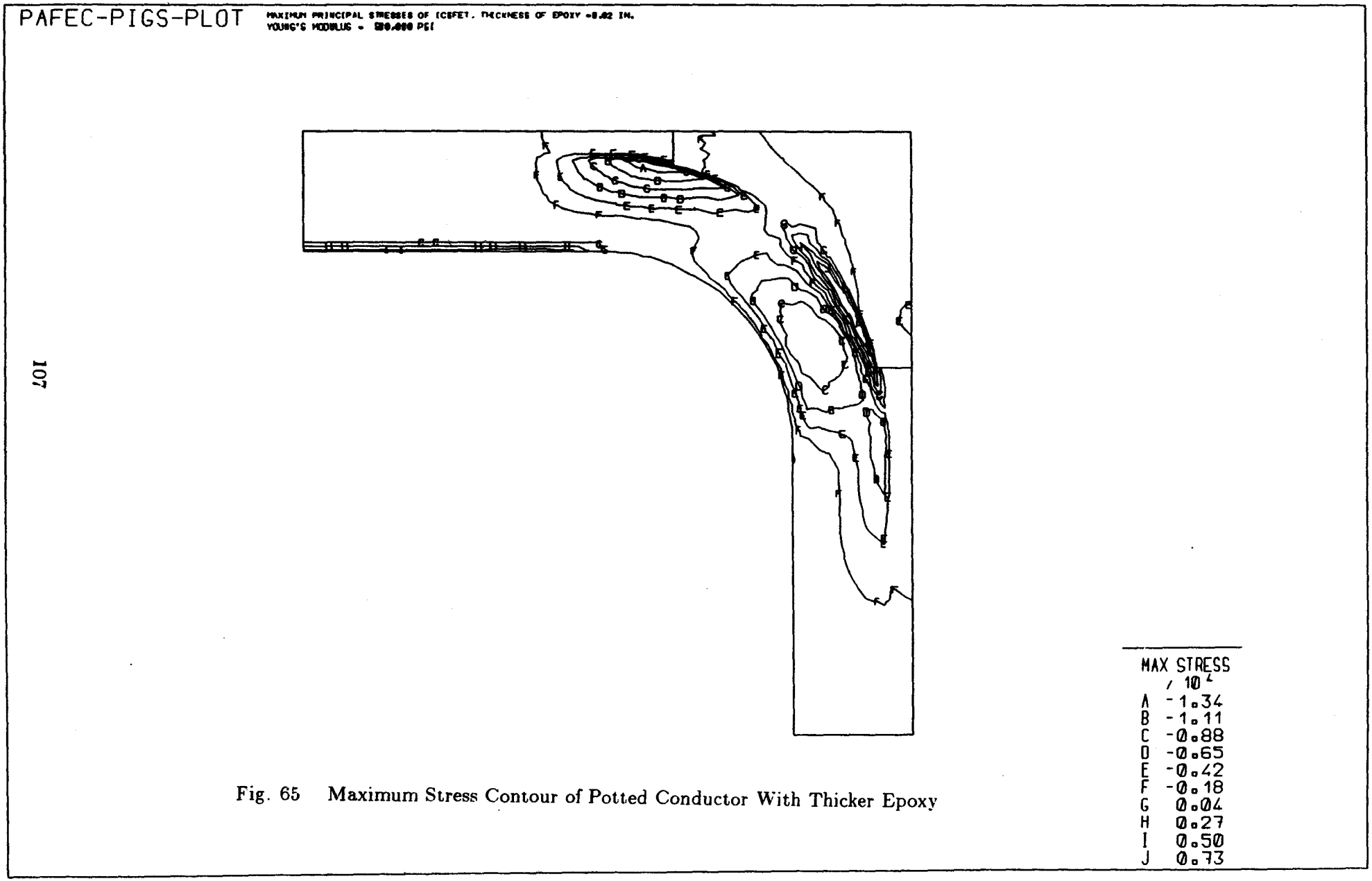

Fig. 65 Maximum Stress Contour of Potted Conductor With Thicker Epoxy

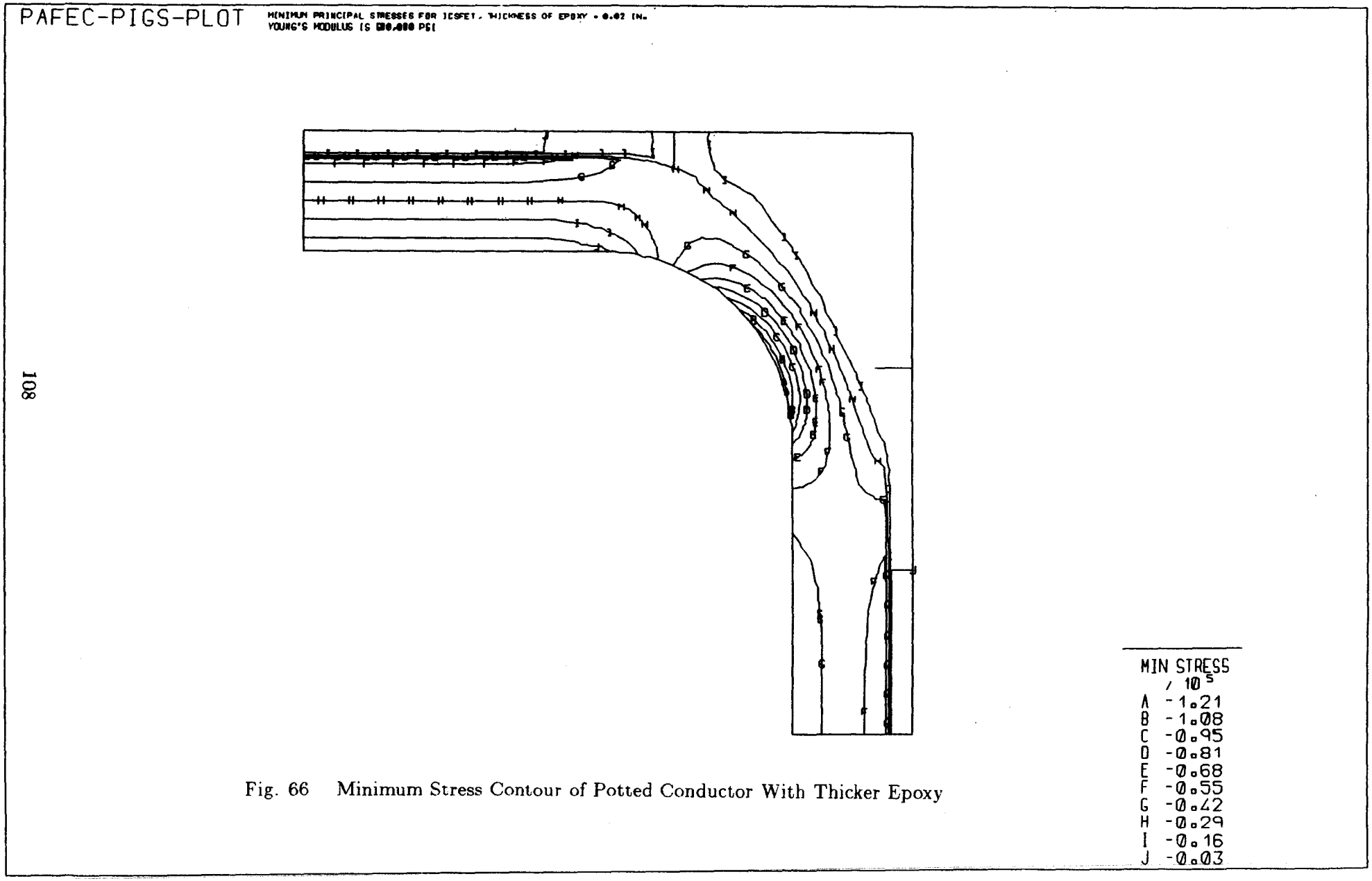

Fig. 66 Minimum Stress Contour of Potted Conductor With Thicker Epoxy

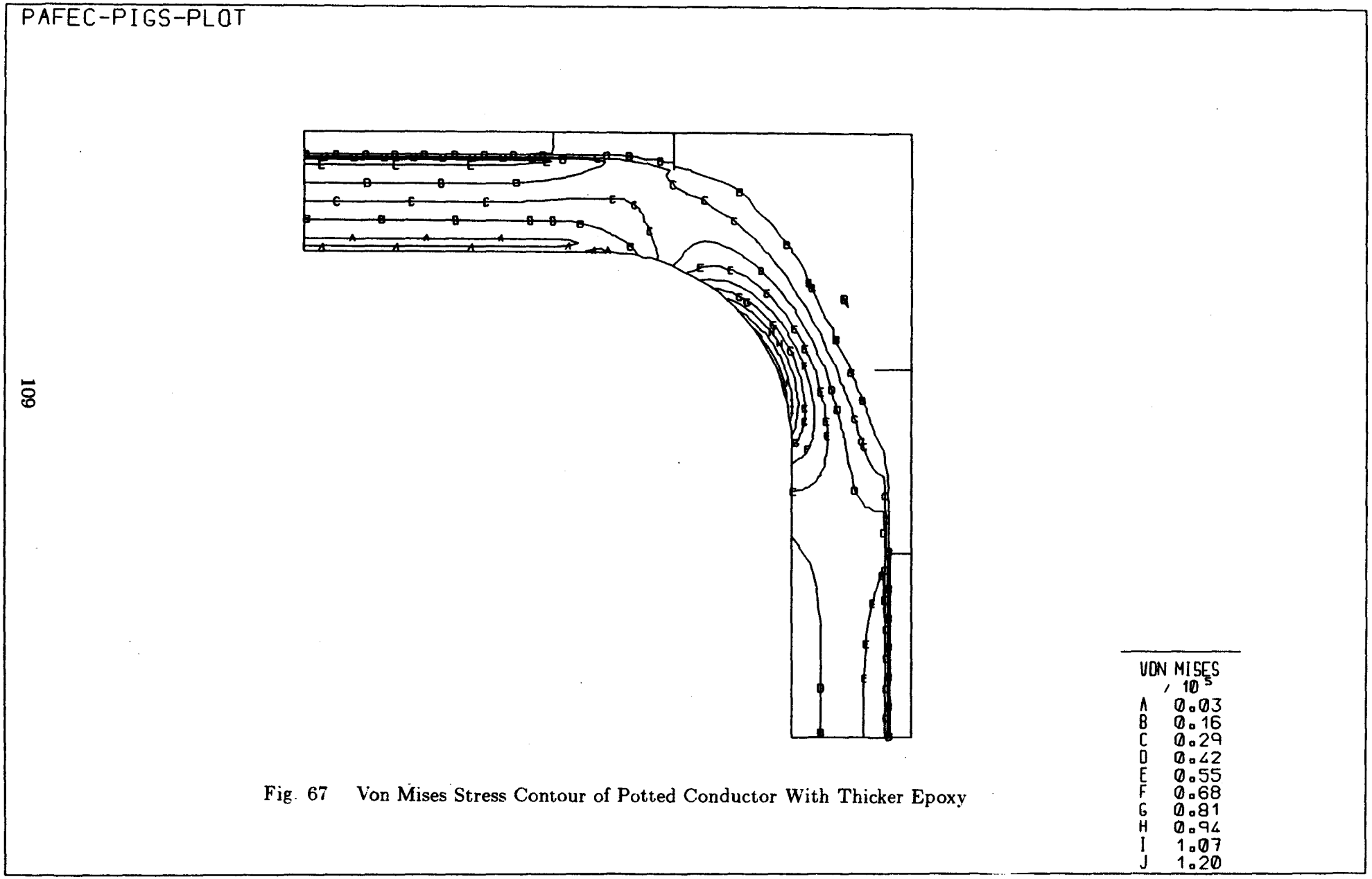

Fig. 67 Von Mises Stress Contour of Potted Conductor With Thicker Epoxy

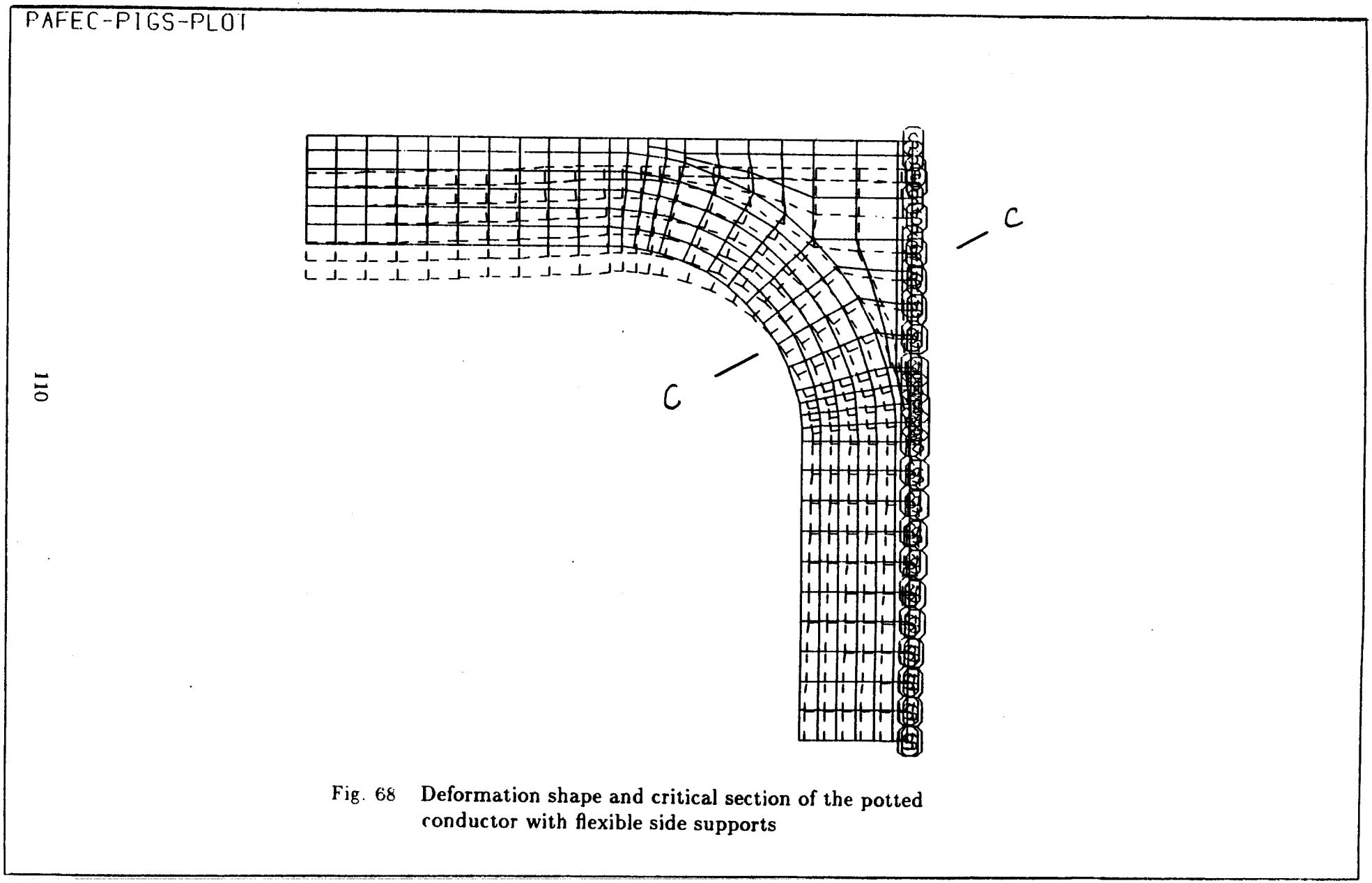

Fig. 68 Deformation shape and critical section of the potted conductor with flexible side supports

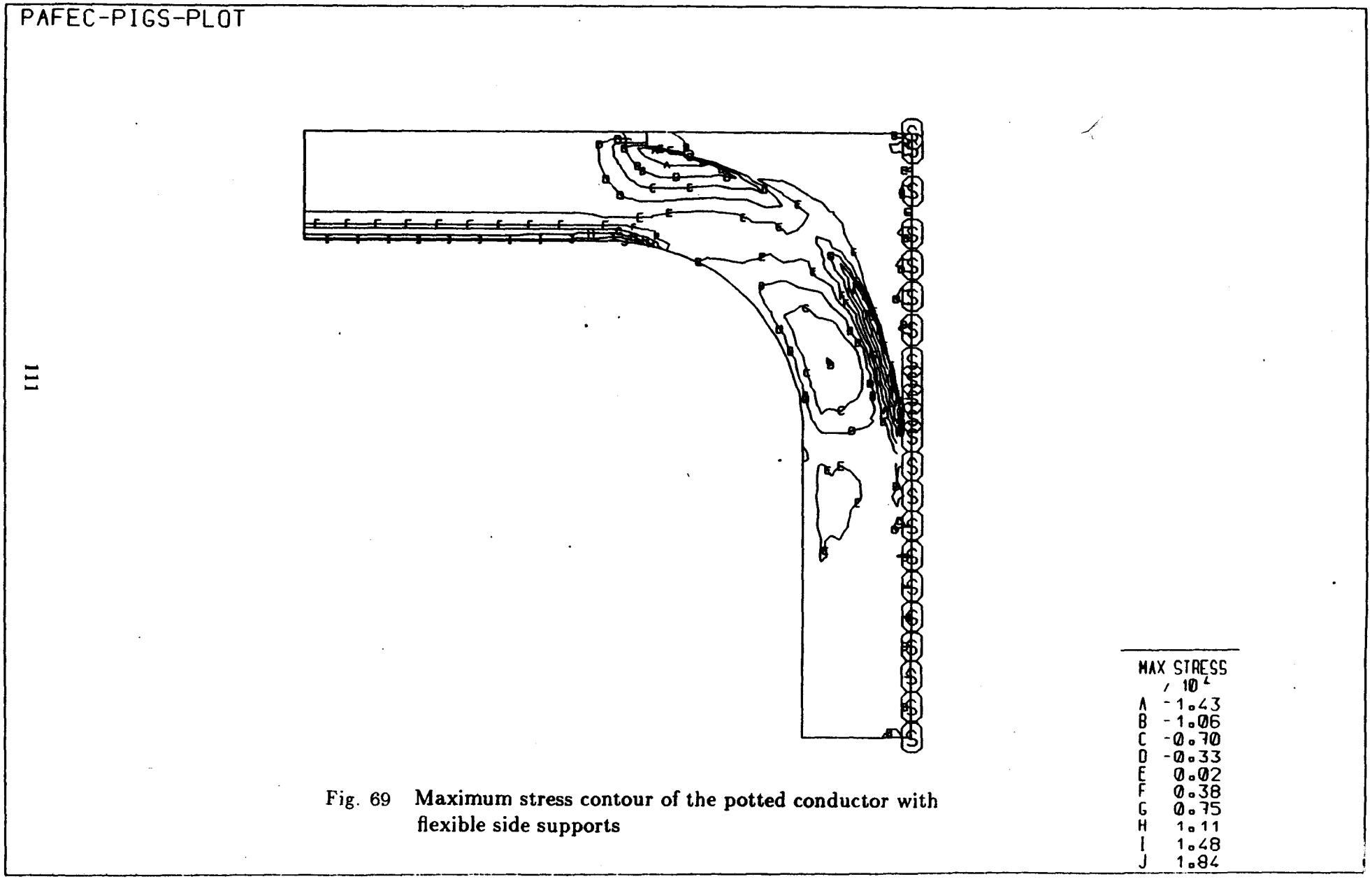

Fig. 69 **Maximum stress contour of the potted conductor with flexible side supports**

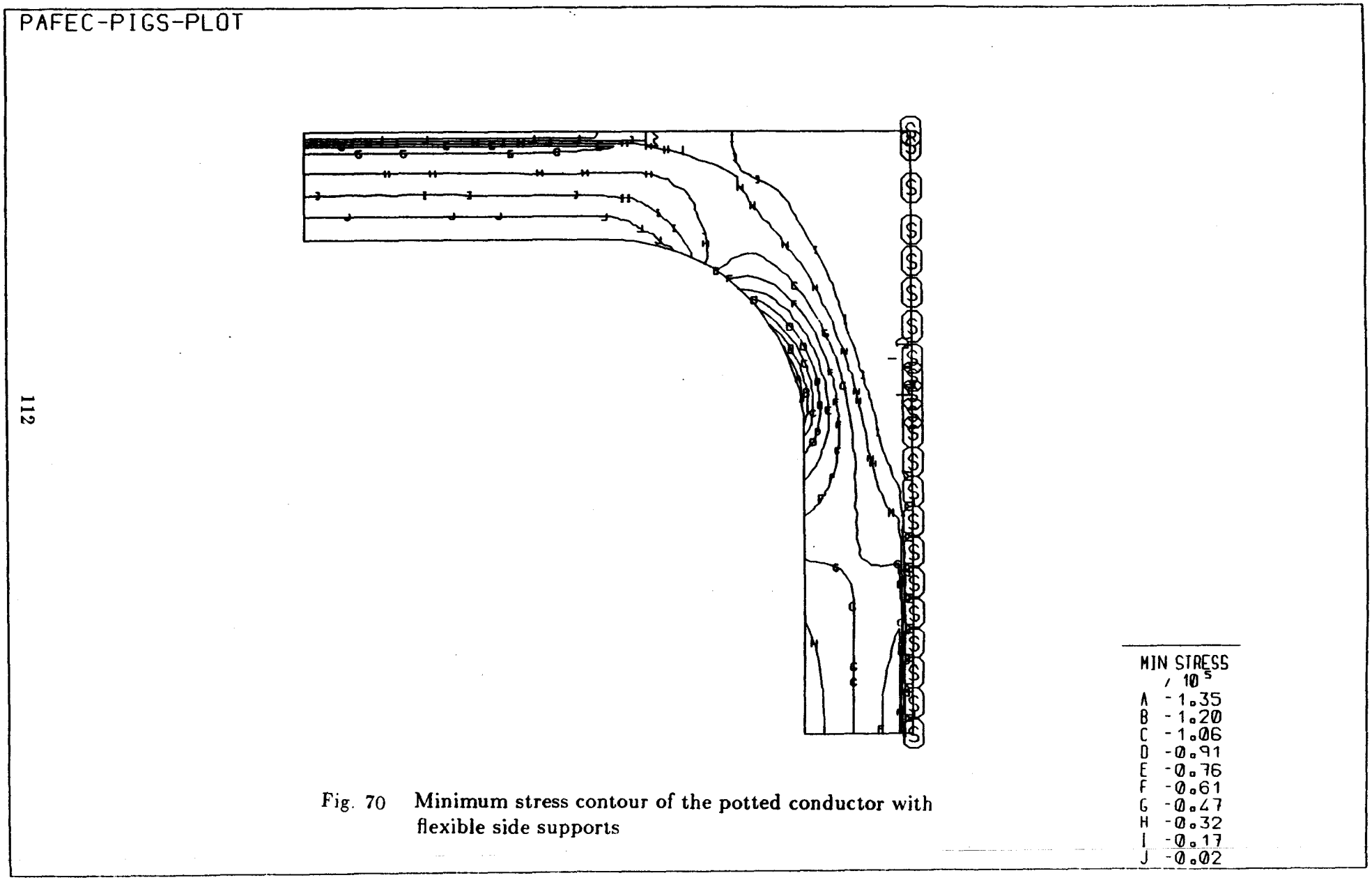

Fig. 70 Minimum stress contour of the potted conductor with flexible side supports

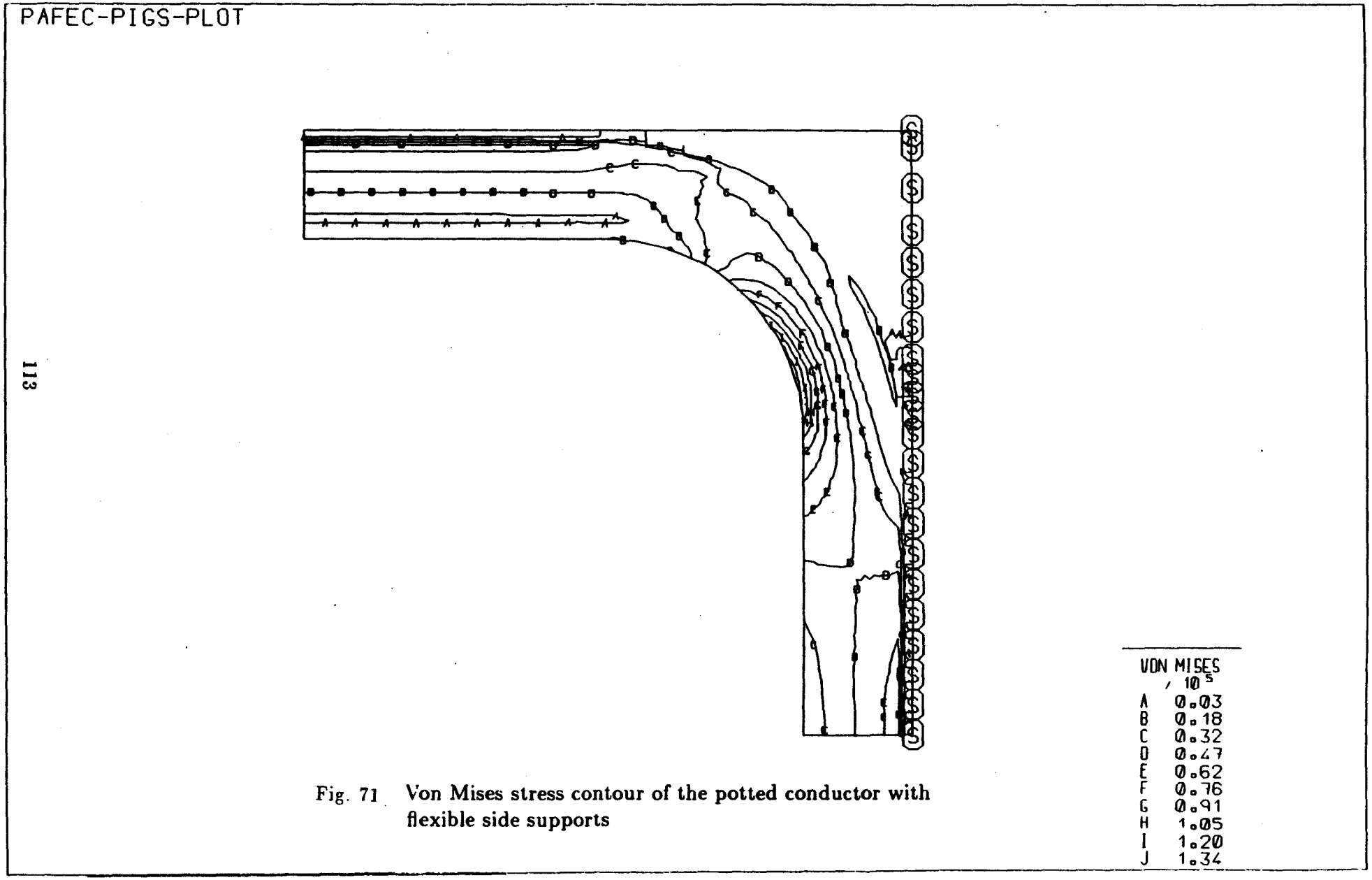

Fig. 71 Von Mises stress contour of the potted conductor with flexible side supports

TABLE 9 SUMMARY OF THE CRITICAL STRESSES AND THE DEFORMATIONS OF THE CONDUCTOR UNDER A WORKING LOAD OF 7250 PSI WITH DIFFERENT SUPPORTING AND POTTING SYSTEMS

(1)		(2)		(3)		(4)	
Se	U	Se	U	Se	U	Sc	U
1.792	4.523	1.752	5.730	1.270	2.404	1.250	1.708

(5)		(6)		(7)	
Sc	U	Sc	U	Sc	U
0.841	0.905	1.300	1.976	1.160	2.043

TITLES OF THE COLUMNS:

(1). LOOSE, RIGID SIDE SUPPORTS, THICKNESS OF CONDUCTOR = 0.065 INCHES

(2). LOOSE, ELASTIC SIDE SUPPORTS, THICKNESS OF CONDUCTOR = 0.065 INCHES

(3). LOOSE, ELASTIC SIDE SUPPORTS, THICKNESS OF CONDUCTOR = 0.130 INCHES

(4). POTTED, RIGID SIDE SUPPORTS, YOUNG'S MODULUS OF EPOXY = 600,000 PSI, THICKNESS OF EPOXY = 0.01 INCHES, THIS AND THE FOLLOWING ITEMS ALL HAVE THE THICKNESS OF CONDUCTOR = 0.065 INCHES

(5). POTTED, RIGID SIDE SUPPORTS, YOUNG MODULUS OF INSULATION = 3,000,000 PSI, THICKNESS OF INSULATION =0.01 INCHES

(6). POTTED, RIGID SIDE SUPPORTS, YOUNG'S MODULUS OF EPOXY = 600,000 PSI, THICKNESS OF EPOXY = 0.02 INCHES

(7). POTTED, FLEXIBLE SIDE SUPPORTS, YOUNG'S MODULUS OF EPOXY = 600,000 PSI, THICKNESS IS 0.01 INCHES

Se MAXIMUM EQUIVALENT STRESS IN 1E5 PSI IN ELASTIC-PLASTIC ANALYSIS

Sc LARGEST MINIMUM PRINCIPAL STRESS IN 1E5 PSI IN ELASTIC ANALYSIS

U DEFORMATION IN 1E3 INCHES OF THE LOADED NODE (IF NO POTTING) OR THAT OF THE LOADED AREA (IF POTTED)

(2) Increasing the thickness of the conductor is an effective way of increasing its strength. However, other methods can be more effective.

(3) The epoxy potting redistributes the applied load and reduces the magnitudes of both stresses and deformations significantly.

(4) The use of an insulation material with higher Young's modulus than that of the proposed epoxy serves to shift both the applied loading and its peak toward the corner, thus reducing the magnitudes of the stresses. The deformations are also reduced significantly.

(5) There is little effect of increasing the thickness of the epoxy on stresses or deformations.

Recommendations

If the magnitudes of critical stresses are excessive, they may be reduced by taking the following actions:

(1) Other insulation materials with a higher Young's modulus may be used.

(2) As an extrapolation of (1), a better design can be achieved by making the conductor into a form such as that shown in Figure 72. The bending stress will be greatly reduced and a pure compressive mode will be approximated.

(3) Less effectively, the thickness of the conductor may be increased.

The three methods described above also serve to reduce the magnitudes of the deformations. In addition, the following measures can be taken to reduce excessive deformations:

(4) Design the arrangement of the conductors so that they have both geometrical and loading symmetry and their deformations are restrained by this symmetry.

(5) A less effective way is be to increase the rigidity of the side restraints.

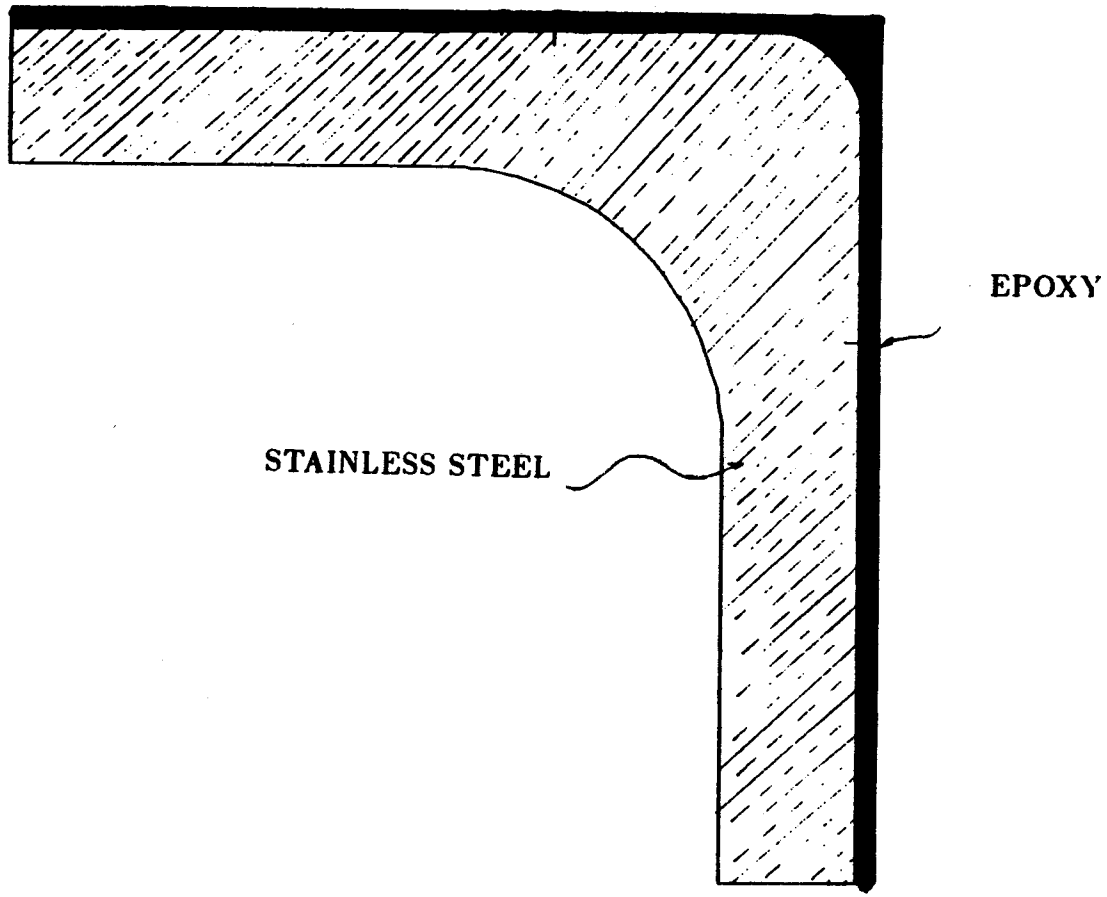

Fig. 72 **Recommended shape of the conductor**

THEORETICAL DETERMINATION OF CONDUIT STRENGTH

Strength-of-materials estimates were made of the maximum load that could be sustained by the JBK-75 conduit wall and the conduit corner. The assumed failure mode was inelastic compressive buckling.

Compression stress-strain curves for JBK-75 have not been found . For these analyses, the Ramberg-Osgood procedure was used to construct a stress-strain curve from which pertinent inelasticity data were derived (Figure 73). Analytic expressions were obtained for both wall and corner strengths, for which the tangent modulus, E_t, was assumed to be the appropriate inelastic stiffness. The predictions show reasonable agreement with the test data.

Wall buckling was calculated on the assumption that the straight regions were simply supported and loaded in uniform membrane compression. Each wall straight section is 0.418 inch long and 0.065 inch thick. If it were assumed to be a simply supported column, the critical stress would be

$$\sigma_{cr} = 0.9E_t(t/L)^2 = 140{,}000 \text{ psi.}$$

The buckling stress of the corner was estimated by assuming each corner to be part of a continuous circular ring under uniform external pressure, for which the critical stress would be

$$\sigma_{cr} = E_t(t/D)^2 = 145{,}000 \text{ psi.}$$

which is essentially the same as for the wall.

Each wall is restrained laterally by the wall of the adjacent conduit on one side and by the elastic foundation action of the conductor cable on the other. However, with the wall buckling stress near yield, it is difficult to determine how much benefit would result from those effects.

The collapse pressure would be $(0.065\times2/0.818)\times975 = 155$ MPa (22,500 psi) which is in good agreement with the maximum measured load on the filled and potted conduit. That agreement is fortuitous, however, since the stress-strain curve was constructed instead of measured and the tangent modulus is sensitive to the curve shape in the yield region. Also, the above assumptions of effective lengths and applicable elastic stiffness can be questioned. Yet the method shown here

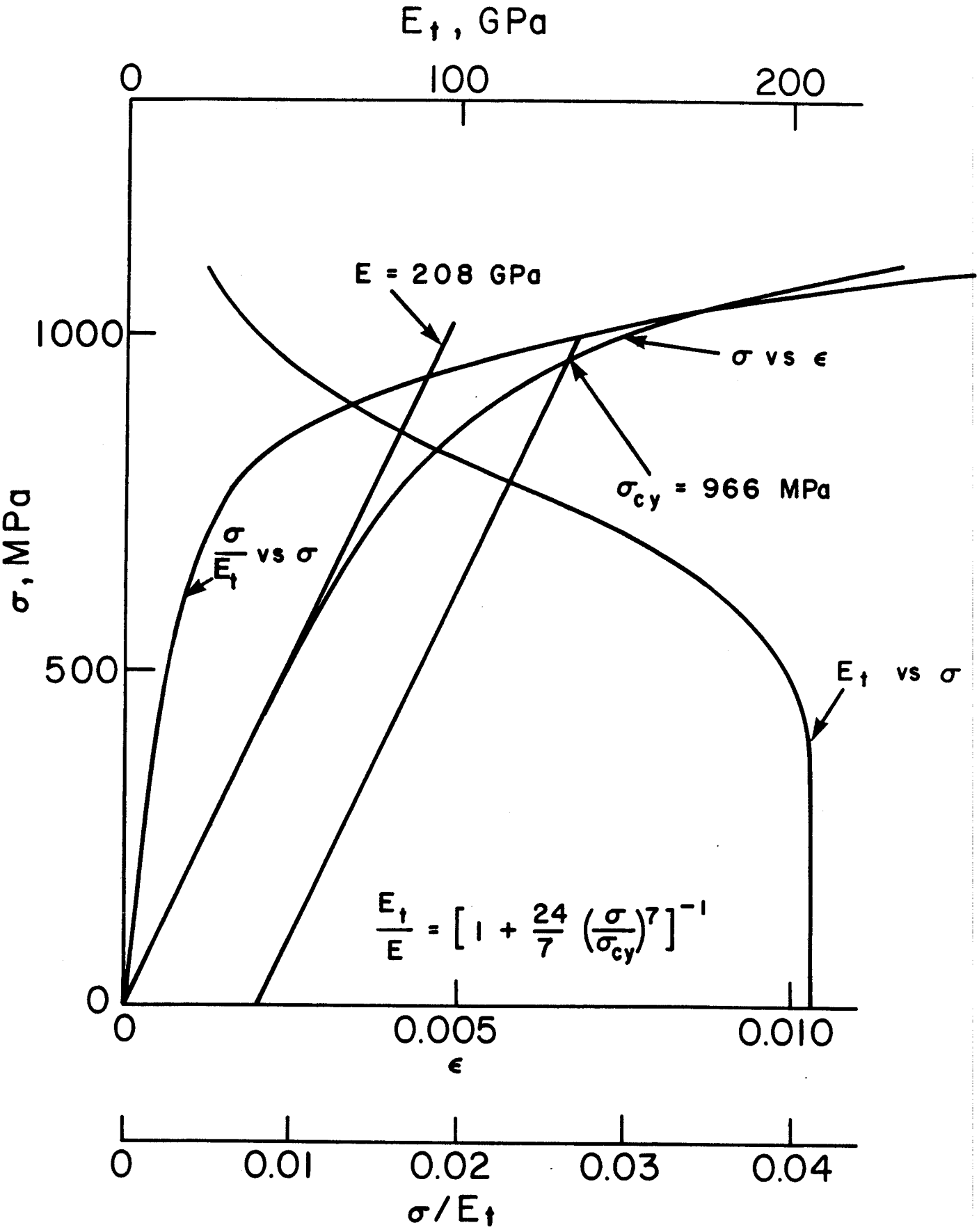

Fig. 73 Assumed Steel Stress-Strain Curve and Derived Tangent Modulus

probably would provide good enough order-of-magnitude values of conduit strengths for various materials.

ANALYSIS OF LOOSE TUBE ARRAYS

Introduction

The loose tube arrays present an opportunity for comparison of a relatively simple theoretical analysis with the experimental data since the directions and locations of the forces are clear and constant. They act vertically on the vertical diameters and horizontally on the horizontal diameters, as shown in Figure 74. The mean radius was used for the strength of materials calculations[15] and linear thin shell theory was assumed to apply. The effect of an elastic foundation for lateral restraint is depicted in Figure 75.

The vertical strain is $\epsilon_v = \Delta v/2R$

When the equations of Figure 74 are substituted in this equation, it is found that

$$E/E_f = [\frac{E}{E_v} - 0.2798\,(\frac{R}{t})^3]/[1 - 0.5601\,(\frac{t}{R})^3(\frac{E}{E_v})].$$

The vertical stiffness, E_v, is obtained from the experimental stress-strain curve.

Under p_v alone,

$$E/E_{v,o} = 0.5601(\frac{t}{R})^3$$

For the 0.41 inch tube, $t/R = 0.317$ and $E_{v,o} = 0.54$ msi. For the 0.875 inch tube, $t/R = 0.149$ and $E_{v,o} = 0.055$ msi.

The stack restraint frame rigidity was estimated to be 0.4 msi. If the flexibility of the insulation is disregarded and the contact-point deformation is considered negligible, then the theoretical E_v values for the 0.41 inch and 0.875 inch tubes would be 0.84 and 0.21 msi, respectively, compared with 1.6 and 0.5 msi obtained experimentally.

The peak bending stress on a ring under vertical load alone is

$$\sigma = \frac{12}{\pi} p(\frac{R}{t})^3.$$

If the stress is assumed to be 80,000 psi, corresponding approximately to the stress at the onset of inelastic behavior, the corresponding pressures would be 2,100 psi and 462 psi for the 0.41 inch and 0.875 inch tubes, respectively.

If the potted tubes are assumed to have been loaded by axisymmetric radial pressure,

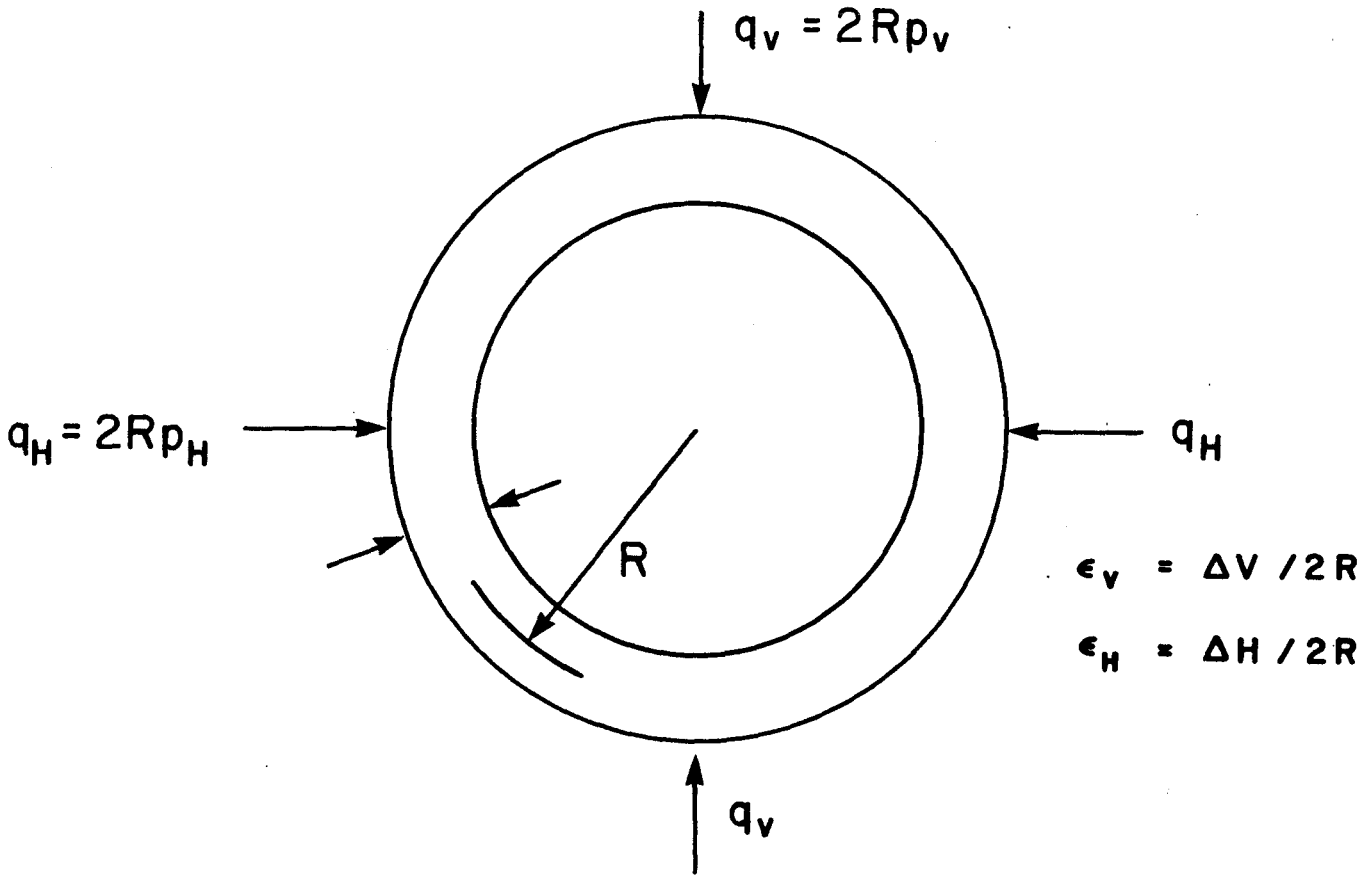

$$\Delta V_V , \Delta H_H = 3.57 \ (P_V , P_H) \ R^4 / Et^3$$

$$\Delta H_V , \Delta V_H = 2.28 \ (P_V , P_H) \ R^4 / Et^3$$

Fig. 74 Tube Loads and Deflections

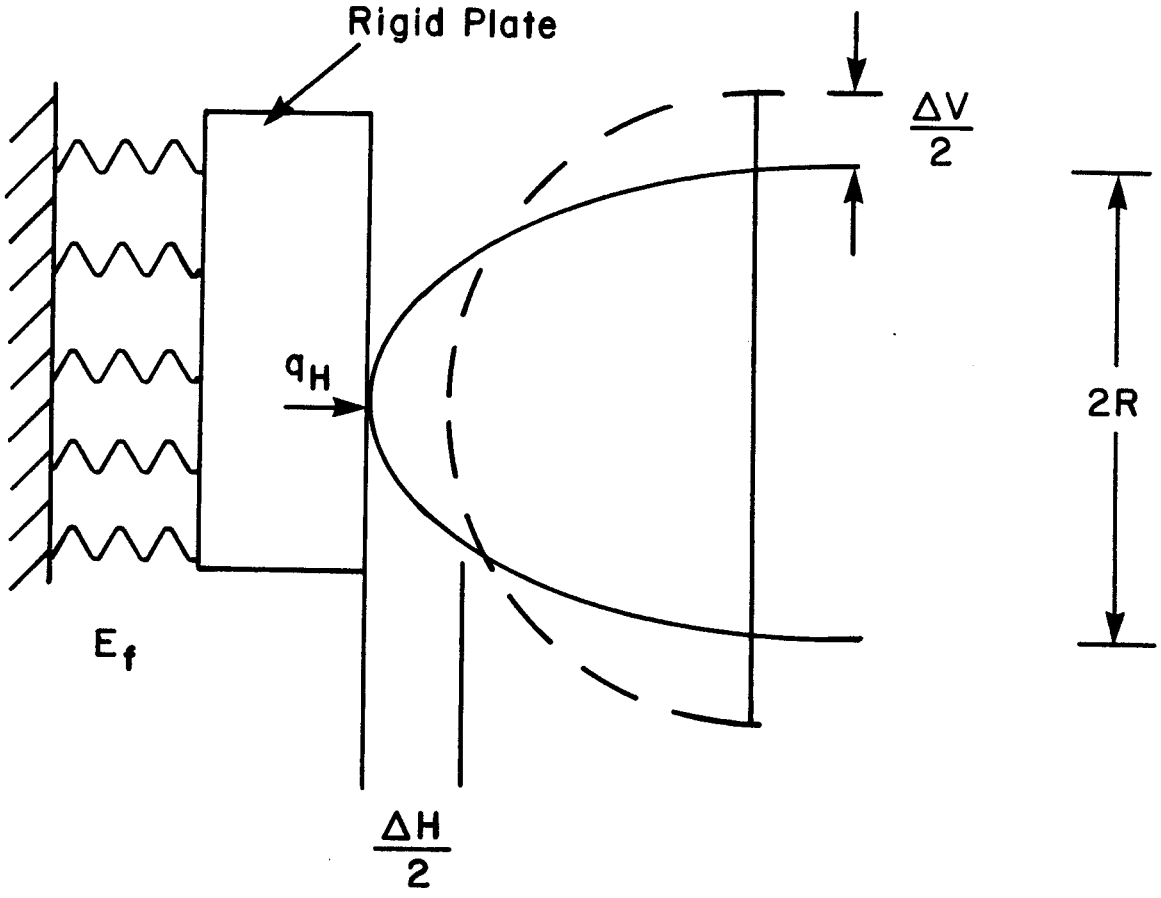

$$\frac{E_f}{E} = \left(\frac{t}{R}\right)^3 \left(1.64\,\frac{P_V}{P_H} - 1.79\right)^{-1}$$

Fig. 75 Interaction of Tube With Foundation

$$\sigma = \frac{pR}{t},$$

$$\epsilon = \frac{pR}{Et}.$$

$$E_v = \frac{p}{\epsilon} = E\,\frac{t}{R}.$$

The theoretical stiffnesses would be 9.51 msi and 4.47 msi for the 0.41 and 0.875 inch tubes, respectively, which are much larger than the experimentally determined values of 1.6 msi and 0.5 msi. This would appear to indicate that the lateral restraint was not great enough to force the potted tube arrays into a hydrostatic loading mode.

The 1.6 msi measured stiffness value for the 0.410 tube array would have required a radial deflection of 9.51 msi/1.6 msi (or 5.94) times the theoretical hydrostatic value. The corresponding ratio for the 0.875 tubes is 4.47/0.5 = 8.94. The larger deflections could have occurred as a result of the flexibility of the lateral restraint frame.

BEARING PRESSURE ON INSULATION

An estimate was made of the bearing pressure on the insulation by assuming that each rounded edge of the conduit square presses against the insulation (Figure 76). The maximum pressure was found from the relation.

$$\sigma_c = 0.798 \frac{q}{D}^{1/2} \left(\frac{1 - \nu_s^2}{E_s} - \frac{1 - \nu_i^2}{E_i} \right)^{-1/2}$$

At the peak pressure of 22,200 psi, $q = 9{,}100$ lb/in. The cylinder diameter would be 0.4 inch. With $(1 - \nu_s^2)/E_s = 1/(33 \times 10^6)$ and $(1 - \nu_i^2)/E_i = 1/(2 \times 10^6)$, $\sigma_i = 120{,}000$ psi, which is twice as high as published values for the transverse compressive strength of typical G-10[14].

The local corner deformations would tend to reduce the curvatures, thereby increasing the effective D in the pressure equation above. Also, the corner is not a solid bar. It is a formed strip, which would tend to be softer than a bar. These features would tend to reduce the local compression stress. However, these effects would be offset, to some extent, by the fact that the midplane of the insulation is probably a plane of symmetry and, as a result, the insulation would be considerably stiffer than a semi-infinite foundation of effective modulus, E_i.

According to the equation, there would be some degree of balance among those factors. In any case, there is theoretical support for the observation of insulation cracking where the flat sides of the conduit meet the round corners.

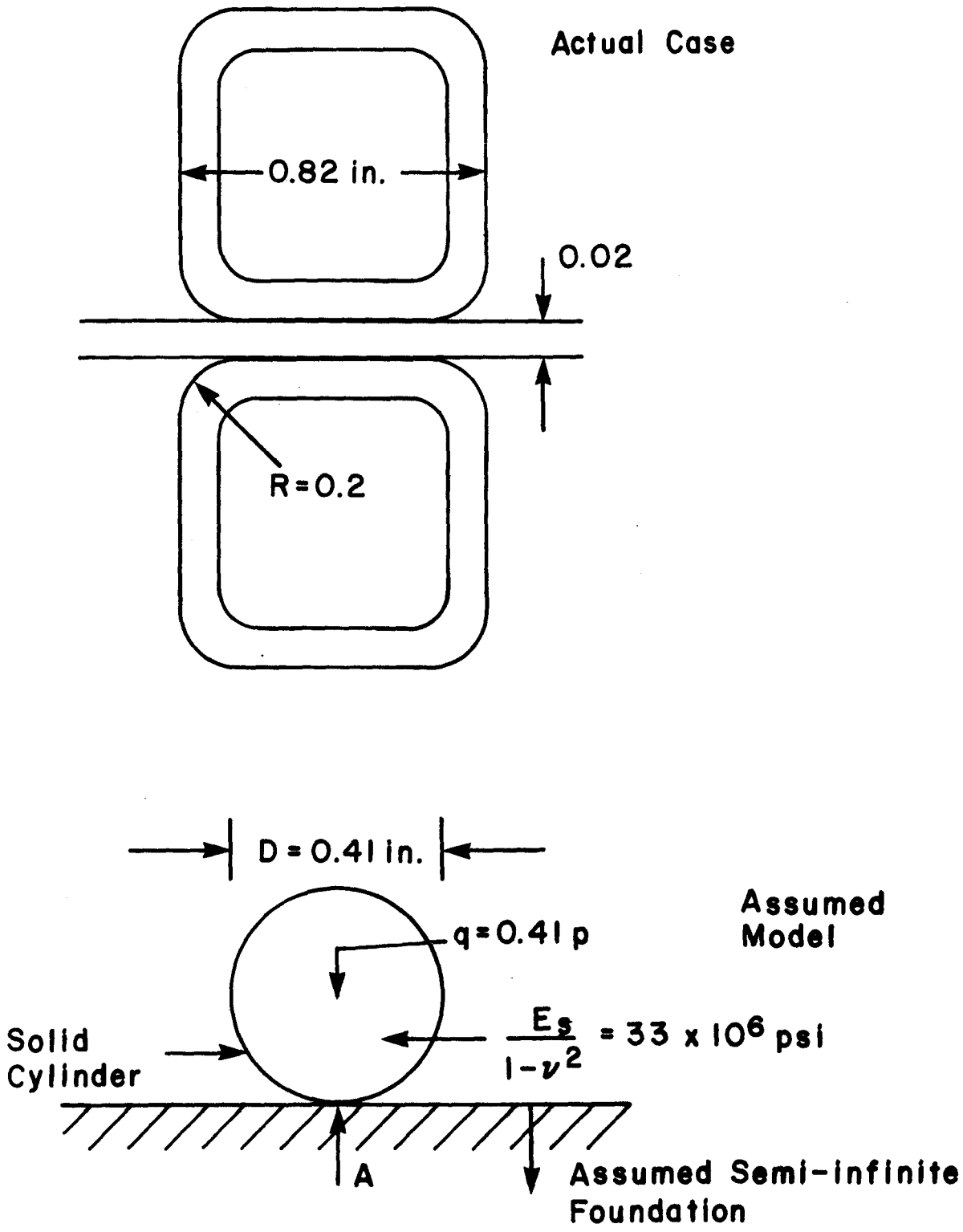

Fig. 76 Bearing on Insulation

EFFECT OF INTERNAL PRESSURE

A linear-elastic plane-strain finite element analysis was performed on the conduit for the condition of 6,000 psi internal pressure to determine the pressure-deflection curve for the wall. The peak stress was calculated to be 248 ksi (Figure 77). It occurs at the 40 degree locations in the rounded corners. The theoretical deflection at the center of each side is seen to be 0.00391 inches (Figure 78), which agrees reasonably well with the linear value of 0.0037 inches measured at dial gauge 1 on the pressure-deflection curves shown in Figure 22.

The localized high peak stress can account for the small net deflection shown on Figure 22. The large-deflection structural effect does not appear to be significant.

If the simple tube equation is used to calculate the proportional limit pressure.

$$p_{pl} = 2\sigma t/W,$$

with σ assumed to be 20 ksi, $t = 0.065$ inch and $W = 0.688$ inch (internal width), then

$$p_{pl} \doteq 3.8 \text{ ksi.}$$

Upon examination of the deflections and permanent sets shown in Figure 78 for the two curves, the amount of deflection due to nonlinear behavior was estimated at 0.00025 inch. That would indicate a proportional limit pressure in reasonable agreement with the calculated value.

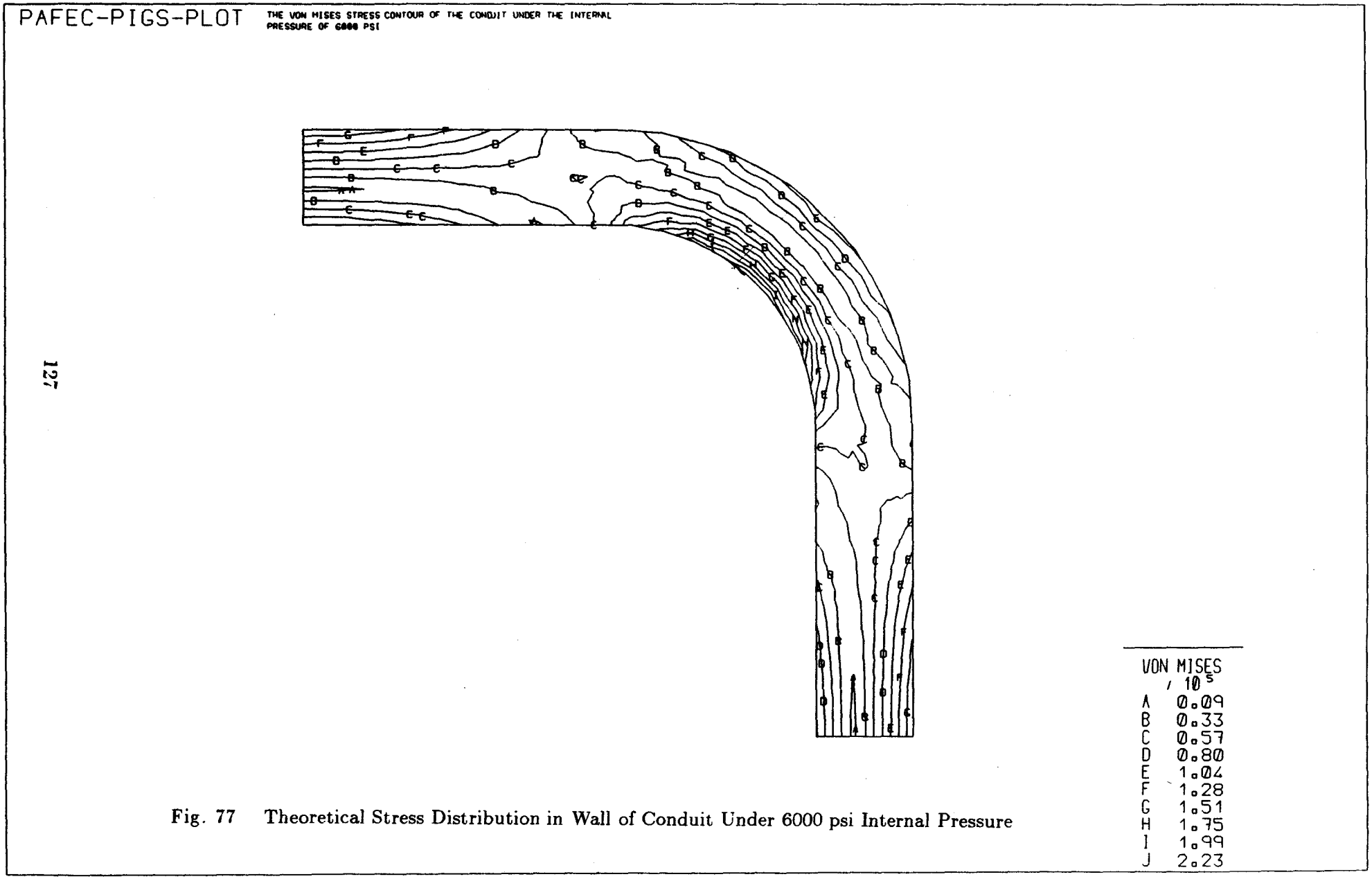

Fig. 77 Theoretical Stress Distribution in Wall of Conduit Under 6000 psi Internal Pressure

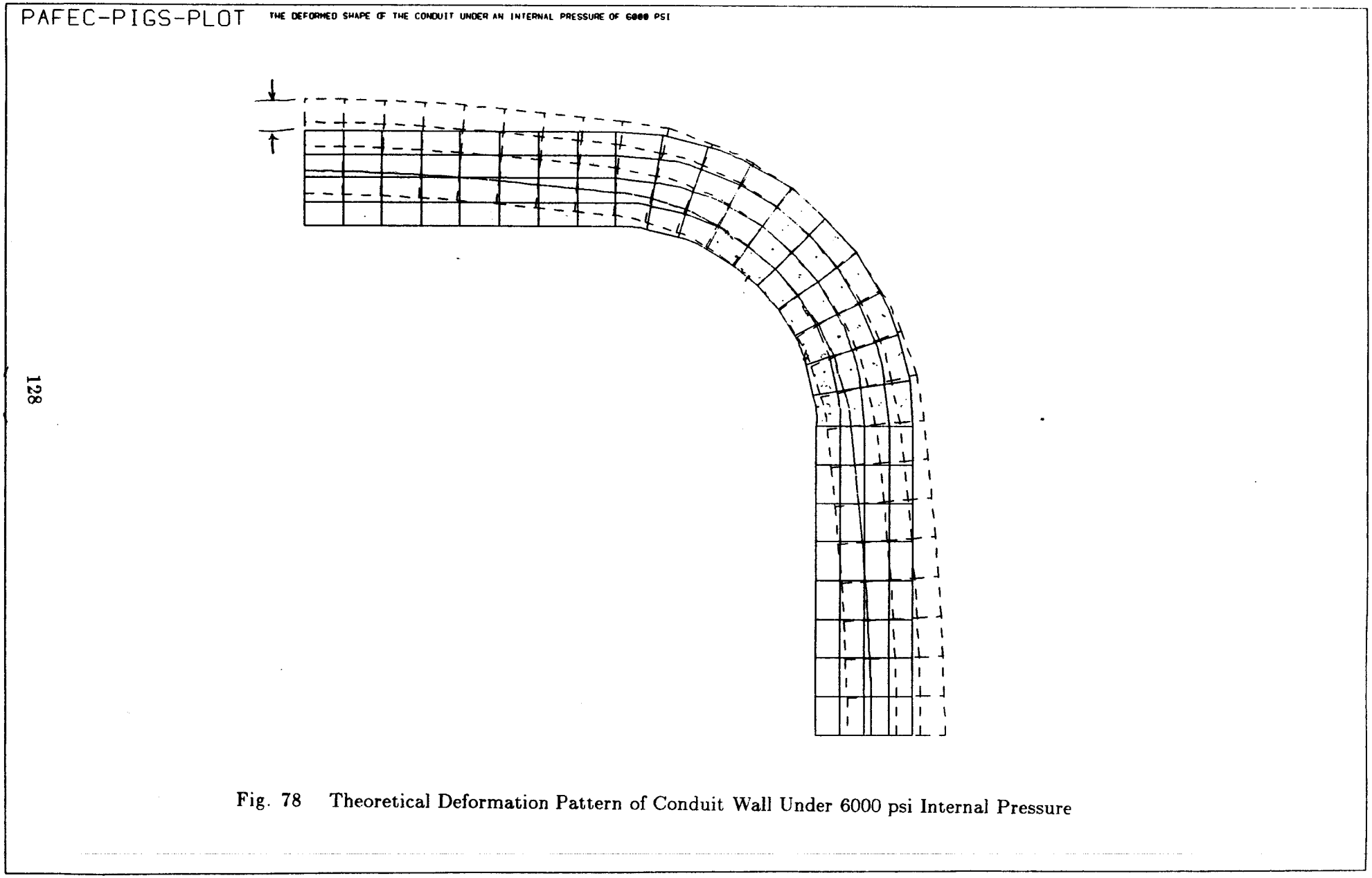

Fig. 78 Theoretical Deformation Pattern of Conduit Wall Under 6000 psi Internal Pressure

REFERENCES

1. H. Becker and J.B. Thompson, "Exploratory Structural Tests on Force-Cooled Superconductors," MIT FBNML Report, 26 December 1978.

2. H. Becker and D.B. Montgomery, "Transverse Strength of ICCS Coils for Alcator DCT," MIT PFC Memorandum, 23 January 1984.

3. G. Vecsey, "Design of the Swiss Test Coil for the IEA Large Coil Task," Proc. 8th Symposium on Engineering Problems of Fusion Research, IEEE Pub. No. 79CH1441-5 NPS Vol. III, pp. 1179-1182, 1979.

4. G. Vecsey, "Status of the Swiss LCT Coil," Proc. 8th Symposium on Engineering Problems of Fusion Research, IEEE Pub. No. 79CH1441-5 NPS Vol. III, pp. 1738-1740.

5. H. Benz et al., "The Conductor for the Swiss LCT Coil," IEEE Transactions on Magnetics, (MT-7, 1981) Volume Mag-17, No. 5, pp. 2213-2216. Also private communication from BBC on selected data from analysis and test of ICCS conduit.

6. Anon., "Superconducting Magnet Coils for the Large Coil Program, Vol. I - Introduction and Verification Testing Report," Phase 2 Final Report to UCC Nuclear Division, Westinghouse Electric Corporation, 31 March 1980.

7. H. Hahn, P.F. Dahl, J.E. Kaugerts, A.G. Prodell, "Upgraded Coil Configuration for Isabelle Magnets," IEEE Trans. Mag., Vol. MAG-17(5), p. 1575, 1981.

8. H. Becker et al., "Radiation Survivability of Organic Insulators," MIT PFC report in preparation.

9. ASME Boiler and Pressure Vessel Code, Section VIII.

10. M. Attaar, "Characterization of Repair Weld in a Fully Processed JBK-75 Sheath Using Burst Tests," Westinghouse Electric Corporation, 10 December 1982.

11. A.J. Jarabak, Addendum to Report Titled "Characterization of Repair Weld in a Fully Processed JBK-75 Sheath Using Burst Test," 10 December 1982.

12. J.W. Lue, C.M. Fitzpatrick, and J.N. Luton, "Pressure Tap Evaluation on Westinghouse Conductor Jacket," 18 November 1983.

13. J.W. Lue, C.M. Fitzpatrick, and J.N. Luton, "Additional Test Results on Pressure Tap Evaluation on Westinghouse Conductor Jacket, Addendum," 2 February 1984.

14. Anon., Handbook on Materials for Superconducting Machinery, MCIC-HB-04, Metals & Ceramics Information Center, Battelle Columbus Laboratories, January 1977.

15. R.J. Roark and W.C. Young, Formulas for Stress and Strain, 5th Ed., McGraw-Hill, 1975.